

AN ABSTRACT OF THE THESIS OF

Derek D. Pross

for the degree of Master of Science in

Geography

presented on May 24, 1991

Title: A Global Scale Analysis of the Spatiotemporal Distribution of Foliar Biomass for 1988.

Abstract approved: \_\_\_\_\_

A. J. Kimerling

Redacted for Privacy

Many ecological systems follow a seasonal cycle affecting primary production, carbon flux, and vegetative gas emissions. The seasonal variation of ecological systems are both affected by and have effects upon climatic factors. A quantitative estimate of the seasonal variation of vegetation is required to characterize ecological systems and their interaction with climate. Monitoring the spatiotemporal variation of foliar biomass density (FBD) over one year will provide a quantitative estimate of the annual cycle and regional variation of photosynthetic activity. FBD is a quantitative measure of leafy material per unit of area produced by photosynthetically active vegetation. This seasonal variation in FBD is an important parameter for global and other large scale investigations of ecological, hydrological, and biogeochemical systems which require data and expertise from a variety of sources and disciplines. Therefore, FBD is potentially of great utility for ecologists, hydrologists, climatologists, and atmospheric scientists.

Recent regional scale investigations of ecological systems concluded that the repetitive coverage and synoptic view of remotely sensed measurements provide data to monitor the seasonal variation of biomass. A method to estimate the seasonal variation of FBD at global scales has not been developed. The objective of this research is to develop a methodology that could be used to estimate the

seasonal variation of FBD for the entire terrestrial biosphere. By coupling global satellite data, measured field data, and a vegetation classification, a model was developed to estimate the global spatiotemporal variation of FBD.

Comparisons between literature estimates of FBD and estimated FBD from this model were made as a means of validation. A more specific comparison was conducted between grasslands based on work conducted in the Senegalese Sahel region in Africa. Finally, a sensitivity analysis was performed to characterize the potential propagation of error associated with the literature FBD estimates used to drive this model.

A Global Scale Analysis of the Spatiotemporal  
Distribution of Foliar Biomass for 1988

by

Derek D. Pross

A THESIS

submitted to

Oregon State University

in partial fulfillment of  
the requirements for the  
degree of

Master of Science

Completed May 24, 1991

Commencement June 1992

APPROVED:

Redacted for Privacy

\_\_\_\_\_  
Professor of Geography in charge of major

Redacted for Privacy

\_\_\_\_\_  
Chairman of Department of Geosciences

Redacted for Privacy

\_\_\_\_\_  
Dean of Graduate School

Date thesis is presented \_\_\_\_\_ May 24, 1991

Typed by \_\_\_\_\_ Derek D. Pross



## ACKNOWLEDGEMENTS

I express my deep thanks and appreciation to my friend Danny Marks for all his help and guidance, both financially and intellectually. I would also like to thank Jon Kimerling for his guidance through my program and his assistance in producing my thesis manuscript. Special thanks to Dave Turner and Don Phillips who provided a surplus of ideas and encouragement that have added greatly to the structure and content of my thesis. Finally, I wish to thank Jayne Dolph, whose trust in me afforded me the chance of my lifetime. I will not forget.

I dedicate this thesis to my mother, Jody Pross, who by example, inspired in me an interest in the wonders of nature, and who has given me the perserverance and compassion to follow my present and future dreams to fruition. I also wish to dedicate this thesis to memory of my father, Donald Pross; a man whose life was taken before I had the chance to know him. My grandparents, Bertram and Alice Halberg, provided me with unlimited love and an interest in the "out-of-doors", and I thank them. Without my family, I would be a man of little substance. This thesis is really the accomplishment of my parents and grandparents in raising me as much as it is my personal scientific accomplishment.

Derek Pross  
Corvallis, 1991

## Table of Contents

CHAPTER 1 .....	1
INTRODUCTION .....	1
CHAPTER 2 .....	5
BACKGROUND .....	5
Spectral Windows for Vegetative Remote Sensing .....	5
Spectral Band Ratioing .....	6
Quantitative Applications of Remote Sensing Data .....	8
Remote Sensing Analysis of Large Areas Over Time .....	9
Remote Sensing and Ecological Models .....	12
Global Vegetation Index (GVI) Data .....	13
Foliar Biomass Estimates and Seasonal Variation .....	14
CHAPTER 3 .....	16
METHODOLOGY .....	16
Data .....	16
Approach .....	20
Methods .....	24
CHAPTER 4 .....	36
RESULTS .....	36
Results and Discussion .....	36
Sensitivity Analysis .....	43
CHAPTER 5 .....	47
CONCLUSIONS .....	47
REFERENCES .....	50
Monthly Images of GVI, January through December .....	59
Derivation of FBD-GVI relationship .....	72
Table of Biome Specific Variables and Constants .....	75
Table of Olson Categories by Number used in the Aggregation .....	76
Temporal Profiles for each Biome .....	77
Calibration Curves for each Biome .....	90
Monthly FBD Surfaces, January through December .....	102
Monthly Histograms of GVI per Biome .....	115
Monthly Histograms of FBD per Biome .....	139

## LIST OF FIGURES

<u>Figure</u>		<u>Page</u>
1.	January GVI Image	18
2.	July GVI Image	19
3.	Statistical relationship between AVHRR NDVI and the foliar biomass of grasslands	21
4.	Statistical relationship between AVHRR NDVI and LAI of Coniferous Forests	22
5.	The temporal profile of GVI for the Northern Temperate Broadleaf Forest	26
6.	The histogram for the Woodlands biome displaying the bimodality associated with two distinct spectral signatures	27
7a.	Olson biome 32, skewed left with a mean of 26.0	28
7b.	Olson biome 43, skewed left with a mean of 26.2	28
8a.	Olson biome 46, skewed right with a mean of 17.4	29
8b.	Olson biome 47, skewed right with a mean of 16.4	29
8c.	Olson biome 48, skewed right with a mean of 7.5	30
8d.	Olson biome 59, skewed right with a mean of 14.9	30
9.	The calibration curve for the Cool Conifer biome derived from the literature	35
10.	January FBD Surface	37
11.	July FBD Surface	38

## LIST OF TABLES

<u>Table</u>	<u>Page</u>
1. The satellite and sensor are shown with the corresponding spatial and temporal resolutions and the number of spectral bands associated with the sensor	10
2. The first aggregation scheme based solely on literature descriptions of vegetation type	25
3. The second aggregation scheme based on the analysis of GVI histograms	31
4. Percentage of biome located in global categories of unique seasonal variations	32
5. The biomes with ranges of GVI values used to calibrate the model	33
6. The maximum and minimum values for FBD expressed in kg/m <sup>2</sup>	34
7. The total foliar biomass for the globe was calculated by converting LAI into foliar biomass and totalling the leaf biomass of each biome	40
8. The total foliar biomass for the forest biomes was calculated by multiplying the total chlorophyll per biome by the foliar biomass/chlorophyll mass values	40
9. This table displays some descriptive statistics in order to quantitatively compare the global categories of seasonal variation of GVI within the tropical biomes	43
10. The estimates of FBD per biome are shown with a $\pm 10\%$ deviation from the minima and maxima	45
11. This table a 10% movement around the maxima and minima FBD estimates found in the literature	46

# **A GLOBAL SCALE ANALYSIS OF THE SPATIOTEMPORAL DISTRIBUTION OF FOLIAR BIOMASS FOR 1988**

## **CHAPTER 1**

### **Introduction**

There are many factors, both of natural and human origin, that determine the climate of the Earth. The driving energy for weather and climate comes from the Sun. Of the solar radiation that the Earth intercepts, about one third is reflected and the rest is absorbed by the components of the climate system (e.g. atmosphere, ocean, ice, land, and biota). As energy is absorbed from solar radiation it is balanced by outgoing radiation from the Earth and atmosphere. The temperature of the Earth-atmosphere system results from this balance (Gates, 1980).

There are several natural factors which can change the balance between the energy absorbed and emitted by the Earth. One of the most important factors is the greenhouse effect. Simply, shortwave radiation can pass through a clear atmosphere relatively unimpeded, but the long wave terrestrial radiation emitted by the warm surface of the Earth is partially absorbed and then re-emitted by a number of trace gases in the cooler atmosphere above. However, if this balance is disturbed then warming or cooling will occur. The main concern over global climate change today is the quantity of water vapor, clouds, and trace gases in the atmosphere and the affect these parameters have upon the mean temperature of the Earth (Houghton *et al.*, 1991).

The key greenhouse gases produced by natural and human activities are CO<sub>2</sub>, CH<sub>4</sub>, N<sub>2</sub>O, water vapor and ozone. All of these trace gases are determined to some degree by photosynthetically active foliar biomass, owing their quantities and locations of sources and sinks in part to the seasonal variation of terrestrial biota. Water vapor has the largest greenhouse effect but, on a global scale, is not affected

by human sources and sinks. The seasonal variation of terrestrial biota does, however, play a significant role in the regulation of the global water balance. Ozone affects incoming solar radiation, but quantifying the climatic effect of ozone change is not yet accurately defined. It is known, however, that biogenic gas emissions, such as isoprene, can affect the concentrations of tropospheric ozone. The sources of  $\text{CH}_4$  and  $\text{N}_2\text{O}$  are the least well known but can be related to the burning and decay of biomass. While the anthropogenic sources and magnitudes of  $\text{CO}_2$  are known, the sources and sinks from the ocean and terrestrial biota are not well known, but it is recognized that the processes of photosynthesis and respiration fix and release carbon. In summary, the seasonal variation of photosynthetically active biota is an important parameter of the global climate system (Rosenzweig and Dickinson, 1986, and Berger *et al.*, 1989).

The interaction between vegetation and climate are affected in both the short and long term. Biophysical processes such as photosynthesis and respiration are dependent on climatic factors and  $\text{CO}_2$  concentration in the short term. Photosynthesis captures atmospheric  $\text{CO}_2$ , water, and solar energy and stores them in organic compounds which are then used for subsequent plant growth, animal growth, and growth of microbes in the soil. All of these organisms release  $\text{CO}_2$  via respiration into the atmosphere. Most land plants have a system of photosynthesis which will respond positively to increased atmospheric  $\text{CO}_2$  but the response varies with species. In the longer term, due to the species response, climate and  $\text{CO}_2$  are among the factors which control ecosystem structure (i.e. species composition, either directly by increasing mortality in poorly adapted species, or indirectly by mediating the competition between species) (Gates, 1980).

Because species respond differently to climatic change, some will increase in abundance and/or range while others will decrease. Ecosystems will therefore

change in structure and composition. For example, some species may be displaced to higher latitudes and altitudes, and may be more prone to local or global extinction whereas other species may thrive. In other words, ecosystem structure and species distribution are particularly sensitive to the rate of change of climate. As a result, the rate of temperature change can be deduced from the paleoclimatological records. These paleoclimatological records account for the photosynthetically active seasonal variation of global ecosystems (Rosenzweig and Dickinson, 1986).

A method is needed to characterize present distributions and seasonal variation of photosynthetically active vegetation because of the importance of accounting for this seasonal variation in order to achieve the best possible estimates for the vegetative component of the global climate system. Field sampling of vegetation is one way to estimate distribution and seasonal variation but problems of spatial and temporal sampling are impossible to overcome in the context of global ecosystems. However, by taking advantage of the same solar radiation characteristics that determine the temperature of the Earth-atmosphere system, it is possible to monitor the terrestrial biosphere with satellite instruments that record data in specific spectral windows to retrieve information relevant to the seasonal variation of photosynthetic processes of ecosystems (Rosenzweig and Dickinson, 1986).

Studies which use satellite data to quantitatively characterize the spatial and temporal variation for the entire terrestrial biosphere have not yet been conducted. Nevertheless, there has been a great deal of research performed on the quantification of foliar biomass from watershed to regional scales. These studies, in general, conclude that: 1) satellite imagery can be qualitatively and quantitatively related to foliar biomass, 2) large scale analysis of foliar biomass can be successfully conducted over large regions through time, 3) great care must be taken to normalize and reduce error within the satellite imagery in order that the data



remain reliable through time.

The objective of this study is to develop a methodology that could be used to model the quantitative seasonal variation of foliar biomass for the entire terrestrial biosphere. Coupling the satellite imagery with measured field data and a vegetation ecosystem classification provides the tools for developing a model to estimate the seasonal distribution of foliar biomass. It is hypothesized that: 1) foliar biomass density (FBD - a quantitative measure of the amount of foliar biomass per unit area) can be mathematically estimated with remotely sensed data, 2) these estimates will provide the spatiotemporal distribution of FBD at a monthly time step for one year, 3) the results will provide a realistic characterization of the seasonal variations of photosynthetically active foliar biomass for present ecosystems. These results are compared to other literature based estimates and another model of grasslands in order to test the validity of the model. Finally, a sensitivity analysis is performed to characterize the propagation of potential error associated with the foliar biomass estimates used to drive this model.

## CHAPTER 2

### Background

The research described in this document presents a model that characterizes the seasonal variation of FBD for the entire terrestrial biosphere with a one year time series of global satellite data. The methodology developed for this work was an extension of previous research that has been conducted to understand the physical and physiological basis of spectral response as a function of foliar biomass. The following discussion traces the establishment of both qualitative and quantitative use of these spectral windows for remote sensing of foliar biomass.

#### Spectral Windows for Vegetative Remote Sensing

Two portions of the electromagnetic spectrum, the red (0.6 - 0.7  $\mu\text{m}$ ) and the near-infrared (NIR, 0.7 - 1.5  $\mu\text{m}$ ), are known to be highly sensitive to foliar biomass. The design of remote sensing instruments used to collect data relevant to vegetation using portions of these spectral windows relies upon the many studies conducted to analyze spectral response as a function of photosynthetically active foliar biomass.

Studies concerning vegetation in the 1960's and 1970's established the fact that different response characteristics of the red and NIR spectral windows are related to photosynthetically active foliar biomass. In one of the earlier studies, Gates *et al.* (1965) found that different plants display different spectral properties; a phenomenon upon which remote sensing of vegetation is based. Knipling (1970) noticed the spectral differences of plants in the visible (0.4 - 0.7  $\mu\text{m}$ ) and the NIR (0.7 - 1.5  $\mu\text{m}$ ) and discussed the physical and physiological reasons for the different spectral responses of plants in these two portions of the electromagnetic spectrum. The spectral reflectance and transmittance properties of leaves was researched by Woolley (1971), leading to a better understanding of light interaction

and instrument response. Tucker (1976) analyzed the 0.50 - 1.00  $\mu\text{m}$  portion of the spectrum to report on the asymptotic nature of grass reflectance as a function of biomass, helping to define appropriate spectral windows for remote sensing purposes. Narrowing the spectral window to 0.750-0.800  $\mu\text{m}$ , Tucker (1977) was able to distinguish three quantitative classes of grass biomass. The spectral contribution of post-senescent grass to photosynthetically active grass was conducted by Tucker (1978), adding further to the foundation of spectral response as a function of photosynthetically active vegetation. Linear combinations of red and NIR spectral bands were shown to be highly sensitive to photosynthetically active biomass by Tucker (1979), who concluded that these combinations could be used to monitor biomass. Tucker (1979) reviewed remote sensing and other non-destructive techniques and concluded that satellite spectral methods work well for monitoring foliar biomass and allow for synoptic coverage of large areas.

### Spectral Band Ratioing

The spectral windows (bands) recorded for remotely sensed imagery are analyzed by using digital imagery processing techniques. For an overview of digital image processing see Jensen 1986. One of the techniques commonly used in digital image analysis is band ratioing where, based on covariance among the spectral bands, the analyst may wish to ratio these bands together in some mathematical function. Rouse *et al.* (1973) was one of the first to ratio the red and the NIR to digitally distinguish vegetation types. This band ratio became known as the normalized difference vegetation index (NDVI)(equation 1).

$$NDVI = \frac{NIR - RED}{NIR + RED} \quad (1)$$

where:

NIR = bandwidth corresponding to near-infrared

RED = bandwidth corresponding to red.

Other band ratios have been used but NDVI is one of the computationally simplest and least instrument dependent, providing digital values that are highly correlated and directly related to photosynthetically active FBD. NDVI also minimizes the spatial heterogeneity of an image due to solar variation and topographic effects, increasing its utility for time series analysis. These factors make NDVI a desirable vegetation index. The following research is presented to explain the factors affecting NDVI.

One of the desirable features of the NDVI ratio is the minimization of solar variation across images through time. NDVI was used to effectively compensate for the variation in irradiational conditions through time to monitor photosynthetically active biomass dynamics (Tucker *et al.* 1979). Kimes (1980) reported on the spatial variability of vegetation canopy reflectance as a function of solar zenith angle. This was a key study for multitemporal image analysis, which is described later in this chapter. The study concluded that diurnal reflectances cannot be clearly understood until the bi-directional measurements of vegetation are more commonly known. However, if satellite data are acquired at the same time each day this problem is minimized. Holben and Justice (1980) used band ratioing as a means to reduce topographic effects on remotely sensed data. Tucker *et al.* (1981) used simple band ratios, including NDVI, to compensate for variation in solar intensities through time while estimating crop biomass accumulation. Kimes (1984) discovered that the NDVI is significantly less sensitive to solar variations than individual bands for all Sun angles at off-nadir viewing angles of less than 45°.

### Quantitative Applications of Remote Sensing Data

The other desirable feature of NDVI is that it can be used to estimate photosynthetically active foliar biomass. Two measures of foliar biomass are foliar biomass density (FBD) and leaf area index (LAI). FBD is a measure of the amount of leafy vegetation per unit area, and LAI is a measure of total leaf area per unit area. Both measurements quantify the amount of foliar biomass per unit area. The red and NIR spectral windows used in satellite remote sensing are sensitive to amount of photosynthetically active foliar biomass per pixel (when digitally analyzed), where the pixel is a measure of unit area. Clearly, the response characteristics of the red and NIR spectral windows are not changed when a different measurement is used to quantify foliar biomass. Therefore, these spectral response characteristics and the NDVI ratio should be similar when related to FBD and LAI.

An early attempt to assess foliar biomass was performed by Jordan (1969), where in situ measurements of LAI based upon spectral properties of trees were made. Pearson (1976) was one the first to model the relationship between airborne spectral remote sensing data and the amount of biomass using a nine band ratio. The study concluded that the ratio predicted 1.15 times the actual biomass present, with a coefficient of 0.98 for 26 biomass ground-truthed samples. Wiegand *et al.* (1979) reported one of the first succesful uses of NDVI as a quantitative measure correlating spectral reflectance of biomass to satellite sensors. Holben *et al.* (1980) discovered that the most significant correlations existed between NDVI and photosynthetically active foliar biomass.

Photosynthetically active LAI was estimated from remote sensing data by Curran (1983) where it was explained that reflectances and radiances in the red are inversely related to the in situ chlorophyll density and the NIR is directly related and proportional to photosynthetically active foliar biomass. Wardley and Curran

(1984) also used remote sensing techniques to estimate photosynthetically active LAI with an accuracy of 50-86% at the 95% confidence level. Conducting a time-series analysis of spectral measurements, Hatfield (1985) discovered that a simple NIR/red ratio remained stable through time and at different locations for wheat.

### Remote Sensing Analysis of Large Areas Over Time

Remote sensing can be used to characterize seasonal variation of vegetation provided that the temporal resolution is relatively high. Temporal spectral measurements of crop biomass development were conducted by Tucker *et al.* (1979) Kimes *et al.* (1981), and Markham *et al.* (1981) where significant relationships were found between NDVI and crop biomass development and crop chlorosis, displaying the usefulness of time series NDVI data. Biomass yield variation as a function of remote sensor response over growing seasons was also modeled by Tucker *et al.* (1980). A similar small scale analysis was conducted by Gallo *et al.* (1985) where estimates of photosynthetically active radiation in corn canopies were calculated, accentuating the utility of multi-temporal analyses.

Most of the studies up to this point were conducted on small areas and for only one homogeneous vegetation type, such as crops. Temporal analyses had also been conducted on these small areas and a new research direction to study large areas was initiated. The National Oceanic and Atmospheric Association (NOAA) satellites carrying the advanced very high resolution radiometer (AVHRR) provides remote sensing of large regions at a high temporal resolution compared to other remote sensing platforms. The choice is narrowed to one satellite platform when considering a suitable platform for monitoring the seasonal variation within global vegetation ecosystems where a high temporal frequency is needed along with synoptic coverage of large regions of the Earth (Table 1).

**Table 1.** The satellite and sensor are shown with the corresponding spatial and temporal resolutions and the number of spectral bands associated with the sensor. The NOAA AVHRR satellite platform has 14.5 orbits per day providing daily global coverage with some resampling discussed in the data section. The information in this table came from Jensen (1986).

System Resolutions			
Sensor	Spatial	Number of bands	Temporal
SPOT Panchrom.	10m	1	26 days
SPOT MSS	20m	3	26 days
Landsat TM	30m	7	16 days
Landsat MSS	79m	5	18 days
NOAA AVHRR	1100m	5	14.5/day

The AVHRR NDVI data were studied to determine if various vegetation types could be differentiated with the coarse spatial resolution of these data. Norwine and Greigor (1983) stratified various vegetation types using the AVHRR imagery, showing the utility of low resolution satellite data to spectrally distinguish vegetation. Goward (1985) mapped different vegetation types for North America with AVHRR NDVI imagery supporting previous work. These studies show that while the spatial resolution is coarse the high temporal resolution more than makes up for any deficiencies the spatial resolution introduces.

A long term regional scale spatiotemporal analysis of portions of Africa using AVHRR NDVI data began in 1980. It was hypothesized that remote sensing can provide invaluable ecological data. Tucker *et al.* 1983 used the AVHRR NDVI data to statistically model relationships of seasonal variation between the satellite data and grasslands. Tucker *et al.* 1985 used an NDVI time series to analyze both the spatial and temporal variability of grassland biomass. Tucker *et al.* (1985) integrated weekly satellite data with respect to time for a twelve month period and produced a remotely sensed estimate of primary production based upon the density and duration of foliar biomass. The dynamics of AVHRR data for Tunisia, Africa, were explained by a combination of vegetation and soil scattering components, and

the NDVI data were also shown to decrease signal variation (Kimes *et al.* 1985).

Further remote sensing research in Africa stresses the need for high frequency temporal satellite data. Tucker and Sellers (1986) estimated primary production under the limitations of off-nadir viewing and atmospheric conditions. These limitations coupled with the need to measure changing surface conditions emphasized the need for multitemporal measurements. Townshend and Justice (1986) showed NDVI response to different vegetative cover types has unique temporal profiles per vegetation type. An estimate of length of a growing season was made using time series NDVI in East Africa by Justice *et al.* (1986) by distinguishing levels of foliar biomass.

Holben and Fraser (1984) noted that cloud contamination, directional reflectance, off-nadir viewing, sun-angle, and shadow effects decrease values of NDVI, leading Holben (1986) to develop the maximum value composite procedure. The computations in this procedure retain the maximum value on a pixel by pixel basis for a number of images acquired for the same area of interest on different dates thereby providing the clearest and least shadowed view of the surface. Justice and Hiernaux (1986) showed the utility of high temporal resolution for monitoring at regional scales and emphasized the importance of the maximum value composite procedure. More recently Gutman (1987) reported that the maximum value composite procedure for AVHRR NDVI data is useful for minimizing cloud contamination, atmospheric scattering and absorption, and solar angle effects in the Great Plains region of the Western U.S.

Prince and Astle (1986) concluded that equations could be constructed to predict biomass, but only if the satellite data/vegetation relationship is applied to the same vegetation type by stratifying the region with a vegetation map. Prince and Tucker (1986) built regression models between the Senegalese grassland



biomass and NDVI which explained 93% - 99% of the variation in NDVI. A qualitative approach suggested that by monitoring rangeland conditions with satellite data one could identify areas of deficiencies in primary production and provide synoptic information in support of regional drought monitoring (Tucker *et al.* 1986). Growing periods were defined by periods of minimum biomass and related to minimum NDVI values by Henricksen and Durkin (1986), emphasizing the ability of NDVI to be used to quantify measures of foliar biomass.

### Remote Sensing and Ecological Models

More recent studies have revealed the potential of the seasonal variation of the AVHRR NDVI as an input for ecological models needing spatiotemporal measures of foliar biomass. Running *et al.* (1986) reported on the first attempt to measure LAI of coniferous forests using satellite data. The study concluded that satellite derived measures of vegetation cover type and LAI may be used to provide more direct estimates of the carbon content and exchange rates of global vegetation than are possible with current data. Running (1988) related AVHRR NDVI to photosynthesis and transpiration of forests in different climates to assess carbon fixation in relation to the global carbon budget. Simulated photosynthesis and evapotranspiration was modeled by coupling the AVHRR NDVI data (used to determine LAI) with an ecosystem model (Running *et al.* 1989). Spanner *et al.* (1990) was able to monitor the seasonal variation of LAI in coniferous forests with AVHRR NDVI data. Goward (1989) states that foliar presence determines local rates of photosynthesis, affects surface albedo, and influences local rates of evapotranspiration as well as other elements of surface energy/mass balance. The report concludes that for the first time, through satellite acquired imagery, a consistent, global means to directly study interactions between climate and vegetation exists. The accuracy of the AVHRR NDVI data at a resolution of 1 km was assessed by

Box *et al.* (1989), who stated that NDVI data were relatively reliable for primary productivity except in areas of complex terrain, for seasonal values at high latitudes, and in extreme deserts. The study also concluded that total biomass (inclusive of woody material) was poorly correlated to the NDVI data. Primary productivity is associated with the amount of foliage present, lending credence to the reliability of using NDVI to estimate FBD.

#### Global Vegetation Index (GVI) Data

The global vegetation index consists of resampled AVHRR NDVI imagery providing weekly global coverage. Malingreau (1986) determined that the GVI product provides a large set of useful information on ecosystem dynamics and cropping practices can be consistently derived from these time series data. Singh (1988 a,b) found that the GVI data remain reliable for high, medium, and low foliar biomass with solar zenith angles of less than 80°. The study also concluded that areas above solar zenith angles of 80° make the GVI data unreliable because the optical depth increases such that the reflectance in the red and NIR is actually a measure of the atmosphere and not the land surface. Holben (1986) referred to this phenomena as the terminator effect. From this fact it was shown that for one GVI image a multitemporal composite image must be made from about four months of imagery. However, the areas of high solar angles lie in a hemisphere's winter during which there is little photosynthetic activity. Lloyd (1990) reported that the GVI data make possible, for the first time, a phenological approach in which classes are defined in terms of the timing, the duration, and the intensity of photosynthetic activity which minimizes this problem of reliability if one is interested only the photosynthetically active foliar biomass.

Goward (1990) cautions against using the GVI data for quantitative purposes due to reasons that Singh (1988 a, b) addresses, but provides methods and ideas to

make the data more reliable. The study stated that it is possible to reduce instrument calibration and off-nadir viewing angle error by approximately 10% with maximum value composite images of at least a one month time resolution. The conclusion suggested that if these errors were corrected a global measure of vegetation green foliage dynamics can be made within a precision of 10% ( $\pm 0.1$  NDVI) at a monthly time resolution.

It has been shown that the NDVI ratio can be used to derive information about photosynthetic activity. The NDVI ratio has been used for both small and large scale analyses and it has been used successfully for multitemporal remote sensing studies. The maximum value composite procedure of the NDVI data minimizes effects of atmosphere and solar variation. There are, however, limitations which must be considered for large and global scale remote sensing analysis. Nevertheless, it is possible to make quantitative estimates of photosynthetic activity at a global scale for the entire terrestrial biosphere.

#### Foliar Biomass Estimates and Seasonal Variation

These quantitative estimates derived from the GVI data will be compared to other estimates of global foliar biomass found in the literature. One estimate of the total amount foliar biomass was found in the literature, and two other global estimates of leaf biomass were calculated by using other global estimates of biophysiological variables in the literature. Estimates of leaf area and chlorophyll exist (Whittaker 1975), as well as relationships between leaf biomass and leaf or leaf area or chlorophyll for the various biomes considered in this research (Whittaker 1962, Whittaker 1966, Whittaker and Woodwell 1969, Whittaker *et al.* 1974, Whittaker and Niering 1975, Lieth and Whittaker 1975, Blasco and Tassy 1975, Edwards and Grubb 1977, Edwards 1977, and Grubb 1977).

One final parameter must be taken into account before building the model. Most biomes occur in both hemispheres and in the Tropics (with a capital T referring to the Tropics of Cancer and Capricorn). Biomes which occur in the northern and southern hemisphere must be analyzed separately by hemisphere because the seasonal variation is offset (i.e. during January the Northern Hemisphere experiences winter while the Southern Hemisphere is in summer). Further, it is clear that the tropics display a seasonal variation that is different than extratropical areas. The geographic classification of tropics is closely aligned with the Tropics due to characteristics of solar angles. The total amount of solar radiation received at any place depends on two factors: the duration and the intensity of insolation. Insolation, precipitation, and wind play key roles in the determination of climate, and hence, the determination of seasonal variation of vegetation within the tropics (Nieuwolt 1977). Therefore, the biomes will be stratified into a global category (e.g. Tropics, Northern or Southern Hemisphere) in order to analyze the seasonal variation of each biome.

The following chapters discuss the methodology to estimate photosynthetically active FBD by using a yearly time series of GVI, a vegetation map, literature values of FBD, and a stratification for seasonal variation to estimate photosynthetically active FBD, as well as validation procedures to assess the results.

## CHAPTER 3

### Methodology

#### Data

The modeling and analysis was performed in a raster based geographic information system (GIS). A raster based GIS provides the appropriate environment for modeling spatial data (Burrough, 1986). The GIS modeling and statistical analysis of these global data sets required approximately 200 megabytes of on-line memory and the CPU power to adequately run the algorithms.

The GVI satellite imagery used in this research was acquired from ACE-CERL in Geographic Resource Analysis Support System (GRASS) (ACE, 1988) raster format for the year 1988 in a weekly time series. The data originated at the National Oceanic and Atmospheric Association (NOAA) whose satellites carry the Advanced Very High Resolution Radiometer (AVHRR) from which daily global coverage is generated across a 56° viewing track. Spatial resolutions are 1.1 km local area coverage (LAC), and ~4 km global area coverage (GAC). Global daily coverage is available only through the GAC data that are generated on board the satellite by resampling the LAC data (Kidwell, 1984), where pixels with greater than 30° off nadir view are not used (Goward *et al.*, 1990). Further sampling, by taking the last pixel mapped into the new grid of 15 km or more in size (Townshend and Justice, 1986), and conversion to the NDVI results in the GVI product as described by Kidwell (1990). GVI data are spatially restricted to land masses between 75° north and 55° south with a final nadir resolution of approximately 8.5 minutes (approximately 256 km<sup>2</sup>). The GVI ratio uses the red (0.58 μm - 0.68 μm) and NIR (0.725 μm - 1.10 μm) spectral bandwidths from the AVHRR instruments.

A maximum value compositing procedure (MVC) is used to minimize effects of topography, solar zenith and azimuth angles, and atmosphere on the NDVI ratio. The effects of topography, solar zenith and azimuth, and atmosphere have a tendency to reduce the NDVI value (Holben and Fraser, 1984). Therefore, by retaining the maximum value for each pixel these effects are minimized.

The MVC procedure used to compile the GVI data means that the pixel least affected by cloud or other atmospheric interference is automatically selected for a given seven day time period (Holben, 1986). Further, the GAC pixel with the highest value is used to represent the entire GVI pixel. The MVC procedure was used in this research to obtain monthly GVI images (Figures 1 - 2), to avoid atmospheric interference, and to retain spatial heterogeneity (Gutman, 1987, Goward *et al.*, 1990). See Appendix A for all twelve monthly images.

Version WE3.0 of the Olson Database of World Ecosystems was used to distinguish different vegetation types in this study, as discussed by Prince and Aslter (1986). This global vegetation database was chosen over others because it offered the highest resolution and because of its classification format. The spatial resolution of 30 minutes is much more coarse than the GVI data, but it offers the needed description of vegetation types at the highest possible resolution. The Olson classification is based on landscape and ecosystem while others like Matthews (1983) are based on potential vegetation excluding anthropogenic influences. The database consists of fifty-four categories of ecosystem/vegetation types at a resolution of 30 minutes which covers the entire earth (Olson *et al.*, 1983, Olson 1990).

As discussed, the seasonal variation of foliar biomass is an important parameter to consider when characterizing photosynthetic activity. Because it is impossible to collect enough field data to characterize the seasonal variation of foliar biomass for the entire terrestrial biosphere, previous research from others must be

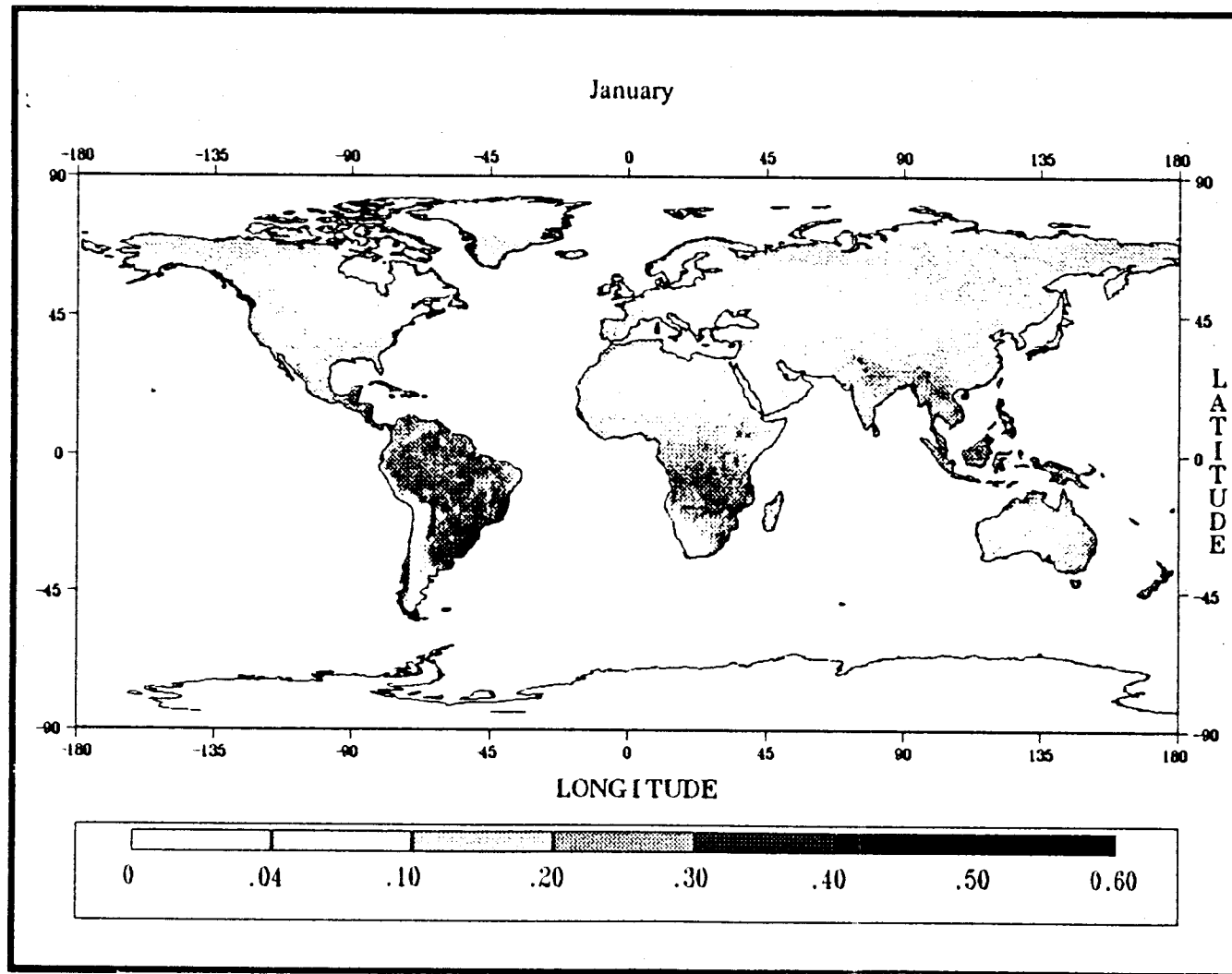


Figure 1. January GVI Image

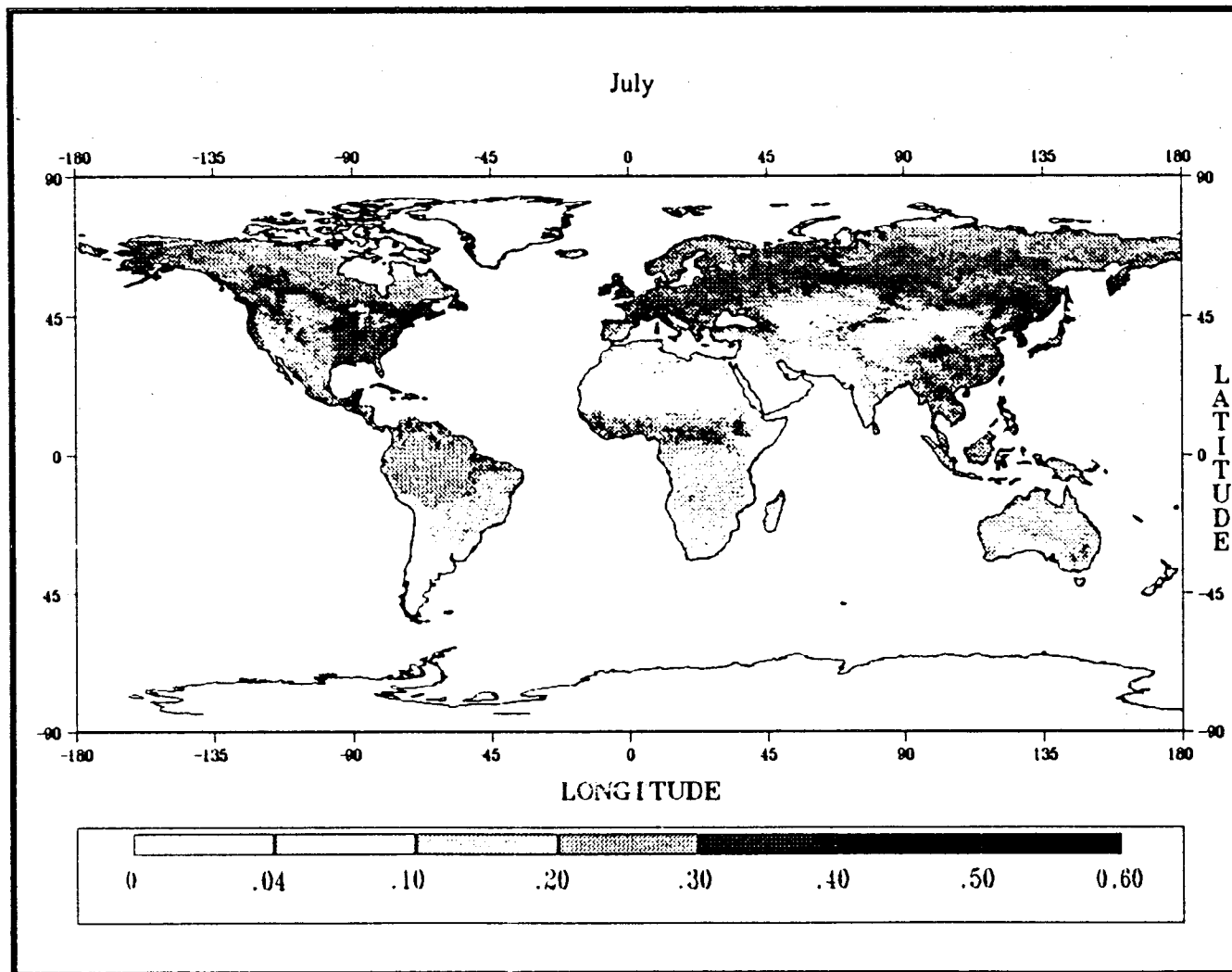


Figure 2. July GVI Image



used. Measurements of FBD for large scale biomes were found in Box (1981) Cannell (1982), and Webb *et al.* 1983. The data found in these sources supplied the maxima and minima of FBD for large scale biomes. This range represents spatial heterogeneity expected of FBD in the biome at peak growth periods.

### Approach

The approach taken to model the spatiotemporal patterns of FBD for one year was to scale the range of FBD values to the range of GVI per biome defined with the Olson map. A general equation of empirical relationships which describes NDVI in terms of FBD exist based on regression analyses. There was a similarity amongst the individual empirical relationships for different vegetation types which confirms the reliability of NDVI for different vegetation types over time. The following discussion details the methodology of this approach.

Empirical relationships between AVHRR NDVI and FBD or LAI exist (for examples see: Tucker *et al.* 1983, Asrar *et al.* 1984, Wardley and Curran 1984, Tucker *et al.* 1985, Hatfield *et al.* 1985, Running *et al.* 1986, Peterson *et al.* 1987, Running *et al.* 1989, Spanner *et al.* 1990). Because FBD and LAI appear spectrally similar in the red and NIR bandwidths, they will also appear similar in the NDVI ratio, and therefore, a regression analysis between FBD, LAI and NDVI will also be quite similar. Regression analysis of both FBD and LAI in grasslands and conifer forests display similar response curves (figures 3 - 4).

They also have identical equations with different empirical constants (Tucker *et al.* 1983, Running *et al.* 1989). Representing the empirical constants with the variables  $a$  and  $b$ , the similarities become more apparent (equations 2a and 2b).

Tucker's model equation (see figure 3):

$$Y = a \ln X - b \tag{2a}$$

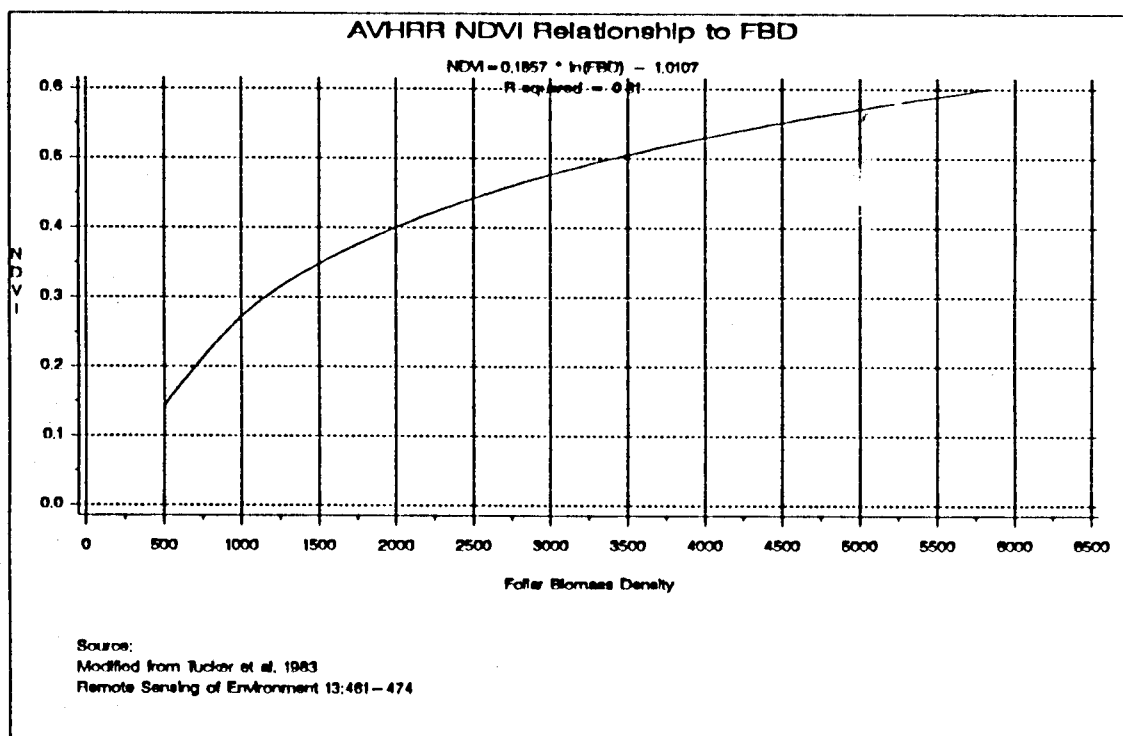


**Figure 3.** Statistical relationship between AVHRR NDVI and the foliar biomass of grasslands. Modified from Tucker *et al.* (1983).

Running's model equation (see figure 4):

$$Y = a \ln \frac{X}{b} \quad (2b)$$

where:

$$Y = NDVI$$

$$X = FBD$$

$a, b$  = empirical constants.

Comparing the two models,  $a$  remains the same while  $b$  is negative in Tucker's model and a negative  $\ln$  in Running's model. This implies that different vegetation types have a similar response curve relating AVHRR NDVI to the similar biophysical variables; FBD and LAI. Further, the equation defining the response curve

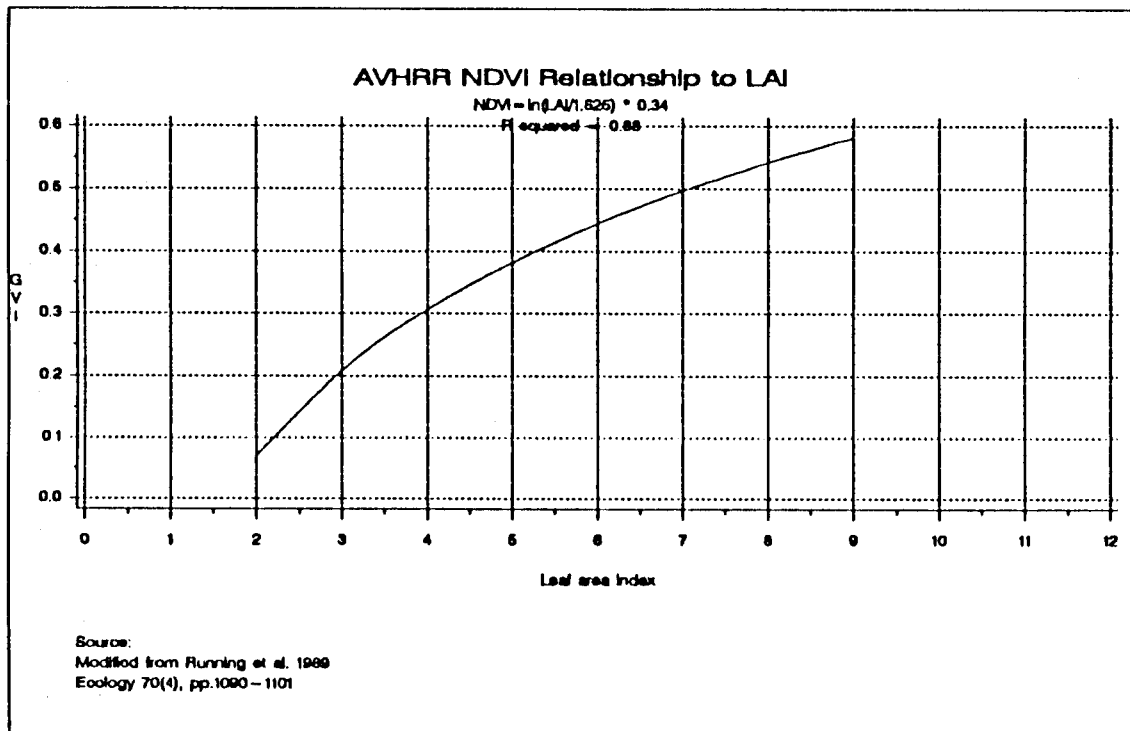


**Figure 4.** Statistical relationship between AVHRR NDVI and LAI of Coniferous forests. Modified from Running and Nemani (1988).

remains the same while the values for  $a$  and  $b$  change. This phenomena suggests that the mathematical equation describing the response curves remains the same for FBD of different vegetation types. The empirical constants, however, will change and may be thought of as variables in this case. Since the general form of the model equation remains constant, the equation may be manipulated to estimate FBD based on the AVHRR NDVI ratio, or GVI. Therefore, derivation of  $a$  and  $b$  based upon GVI will provide unique relationships between FBD and GVI for different vegetation types.

The model presented here is constructed by using the general form of these of equations which, for simplicity, is taken to be equation (2b). Inverting equation (2b), the FBD variable becomes dependent, or in other words, it may be predicted

(equation 3).

$$X = a \exp \frac{Y}{b} \quad (3)$$

where:

$$Y = \text{NDVI}$$

$$X = \text{FBD}$$

$a, b$  = biome specific constants.

As previously discussed, the range of FBD per vegetation type supplies only the maxima and minima to which the GVI data can be scaled. Derivation of the biome specific constants must be calculated to define the parameters of the model on a per vegetation type (biome) basis. Two new equations derived from equation 2 describe the biome specific constants in terms of both the biomass and GVI minima and maxima (equations 4a and 4b), respectively.

$$F_{min} = a \exp \frac{N_{min}}{b} \quad (4a)$$

$$F_{max} = a \exp \frac{N_{max}}{b} \quad (4b)$$

where:

$F_{min}$  = FBD minimum value per biome

$F_{max}$  = FBD maximum value per biome

$N_{min}$  = GVI minimum value per biome

$N_{max}$  = GVI maximum value per biome

$a, b$  = biome specific constants.

In order to solve for the biome specific constants  $a$  and  $b$  equations 4a and 4b can be simultaneously solved to create equations 5a and 5b.

$$b = \frac{N_{max} - N_{min}}{\ln ( F_{max} / F_{min} )} \quad (5a)$$

$$a = F_{max} \exp \frac{-N_{max}}{b} \quad (5b)$$

See appendix B for full the solution and appendix C for the biome specific parameters and constants. The model is now calibrated and can be driven by the monthly GVI images to create monthly FBD surfaces.

### Methods

The components of the model are now complete. The seasonal variation and the vegetation types will be stratified, the literature values of FBD will be used to parameterize the model, and the range of GVI values will be used to estimate the spatial heterogeneity of FBD by applying equation 3 on a per biome basis. The first step, however, is to equate the biomes described in the literature to the Olson classification. The Olson classification defines fifty-four categories which were aggregated into eighteen categories representing the literature biomes (Table 2).

The range of FBD in the literature describes the spatial heterogeneity one may find under normal peak growing conditions (see Chapter 2). Because GVI is positively related to FBD, the monthly image with the highest GVI values for each biome can be used to represent the time of peak growth. The month with the maximum mean value for each biome was used to represent the highest GVI values. These months were established by tracking the monthly distributions of GVI for the year (figure 5). These maximum mean data sets for each biome provided the range of GVI values to calibrate the model with the FBD values.

**Table 2.** The first aggregation scheme based solely on literature descriptions of vegetation type. The second column displays the number of Olson categories which were aggregated into the global areal extents shown in the last column.

First Aggregation of Olson Categories and their Areal Extent			
Aggregated Category Names	Olson Cats. used	Areal Extent in km <sup>2</sup>	Percent Area *
Water; no data	1	32,366,200	0.00
Ice	2	1,247,000	1.96
Desert	6	18,406,600	11.97
Tundra	4	10,057,700	13.96
South Temperate BLF	1	714,800	0.51
Grassland	3	21,356,200	14.16
Farms/Towns	2	12,260,700	8.69
Nonpaddy Irrigated Dryland	3	1,579,000	1.07
Forest/Fields/Woods	4	9,196,300	6.60
North Temperate BLF	1	786,900	0.64
Cool Conifer Hardwood	2	3,550,900	2.70
Tropical Montane	1	1,175,400	0.66
Wetlands/Hinterlands/Shore	7	3,578,700	2.60
Woodlands	6	19,902,500	11.62
Warm Conifer	1	399,200	0.28
Paddyland	1	1,994,100	1.19
Taiga	5	11,489,500	12.94
Trop. Seasonal Humid BLF	1	6,173,800	3.47
Trop/Subt Humid BLF	2	4,237,200	2.34
Cool Conifer	1	3,102,100	2.63
Total		454,871,000	100.00

\* The water class was excluded from the percentage calculations.

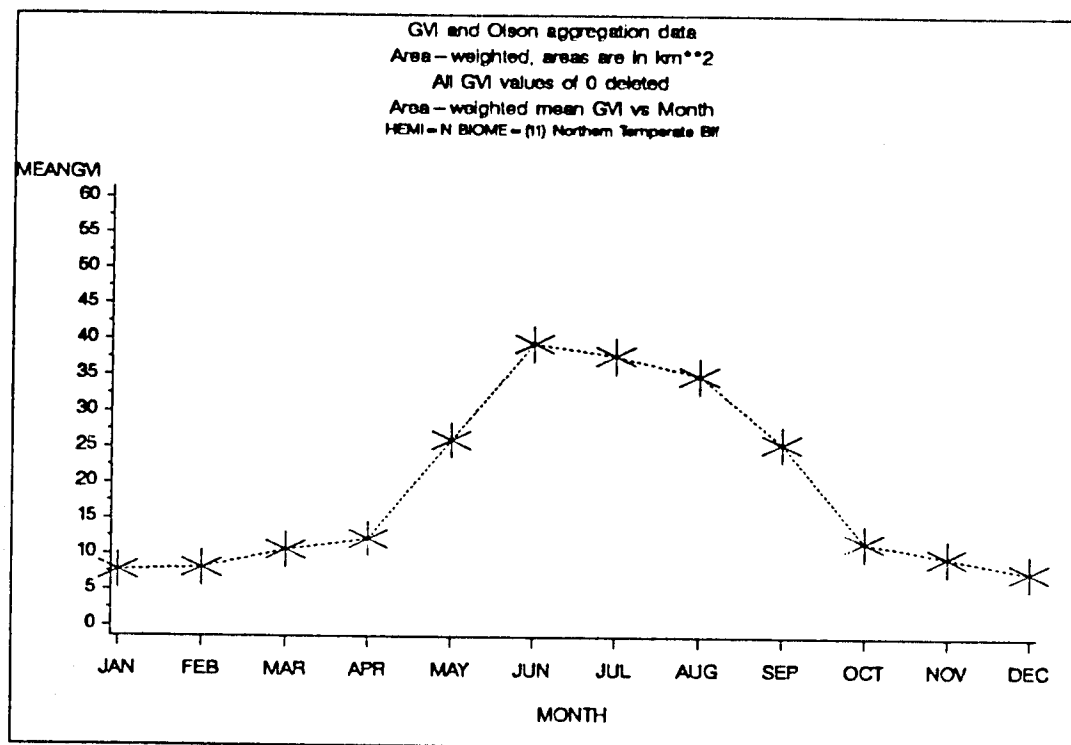


**Figure 5.** The temporal profile of GVI for the Northern Temperate Broadleaf Forest. (see appendix D for the temporal profiles of all the biomes.)

The possibility exists, however, that two or more of Olsons original vegetation types may have been classified as one due to descriptive ambiguity of the definitions for the vegetation types. These categories were digitally analyzed to determine if the classification agreed with a spectral classification using GVI. Histograms of GVI were produced for the fifty-four original Olson categories and the aggregate biomes (Table 2). These distributions of GVI were used to examine the original classifications and the aggregates. If the distribution of GVI is clearly bimodal in the aggregations then the possibility exists that there are two spectrally distinct vegetation types as defined by the original Olson classification.

Bimodality was noticed for the woodlands (figure 6), grasslands, and the desert biomes suggesting the aggregation scheme incorporated dissimilar biomes.

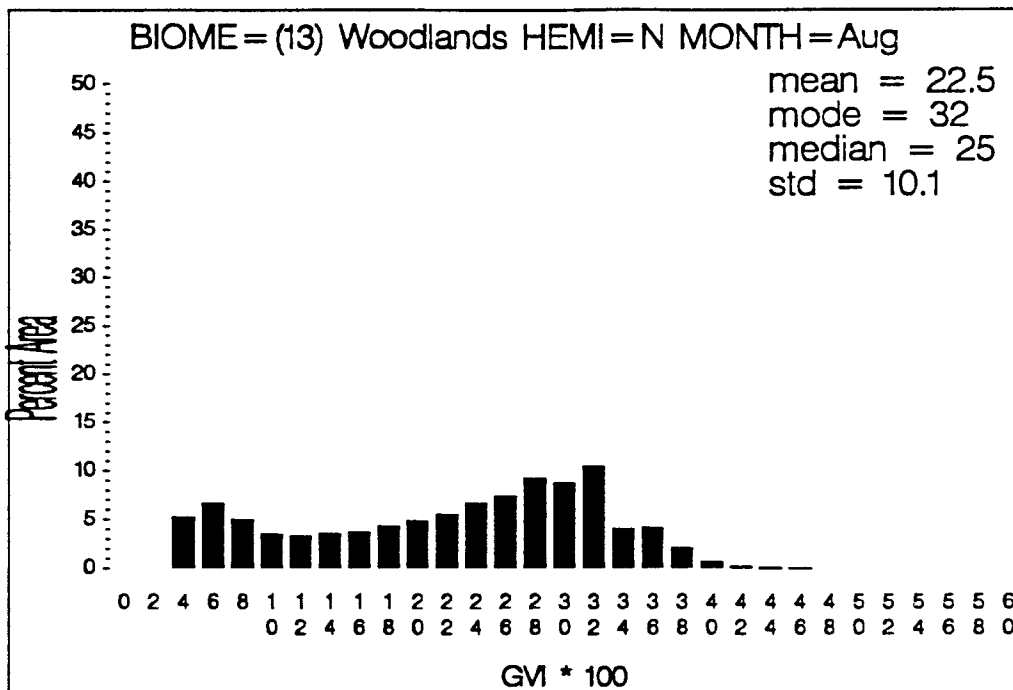


**Figure 6.** The histogram for the Woodlands biome displaying the bimodality associated two distinct spectral signatures.

Checking these aggregates where bimodality occurred against histograms of the original Olson biomes, two distinct groups could be separated representing each mode (figures 7a-b and figures 8a-d).



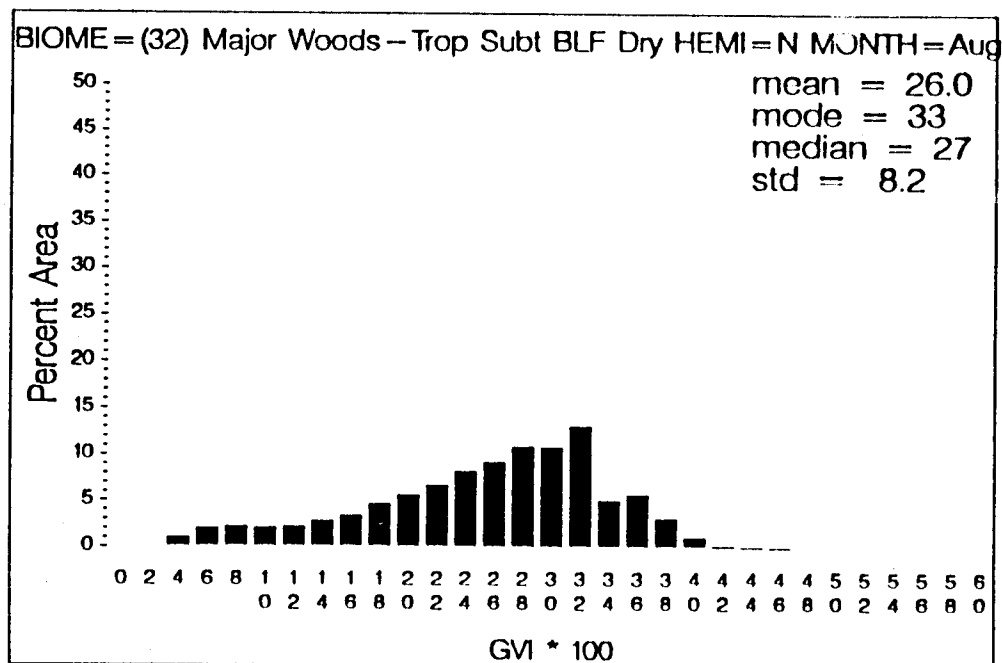


Figure 7a. Olson biome number 32, skewed left with a mean of 26.0.

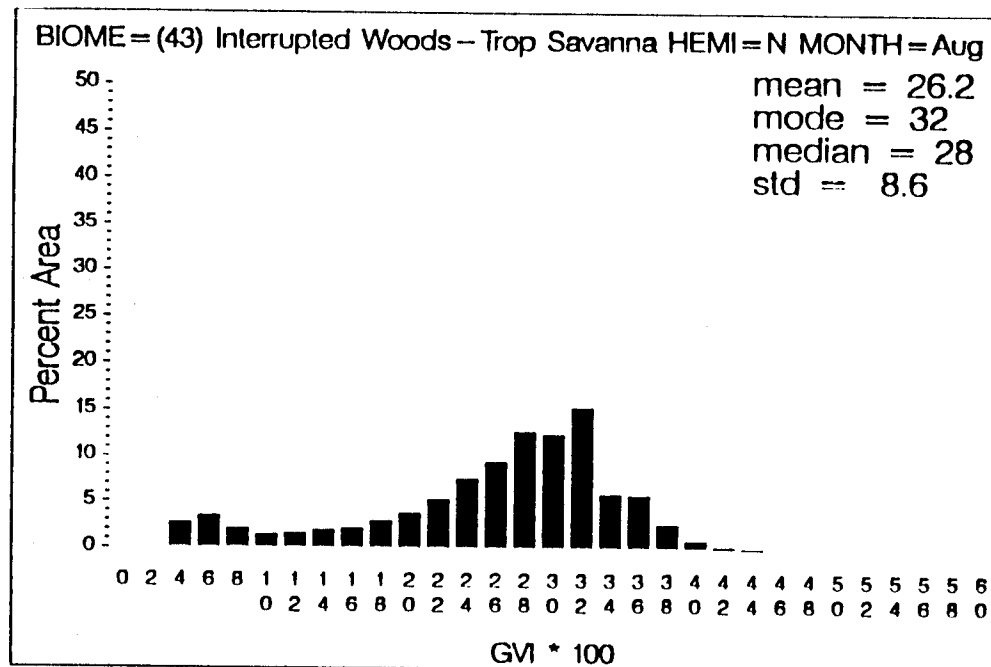


Figure 7b. Olson biome number 43, skewed left with a mean of 26.2.

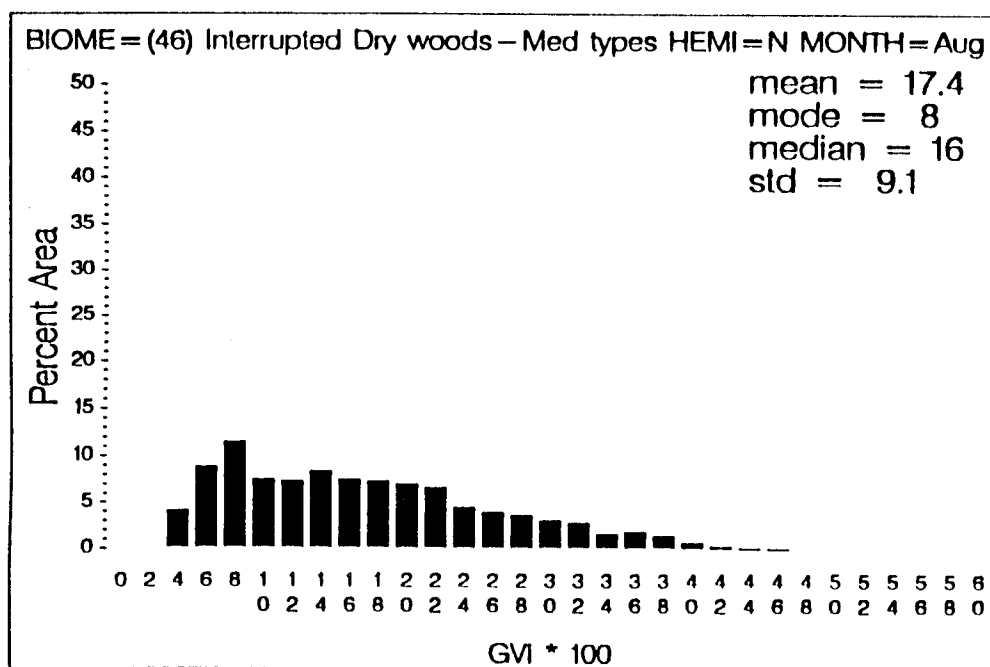


Figure 8a. Olson biome number 46, skewed right with a mean of 17.4.

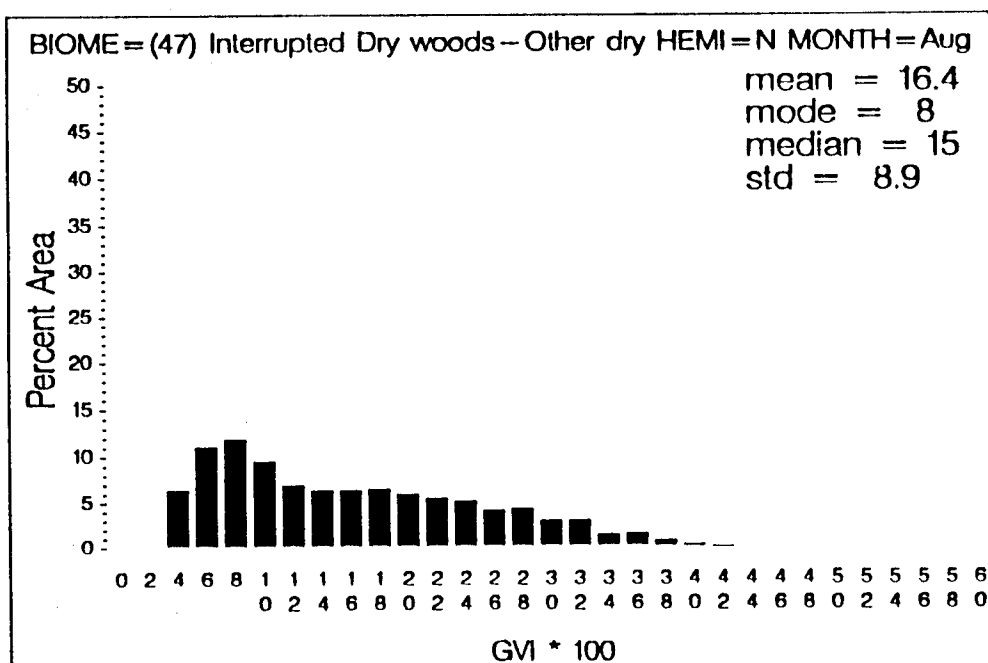


Figure 8b. Olson biome number 47, skewed right with a mean of 16.4.

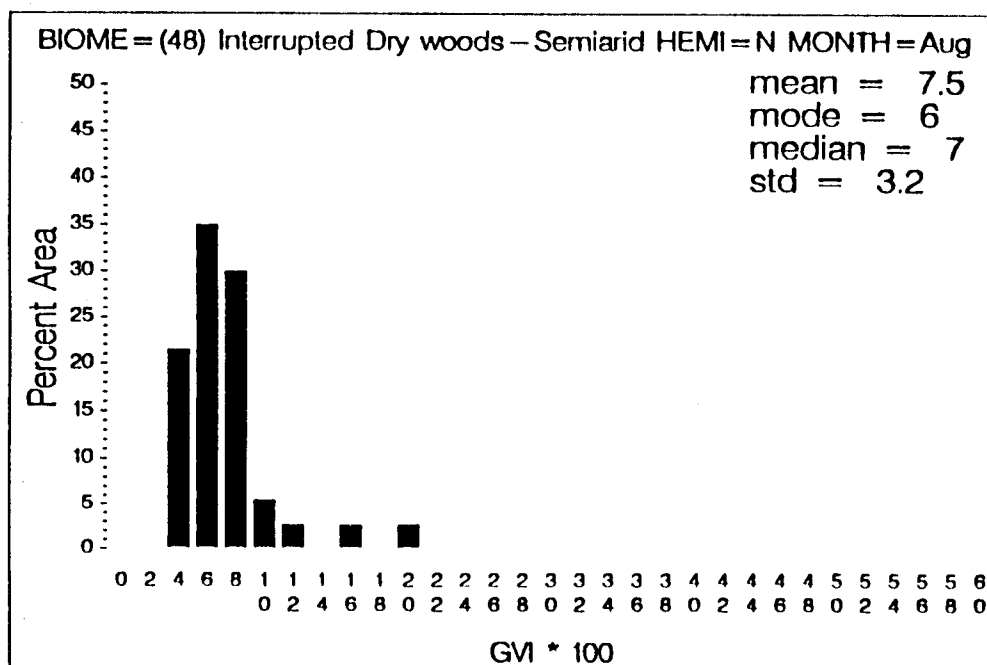


Figure 8c. Olson biome number 48, skewed right with a mean of 7.5.

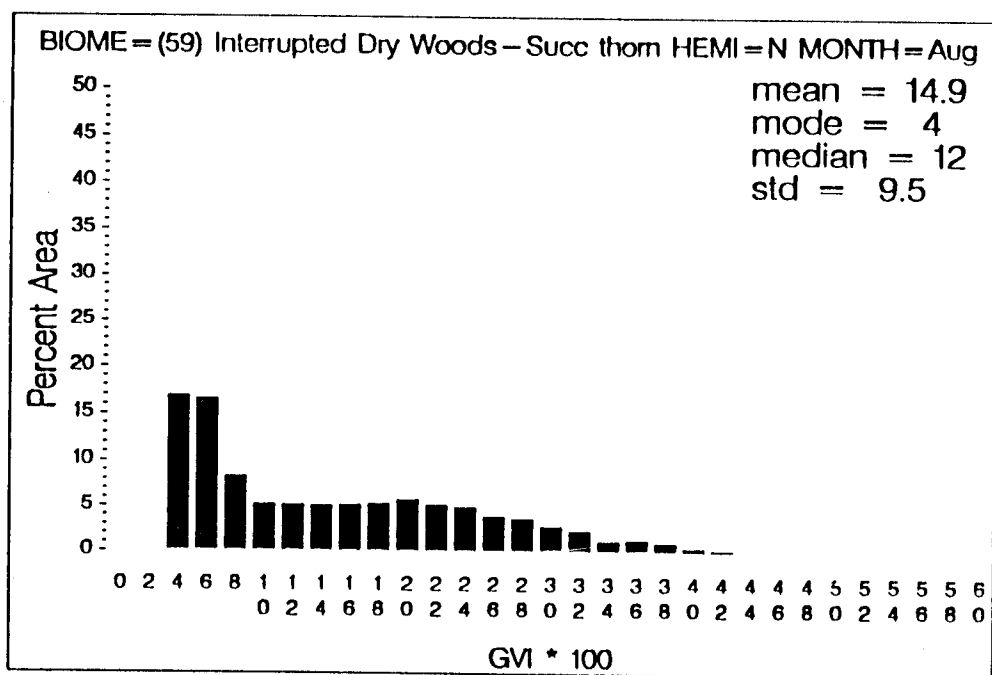


Figure 8d. Olson biome number 59, skewed right with a mean of 14.9.

The same analysis separated the grassland and desert biomes into two new distinct classes as well. These new groups were then added to the aggregation scheme

resulting in the new aggregates (Table 3).

**Table 3 .** The second aggregation scheme based on the analysis of GVI histograms. The second column displays the number of Olson categories which were aggregated.

Second Aggregation of Olson Categories and their Areal Extent			
Aggregated Category Names	Olson Cats. used	Areal Extent in km <sup>2</sup>	Percent Area *
Water; no data	1	32,366,200	0.00
Ice	2	1,247,000	2.00
Nonpolar Desert	4	2,252,700	1.93
Polar Desert	2	16,153,900	10.30
Tundra	4	10,057,700	12.14
South Temperate BLF	1	714,800	0.52
Grassland	2	4,084,200	3.41
Shrubland	1	17,272,000	11.06
Farms/Towns	2	12,260,700	8.87
Nonpaddy Irrigated Dryland	3	1,579,000	1.09
Forest/Fields/Woods	4	9,196,300	6.73
North Temperate BLF	1	786,900	0.66
Cool Conifer Hardwood	2	3,550,900	2.76
Tropical Montane	1	1,175,400	0.68
Wetlands/Hinterlands/Shore	7	3,578,700	2.66
Dry Forest and Woodlands	2	11,427,500	6.59
Semi-arid Woodlands	4	8,474,900	5.28
Warm Conifer	1	399,200	0.29
Paddyland	1	1,994,100	1.22
Taiga	5	11,489,500	13.22
Trop. Seasonal Humid BLF	1	6,173,800	3.54
Trop/Subt Humid BLF	2	4,237,200	2.39
Cool Conifer	1	3,102,100	2.69
Total		454,871,000	100.00

\* The water class was excluded from the percentage calculations.

The aggregated version of Olson vegetation types was then used to group the GVI data into unique spatial categories corresponding to the biomes of the literature.

These biomes were then stratified into global categories (e.g. Northern Hemisphere, Southern Hemisphere, or the Tropics) that represent distinct seasonal variation within each geographic area. The areal extents, by percentage, of biomes in the northern hemisphere and in the Tropics were used to determine in which category the majority of the biome occurred (Table 4). The area where the majority

of the biome occurred was used to calibrate the model by extracting the range of GVI values from inside the geographic constraints of these global categories.

**Table 4** . Percentage of biome located in global categories of unique seasonal variations.

Percentage of Biome in the Tropics, Northern, and Southern Hemisphere			
Aggregated Category Names	Tropics	Northern Hemi.	Southern Hemi.
Nonpolar Desert	1.8	66	32.2
Polar Desert	35.7	54.5	0.8
Tundra	1.1	60.1	38.8
Southern Temperate BLF	0.0	57.7	42.3
Grassland	0.0	96.7	3.3
Shrubland	42.4	42.8	14.8
Farms/Towns	25.7	63.8	10.5
Nonpaddy Irrigated Dryland	19.8	68.6	11.6
Forest/Fields/Woods	25.3	64.9	9.8
Northern Temperate BLF	0.0	93.8	6.2
Cool Conifer Hardwood	10.9	82.0	7.1
Tropical Montane	91.2	8.8	0.0
Wetlands/Hinterlands/Shore	42.8	45.6	11.6
Dry Forest and Woodlands	97.1	1.4	1.5
Semi-arid Woodlands	47.1	18.7	34.2
Warm Conifer	5.2	92.3	2.5
Paddyland	51.4	48.2	0.4
Taiga	0.0	100	0.0
Trop. Seasonal Humid BLF	94.6	2.9	2.5
Trop-Subt Humid BLF	99.7	0.3	0.0
Cool Conifer	0.0	100	0.0

For example, 96.7% of the grassland biome is present in the northern hemisphere, therefore, all the GVI data extracted to characterize grasslands was taken from the northern hemisphere. The stratification allows for a more realistic characterization of seasonal variation rather than arbitrarily dividing the biome at the equator and analyzing two different data sets. The biomes are now geographically restricted to one of the global categories for the rest of the calibration procedure.

Again the mean of the GVI values per biome, along with the fifth and ninety-fifth percentile, were tracked by month for the year to determine the peak growth period. The fifth and ninety-fifth percentiles were chosen to represent the entire range of GVI to remove any noise associated with the two distinct boundaries caused by the resolution differences between the Olson map and the GVI imagery

(Table 5).

**Table 5.** The biomes with ranges of GVI values used to calibrate the model. Also, the global category in which the range occurred is shown as well as the maximum mean GVI value and the month when the maximum mean occurred.

Biome	Global Category	Month of Max. Mean	Maximum Mean	5 <sup>th</sup> %ile	95 <sup>th</sup> %ile
Nonpolar Desert	North	Jun	19.5069	5	36
Polar Desert	North	Mar	8.0313	4	12
Tundra	North	Jul	21.5753	6	38
Southern TemperateBlf	North	Jun	31.1673	8	46
Grassland	North	Jul	26.1649	10	43
Shrubland	North	Aug	17.0670	4	35
Farms/Towns	North	Jul	27.6886	9	42
Nonpaddy Irrigated Dryland	North	Aug	19.4412	4	37
Forest/Fields/Woods	North	Jun	32.5523	11	46
Northern Temperate Blf	North	Jun	39.5085	20	50
Cool Conifer Hardwood	North	Jun	32.2999	11	46
Tropical Montane	Tropic	Nov	32.0610	15	45
Wetlands	North	Jul	27.7999	7	42
DryForest and Woodland	Tropic	Nov	25.7458	10	42
Semi-arid Woodland	South	Jan	19.5504	8	36
Warm Conifer	North	Jun	29.7677	14	41
Paddyland	North	Jul	26.4018	10	38
Taiga	North	Jul	29.3820	20	40
Trop. Seasonal Humid BLF	Tropic	Nov	34.6479	22	45
Trop/subt Humid BLF	Tropic	Dec	34.5576	20	44
Cool Conifer	North	Jul	33.0470	17	45

Ranges of FBD from the literature (Table 6) were then scaled to the GVI by equation 2. See appendix C for the derived constants.

For values of GVI that are greater than the value of the 95<sup>th</sup> percentile, FBD is set to a constant value in order to eliminate anomalous occurrences of exceedingly high GVI values that would convert to exaggerated FBD values. This upper FBD limit was specific for each biome. Using the model equation response curves displaying FBD in terms of GVI were calculated (figure 9).

**Table 6.** The maximum and minimum values for FBD expressed in kg/m<sup>2</sup>.

Biome	Mimimum FBD	Maximum FBD
Nonpolar Desert	0.01	0.05
Polar Desert	0.01	0.10
Tundra	0.01	0.05
Southern Temperate BLF	0.2	0.8
Grassland	0.05	0.5
Shrubland	0.1	0.5
Farm/Town	0.1	0.5
Nonpdy Irrigated Dryland	0.1	0.5
Forest/field/woods	0.1	0.8
Northern Temperate BLF	0.3	0.6
Cool Conifer Hardwood	0.3	1.0
Tropical Montane	0.3	0.7
Wetlands	0.1	0.5
Dry Forest and Woodland	0.1	0.5
Semi-arid Woodlands	0.1	0.3
Warm Conifer	0.1	1.0
Paddyland	0.1	0.5
Taiga	0.3	1.5
Trop Seasonal Humid BLF	0.3	0.8
Trop/subt Humid BLF	0.3	1.3
Cool Conifer	0.5	2.0

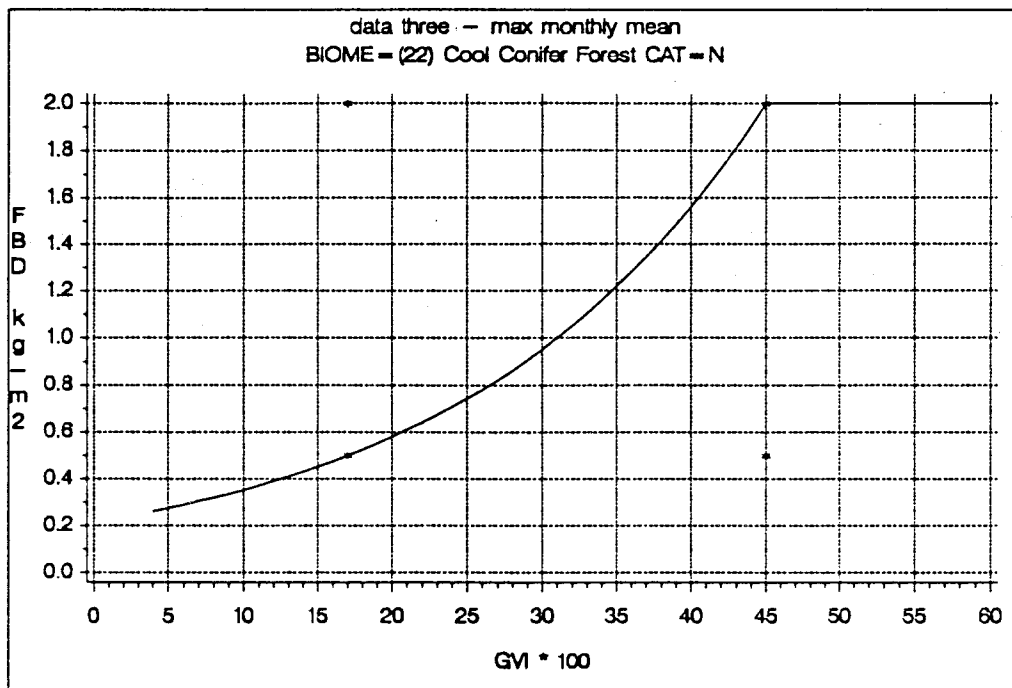


**Figure 9.** The calibration curve for the Cool Conifer biome derived from the literature. See appendix E for all the calibration curves for the biomes.

These biome specific relationships were used to spatially distribute the estimates of FBD for each of the monthly GVI images in the GRASS raster GIS environment. GVI has now been used to estimate FBD values between 75° N and 55° S for the terrestrial biosphere in a monthly time series for twelve months. These FBD surfaces display values from 0 - 2.0 kg/m<sup>2</sup> simulating the seasonal variation of GVI values (Appendix F).



## CHAPTER 4

### Results

#### Results and Discussion

Spatiotemporal patterns of FBD that follow characteristics of seasonal variation can be observed for the terrestrial biosphere. The seasonal variation is clear when comparing the January FBD surface (Figure 10) to the July FBD surface (Figure 11). For example, the northern hemisphere in the January surface is void of any high values of FBD while the southern hemisphere and the Tropics contain the high FBD values. The July surface shows the opposite situation with the equatorial region showing high values again.

The MVC procedure used to make these monthly images highlights a problem caused by solar angles that present a limitation of this procedure. The GVI images during winter in the northern hemisphere, particularly January (Figure 10) have a band of high values in the extreme northern latitudes over the terrestrial biosphere. The solar angles are so low that the optical depth of the atmosphere is increased. The satellite sensor at this point is essentially recording atmospheric reflectance rather than surface reflectance. Applying the MVC procedure retains the highest noise values and creates bogus data in these high latitudes during times of low solar zenith angles. Holben (1986) referred to this phenomena as the terminator effect. Because the GVI data are the NDVI ratio, they cannot be broken apart into the original red and NIR values which could be corrected. This is a limitation of using just the NDVI ratio without having the red and NIR spectral bands to analyze.

The total foliar biomass calculated for the terrestrial biosphere during 1988, considering the discussed limitations, is 47.7 gigatons (Gt). Assuming maximum FBD values per biome a global total for foliar biomass was calculated to be 77.9 Gt. Accounting for the seasonal variation of FBD decreases the yearly global

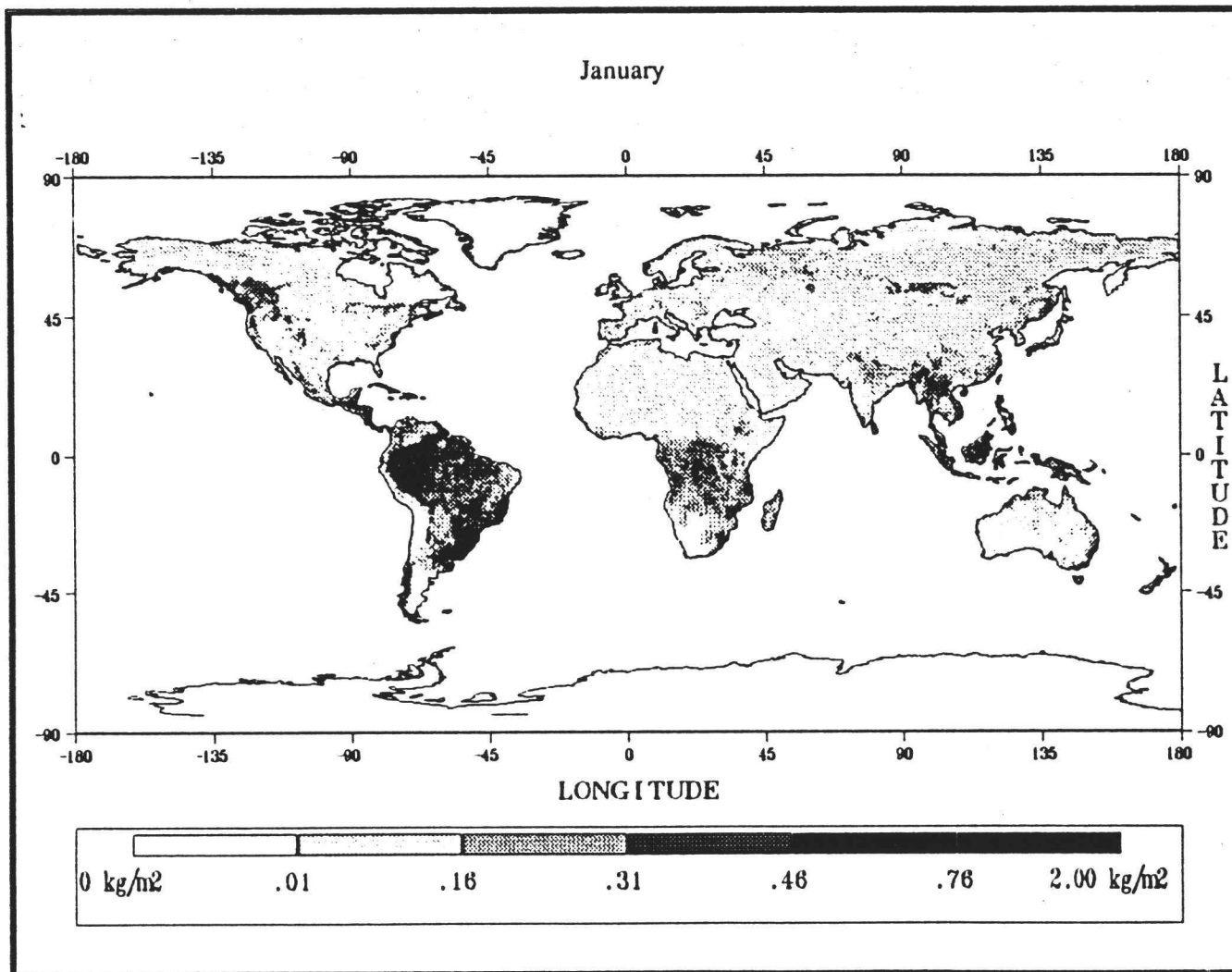


Figure 10. January FBD Surface

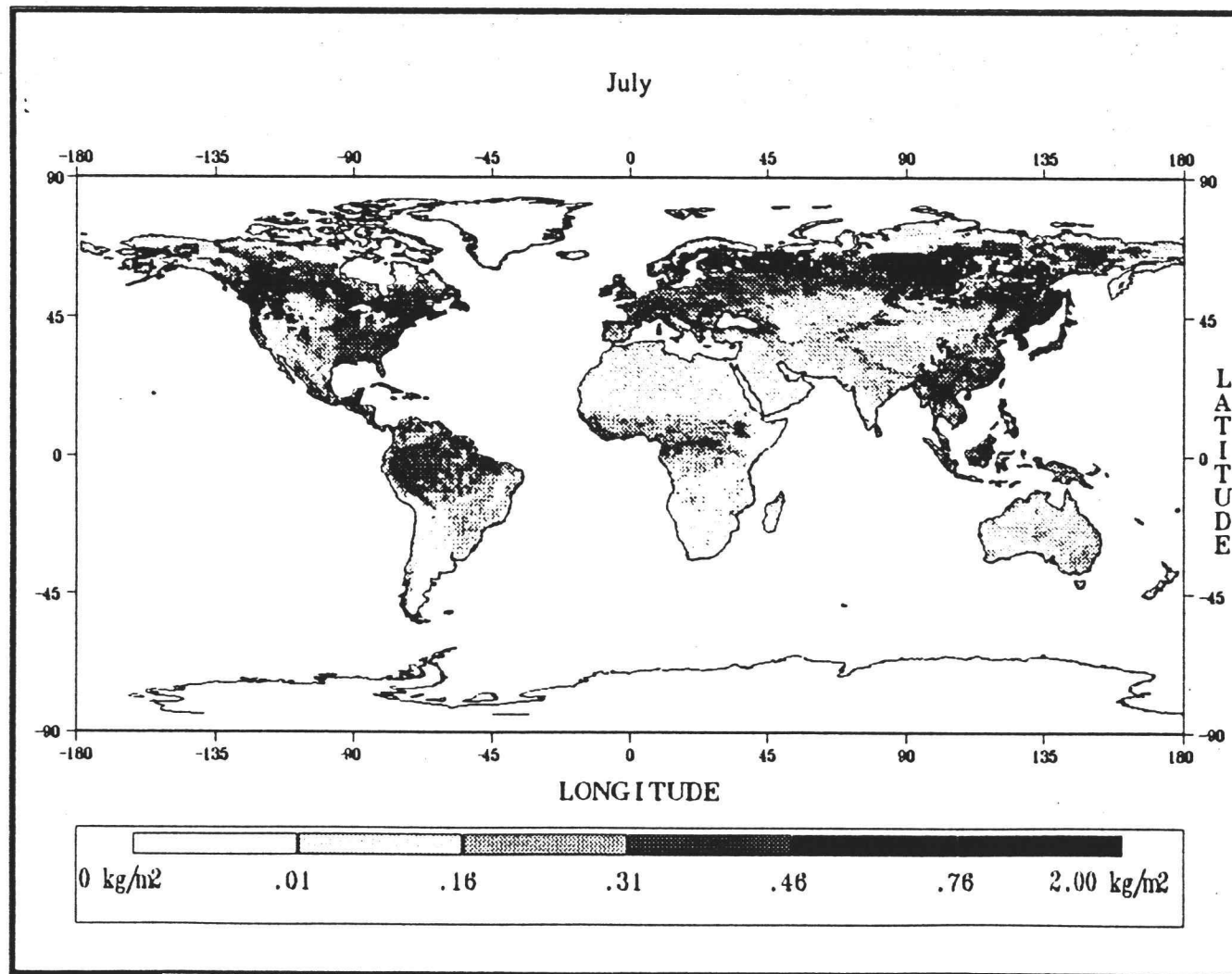


Figure 11. July FBD Surface

estimate for foliar biomass, as expected. The next step is to compare these estimates to other global estimates of foliar biomass for validation. Comparison on a biome specific basis would be advantageous, but the problem of non-comparability of classification schemes would introduce additional uncertainties.

The one global total of foliar biomass found in the literature was 75 Gt (Box, 1981). Lieth and Whittaker (1975) and Whittaker (1975) provided terrestrial biome and global totals of leaf area and chlorophyll. Other sources contained relationships between foliar biomass and leaf area or chlorophyll (using their biome classification scheme). Foliar biomass/area values were determined from data on tropical rain forests (Grubb 1977, Edwards and Grubb 1977, Blasco and Tassy 1975, and Tanner 1977), and temperate deciduous forests, temperate evergreen forest, woodlands, and shrublands (Lieth and Whittaker 1975, Whittaker and Niering 1975, Whittaker and Woodwell 1969, Whittaker *et al.* 1974, Whittaker 1966, Whittaker 1962). The values ranged from 50 tons/km<sup>2</sup> leaf area to 178 tons/km<sup>2</sup> leaf area. A value of 100 tons/km<sup>2</sup> leaf area was taken as representative for forests, woodlands, and shrublands. These values were multiplied by the total leaf area estimates for each biome indicated in the literature to calculate total foliar biomass of 87.5 Gt for the globe (Table 7).

Another comparison involves converting chlorophyll mass to foliar biomass. Foliar biomass conversion factors were used only for forests, woodlands and shrublands. These values ranged from 127 g/g (foliar biomass/chlorophyll mass) to 366 g/g for temperate deciduous forests and woodlands. 250 g/g was taken as representative for these biomes as well as the tropical rain and seasonal forests. A value of 453 g/g (rounded to 450 g/g) was used for the temperate evergreen forest (spruce-fir). These were used to calculate total foliar biomass for the forest biomes (Table 8).

**Table 7.** The total foliar biomass for the globe was calculated by converting LAI into foliar biomass and totalling the leaf biomass of each biome.

Biome	Areal Extent in $\text{km}^2 \times 10^6$	LAI	LAI $\times$ Area in $\text{km}^2 \times 10^6$	Tons/ $\text{km}^2$ Leaf Area	Foliar Biomass Gigatons
Tropical Rain Forest	17.0	8	136	100	13.6
Tropical Seasonal Forest	7.5	5	38	100	3.8
Temperate Evergreen Forest	5.0	12	60	100	6.0
Temperate Deciduous Forest	7.0	5	35	100	3.5
Boreal Forest	12.0	12	144	100	14.4
Woodland/Shrubland	8.5	4	34	100	3.4
Savanna	15.0	4	60	100	6.0
Temperate Grassland	9.0	3.5	32	460	14.7
Tundra and Alpine	8.0	2	16	300	4.8
Desert/Semi-desert	18.0	1	18	100	1.8
Extreme Desert	24.0	0.05	1.2	100	0.1
Cultivated Land	14.0	4	56	250	14.0
Swamp/Marsh	2.0	7	14	100	1.4
Total Foliar Biomass for the Globe					87.5 Gt

**Table 8.** The total foliar biomass for the forest biomes was calculated by multiplying the total chlorophyll per biome by the foliar biomass/chlorophyll mass values.

Biome	Chlorophyll tons $\times 10^6$	Foliar biomass/ Chlor. mass	Foliar biomass Gigatons
Tropical Rain Forest	51.0	250	12.8
Tropical Seasonal Forest	18.8	250	4.7
Temperate Evergreen Forest	17.5	450	7.9
Temperate Deciduous Forest	14.0	250	3.5
Boreal Forest	36.0	450	16.2
Woodland/Shrubland	13.6	250	3.4
Total Foliar Biomass for the Forests			48.5 Gt

The total foliar biomass estimates for these six biomes using the chlorophyll conversion equalled 48.5 Gt, comparing favorably to the total of 34.2 Gt using the leaf area conversions for global total foliar biomass estimates considering the uncertainties associated with the calculations and the potential noncomparability between the biome classifications.

These two comparisons produced similar results. Each estimate using leaf area or chlorophyll conversion is higher than the estimates produced in this research. Nevertheless, considering the uncertainties associated with conversion estimates and that the estimates from both conversion calculations and the model estimates are of the same order of magnitude, the results are considered satisfactory.

In the final validation procedure, the grassland biome described in this study is compared to a regional analysis of the Senegalese Sahel grassland described by Tucker *et al.* (1983) and Tucker *et al.* (1986). The grassland biome presented in this study was isolated for this analysis. Tucker's model (equation 6) was run using the GVI data for the grassland biome and compared to the grassland model derived in this analysis (equation 7).

$$FBD = \exp \frac{GVI + 1.0107}{0.1857} \quad (6)$$

$$FBD = 0.2485 \exp \frac{GVI * 100}{14.3317} \quad (7)$$

GRASS raster (cell) format requires integers, therefore, the GVI data in equation 2 is multiplied by 100. (Consult Appendix C to see all the derived biome specific coefficients.)

It is not possible to compare both models within the geographic confines of Tucker's study area. Tucker describes his study area as grassland while the aggregated Olson classification used in this analysis describes this same geographic area as 15% Farms/Towns, 26% Nonpaddy Irrigated Dryland, and 59% Dry Forest and Woodlands.

However, it is possible to apply Tucker's model to the entire grassland biome described by Olson for comparison. The resulting estimated range of Tucker's

model as applied to the grassland biome is  $.02 - 0.58 \text{ kg/m}^2$  while the range taken from the literature for this analysis was  $.05 - 0.5 \text{ kg/m}^2$ . Running Tucker's model at the same monthly time step produces a global grassland estimate of 0.528 Gt of FBD for 1988, while this model estimates 0.947 Gt of FBD in 1988.

It appears, however, that this model overestimates grassland with the GVI data. One explanation is that the entire grassland biome which this model is based on, likely has different characteristics than the geographically restricted grasslands of the Senegalese Sahel. This would result in different empirical constants creating the different results. Another explanation is that the grassland that is described by Tucker is really what Olson would call Dry Woodland and Forest. Either of these explanations would account for differences in the results. Considering the limitations of these comparison, it is difficult to say whether the model developed in this research overestimates or underestimates foliar biomass. Nevertheless, the results of this model were always of the same order of magnitude with the validation estimates, lending credence to its validity.

The results of the statistical analysis to isolate biomes of similar seasonal variations are presented. As previously discussed, the tropical biomes were determined by the majority of their areal extent with respect to their geographic locations. Nevertheless, the descriptive statistics of the monthly GVI data sets concerning the tropical biomes, as defined in this study, were also used to determine and justify which biomes should be considered tropical (Table 9).

Comparing the months of maximum mean GVI and the coefficient of variation it is clear that these biomes were similar before being combined into the tropical category. For example, the Tropical Montane biome has months of maximum mean and coefficient of variation for the northern and southern hemisphere of, November, 0.283, and November, 0.303, respectively. When combined into the

**Table 9** . This table displays some descriptive statistics in order to quantitatively compare the global categories of seasonal variation of GVI data within the tropical biomes.

Monthly GVI Data Sets						
Descriptive Statistics of Tropical Biomes by Hemispheres						
Biome	Global Category	Month of Max. Mean	Coefficient of Variation	5th %ile	95th %ile	Median GVI
Trop. Montane	North	November	0.283	15	44	36
Trop. Montane	South	November	0.303	13	46	32
Dry Forest/Wdld	North	August	0.324	7	37	26
Dry Forest/Wdld	South	December	0.318	12	44	32
Trop. Seas. Frst	North	November	0.183	24	44	36
Trop. Seas. Frst	South	December	0.198	22	45	36
Trop/Subt. Frst	North	December	0.224	19	43	35
Trop/Subt. Frst	South	December	0.197	22	44	37
Descriptive Statistics of Tropical Biomes by Tropics						
Biome	Global Category	Month of Max. Mean	Coefficient of Variation	5th %ile	95th %ile	Median
Trop. Montane	Tropic	November	0.293	15	45	33
Dry Forest/Wdld	Tropic	November	0.375	10	42	26
Trop. Seas. Frst	Tropic	November	0.205	22	45	36
Trop/Subt. Frst	Tropic	November	0.209	20	44	36

tropic category the month of maximum mean and the coefficient of variation are November and 0.293, respectively. This similarity of all the tropical biomes is an indication that the arbitrary north-south division is not necessary, and perhaps wrong. The Dry Forest and Woodland biome displays the greatest variance because it is located in higher latitudes of the tropics.

### Sensitivity Analysis

A sensitivity analysis was performed to characterize the sensitivity of the model to the maximum and minimum estimates of FBD found in the literature. To assess the sensitivity of global estimates of foliar biomass, the biome specific FBD values were arbitrarily changed by  $\pm 10\%$  around the minima and maxima (Table 10). For each one of the four deviations about the maxima and minima, new coefficients were derived to run the model. Global totals of foliar biomass were



calculated to compare the magnitude of change associated with each of these deviations (Table 11).

Clearly, movement about the maxima has the greatest effect on overall quantities of estimated FBD. A 20% change in the maxima causes about 7 Gt difference to be estimated while the minima causes approximately 2 Gt of change. The 5.54% change of foliar biomass associated with +10% maxima shown in table 11 would be greater if the maximum values of estimated FBD were not held constant to the maximum limit defined by the 95<sup>th</sup> percentile GVI value on a per biome basis (Figure 9).

**Table 10.** The estimates of FBD per biome are shown with a  $\pm 10\%$  deviation from the minima and maxima. These percentages in FBD are used to characterize the potential of error in the estimates of FBD presented in this research.

Ten Percent Change About the Minima and Maxima Foliar Biomass Estimates						
Biome	Minima kg/m <sup>2</sup>	-10% kg/m <sup>2</sup>	+10% kg/m <sup>2</sup>	Maxima kg/m <sup>2</sup>	-10% kg/m <sup>2</sup>	+10% kg/m <sup>2</sup>
Nonpolar Desert	.01	.009	.011	.05	.045	.055
Polar Desert	.01	.009	.011	.10	.09	.11
Tundra	.01	.009	.011	.05	.045	.055
South Temperate BLF	.2	.18	.22	.8	.72	.88
Grassland	.05	.045	.055	.5	.45	.55
Shrubland	.1	.09	.11	.5	.45	.55
Farms/Towns	.1	.09	.11	.5	.45	.55
Nonpaddy Irrigated Dryland	.1	.09	.11	.5	.45	.55
Forest/Fields/Woods	.1	.09	.11	.8	.72	.88
North Temperate BLF	.3	.27	.33	.6	.54	.66
Cool Conifer Hardwood	.3	.27	.33	1.0	.9	1.1
Tropical Montane	.3	.27	.33	.7	.63	.77
Wetlands/Hinterlands/Shore	.1	.09	.11	.5	.45	.55
Dry Forest and Woodlands	.1	.09	.11	.5	.45	.55
Semi-Arid Woodlands	.1	.09	.11	.3	.27	.33
Warm Conifer	.1	.09	.11	1.0	.9	1.1
Paddyland	.1	.09	.11	.5	.45	.55
Taiga	.3	.27	.33	1.5	1.35	1.65
Trop seas Humid BLF	.3	.27	.33	.8	.72	.88
Trop/subt Humid BLF	.3	.27	.33	1.3	1.17	1.43
Cool Conifer	.5	.45	.55	2.0	1.8	2.2

**Table 11** . This table displays a 10% movement around the maxima and minima FBD estimates found in the literature. The estimated global totals are shown each 10% change in maxima and minima as well as the percent change.

Change in Global Quantities of Estimated FBD		
% Change of Foliar Biomass	Foliar Biomass in Gigatons	% Change in Total Foliar Biomass
Estimated Foliar Biomass	47.7	0
Maxima +10%	50.5	5.54
Maxima -10%	43.7	8.39
Minima +10%	48.8	2.86
Minima -10%	46.4	2.72

## CHAPTER 5

### Conclusions

This study represents a first attempt to model the seasonal variation of FBD across the terrestrial biosphere by quantitatively using global satellite data and other global vegetation data. The approach has proven useful to capture the gross spatiotemporal patterns of the distribution of photosynthetically active FBD. The seasonal variation of GVI was shown to adequately estimate the seasonal variation of FBD. The model estimates of FBD were sufficient when compared to other estimates of global totals of FBD considering uncertainties involved with both estimates.

The GVI data does, however, have these limitations as presented by Singh (1988a), Singh (1988b), and Holben (1986). It is suspected that the addition of snow in the winter months also has a strong effect on the NDVI ratio by decreasing the GVI values for conifer forests where such a drastic decrease is not expected (Appendix D).

The division of the Earth into three unique zones of seasonal variation was shown to be acceptable. The Northern and Southern Hemispheres were obviously different, but the Tropics were shown to present their own seasonal variation. The tropical biomes showed little seasonal variation. This can be seen by looking at the annual time course for the tropical biomes where GVI data and estimated FBD remained relatively stable. (see appendix G and H for monthly distributions of GVI and FBD, respectively.) The arbitrary equatorial division through the tropical biomes was statistically shown to be unnecessary and perhaps wrong. Therefore, the equatorial region should not be divided at the equator and, further, the region between 23°N and 23°S should be isolated for analysis of seasonal variation. Also, the Northern and Southern Hemispheres should start at 23°N and 23°S,

respectively, and extend to the poles for analysis of seasonal variation. This provides three global bands described by latitude that represent three unique zones of seasonal variation.

The biggest limitation in this approach is the model itself because the model depends upon scarce data. not the quantitative use of the imagery, but instead the data on spatial heterogeneity for FBD and on the global vegetation maps. After scanning the literature for spatial FBD data only the sources documented in this manuscript were consulted. Other sources were inappropriate or not available, indicating an extremely low availability of this kind of vegetation data. Because there is such a scarcity of global vegetation data, this model was calibrated with these data, and as a result a high amount of faith was placed in their validity. With the upcoming EOS platforms researchers may better relationships between biophysical variables and the remotely sensed data. But unless there is future research undertaken to establish ranges of FBD, LAI, and other variables and uncertainty associated with these ranges, quantitative estimates of biophysical variables may not drastically improve.

A sensitivity analysis was performed on the FBD parameters taken from the literature in light of the high amount of faith placed in the accuracy of these FBD ranges. The potential error was characterized in percentages and can be used as a guide to assess the effect that error may have upon the global totals of FBD that were estimated by this model.

In the interest of global climate change and tropospheric chemistry, the FBD surfaces were used as variables in a biogenic gas emissions model. The results of this research used as an input for an isoprene model yielded favorable results (Turner *et al.*, submitted). The results are also being input into a water balance model and a carbon flux model (Marks, submitted, and Gucinski, submitted).

There is a need to refine the relationships between the satellite data and FBD, as well as other biophysical variables. The new EOS platforms will provide much improved data over present systems that will not only provide better relationships for biophysical variables but will demand that the scientific community clearly understand concepts associated with all aspects of remote sensing.

To go beyond empirical relationships based on satellite vegetation indices to physical relationships based on radiative properties of vegetation is a highly desirable research priority that would enhance the quantitative application of satellite data. Ongoing remote sensing experiments such as FIFE, HAPEX-MOBLY, and BOREAS may help to establish a more physiologically based model. The more physiologically based a model becomes the less dependent the model becomes on vegetation maps and other vegetation data. This is highly desirable for global and regional remote sensing studies of vegetation where, as previously discussed, there is a scarcity of physiological data to couple with the remote sensing data, because one may not have to couple physiological data with remote sensing data.

## REFERENCES

- Berger, A., R. E. Dickinson, and J. W. Kidson, *Understanding Climate Change*, 187 pp., American Geophysical Union, Washington, D.C., 1989.
- Box, E. O., Foliar biomass: Data base of the international biological program and other sources, in *Atmospheric Biogenic Hydrocarbons*, edited by J. J. Bufalini and R. R. Arnst, vol. 1, pp. 121-148, Ann Arbor Science Publishers, Inc., Ann Arbor, MI, 1981.
- Box, E. O., B. N. Holben, and V. Kalb, Accuracy of the AVHRR vegetation index as a predictor of biomass, primary productivity, and net CO<sub>2</sub> flux, *Vegetatio*, 80, 71-89, 1989.
- Burrough, P. A., *Principles of Geographical Information Systems for Land Resources Assessment*, 135 pp., Clarendon Press, Oxford, 1986.
- Cannell, M. G. R., *World Forest Biomass and Primary Production Data*, 578 pp., Academic Press, New York, NY, 1982.
- Curran, P. J., Multispectral remote sensing for the estimation of green leaf area index, *Phil. Trans. R. Soc. Lond. A*, 309, 257-270, 1983.
- Edwards, P. J., Aspects of mineral cycling in a New Guinean montane forest II The production and disappearance of litter, *Journal of Ecology*, 65, 42-61, 1977.
- Edwards, P. J. and P. J. Grubb, Aspects of mineral cycling in a New Guinean montane forest I: The distribution of organic matter in the vegetation in soil, *Journal of Ecology*, 65, 23-41, 1977.
- Gallo, K. P., C. S. T. Daughtry, and M. E. Bauer, Spectral estimation of absorbed photosynthetically active radiation in corn canopies, *Remote Sensing of Environment*, 17, 221-232, 1985.

- Gates, D. M., *Biophysical Ecology*, 611 pp., Springer-Verlag, New York, NY, 1980.
- Gates, D. M., H. J. Keegan, J. C. Schleter, and V. P. Weidner, Spectral properties of plants, *Journal of Applied Optics*, 4, 11-20, 1965.
- Goward, S. N., Satellite Bioclimatology, *Journal Climate*, 2, 710-720, 1989.
- Goward, S. N., B. Markham, D. G. Dye, W. Dulaney, and J. Yang, Derivation of quantitative normalized difference vegetation index measurements from advanced very high resolution radiometer observations, (*submitted to Remote Sensing of Environment*), 1990.
- Goward, S. N., C. J. Tucker, and D. G. Dye, North American vegetation patterns observed with the NOAA-7 advanced very high resolution radiometer, *Vegetatio*, 64, 3-14, 1985.
- Grubb, P. J., Control of forest growth and distribution on wet tropical mountains, *Annual Review of Ecological Systems*, 8, 83-107, 1977.
- Gucinski, H., *Proposed Initiative: Global Biome Program*, 8 pp., U.S.EPA ORD, Corvallis, OR, 1991.
- Gutman, G., The derivation of vegetation indices from AVHRR data, *International Journal of Remote Sensing*, 8, 1235-1243, 1987.
- Hatfield, J. L., E. T. Kanemasu, G. Asrar, R. D. Jackson, P. J. Pinter, Jr., R. J. Reginato, and S. B. Idso, Leaf-area estimates from spectral measurements over various planting dates of wheat, *International Journal of Remote Sensing*, 6, 167-175, 1985.
- Henricksen, B. L. and J. W. Durkin, Growing period and drought early warning in Africa using satellite data, *Internationalal Journal of Remote Sensing*, 7, 1583-1608, 1986.



- Holben, B. and C. Justice, An examination of spectral band ratioing to reduce the topographic effect on remotely sensed data, *Technical Memorandum 80640*, 28 pp., NASA Goddard Space Flight Center, Greenbelt, MD, 1980.
- Holben, B. H., C. J. Tucker, and J. W. Robinson, Limitations on the application of a ground-based spectral technique for determining rain forest leaf area index, *Photogrammetric Engineering and Remote Sensing*, 46, 1980.
- Holben, B. N. and R. S. Fraser, Red and near-infrared response to off-nadir viewing, *International Journal of Remote Sensing*, 5, 145-156, 1984.
- Houghton, J. T., G. J. Jenkins, and J. J. Ephraums, *Climate Change: The IPCC Scientific Assessment*, 364 pp., Cambridge University Press, New York, NY, 1991.
- Jensen, J. R., *Digital Image Processing: A remote sensing perspective*, Prentice-Hall, Englewood Cliffs, NJ, 1986.
- Jordan, C. F., Derivation of leaf area index from quality of light on the forest floor, *Ecology*, 50, 663-666, 1969.
- Justice, C. O. and P. H. Y. Hiernaux, Monitoring the grasslands of the Sahel using NOAA AVHRR data: Niger 1983, *International Journal of Remote Sensing*, 7, 1475-1498, 1986.
- Justice, C. O., B. N. Holben, and M. D. Gwynne, *Monitoring East African vegetation using AVHRR data*, 7, pp. 1453-1474, 1986.
- Kidwell, K. B., *NOAA Polar Orbiter Data (TIROS-N, NOAA-6, NOAA-7, and NOAA-8) User Guide*, NOAA/NESDIS, Washington, DC, 1984.
- Kidwell, K. B., Global vegetation index user's guide, in *NOAA National Climate Data Center*, p. 38, Washington, D.C., 1990.

- Kimes, D. S., B. N. Holben, C. J. Tucker, and W. W. Newcomb, Optimal directional view angles for remote-sensing missions, *International Journal of Remote Sensing*, 5, 887-908, 1984.
- Kimes, D. S., B. L. Markham, C. J. Tucker, and J. E. McMurtrey III, Temporal relationships between spectral response and agronomic variables of a corn canopy, *Remote Sensing of Environment*, 11, 401-411, 1981.
- Kimes, D. S., W. W. Newcomb, C. J. Tucker, I. S. Zonneveld, W. Van Wijngaarden, J. De Leeuw, and G. F. Epema, Directional reflectance factor distributions for cover types of Northern Africa, *Remote Sensing of Environment*, 18, 1-19, 1985.
- Kimes, D. S., J. A. Smith, and K. J. Ranson, Vegetation reflectance measurements as a function of solar zenith angle, *Photogrammetric Engineering and Remote Sensing*, 46, 1563-1573, 1980.
- Knipling, E. B., Physical and physiological basis for the reflectance of visible and near infrared radiation from vegetation, *Remote Sensing of Environment*, 1, 115-119, 1970.
- Lieth, H. and R. H. Whittaker, *Primary productivity of the biosphere*, Springer-Verlag, New York, NY, 1975.
- Lloyd, D., A phenological classification of terrestrial vegetation cover using shortwave vegetation index imagery, *International Journal of Remote Sensing*, 11, 2269-2279, 1990.
- Malingreau, J. P., Global vegetation dynamics: satellite observations over Asia, *International Journal of Remote Sensing*, 7, 1121-1146, 1986.
- Markham, B. L., D. S. Kimes, C. J. Tucker, and J. E. McMurtrey III, Temporal spectral response of a corn canopy, *Photogrammetric Engineering and*

- Remote Sensing*, 48, 1599-1605, 1981.
- Marks, D., A Continental-Scale Simulation of Potential Evapotranspiration for Historical and Projected Doubled-CO<sub>2</sub> Climate Conditions, (*submitted to Journal of Geophysical Research*), (1991).
- Matthews, E., Global vegetation and land use: new high-resolution data bases for climate studies, *J. Clim. Appl. Meteor.*, 22, 474-487, 1983.
- Nieuwolt, S., *Tropical Climatology*, pp. 1-14, John Wiley & Sons, New York, NY, 1977.
- Norwine, J. and D. H. Greigor, Vegetation classification based on advanced very high resolution radiometer (AVHRR) satellite imagery, *Remote Sensing of Environment*, 13, 69-87, 1983.
- Olson, J. S., *Documentation for WE3.0 Database of World Ecosystems*, pp. 1-7, Global Patterns Company, Lenoir City, TN, 1990.
- Olson, J. S., J. A. Watts, and L. J. Allison, Carbon in live vegetation of major world ecosystems, in *ORNL-5862*, pp. 1-180, Oak Ridge National Laboratory, Oak Ridge, TN, 1983.
- Pearson, R. L., C. J. Tucker, and L. D. Miller, Spectral mapping of shortgrass prairie biomass, *Photogrammetric Engineering and Remote Sensing*, 42, 317-323, 1976.
- Prince, S. D. and W. L. Astle, Satellite remote sensing of rangelands in Botswana I Landsat MSS and herbaceous vegetation, *Internationalal Journal of Remote Sensing*, 7, 1533-1553, 1986.
- Prince, S. D. and C. J. Tucker, Satellite remote sensing of rangelands in Botswana II NOAA AVHRR and herbaceous vegetation, *International Journal of Remote Sensing*, 7, 1555-1570, 1986.

- Rosenzweig, C. and R. E. Dickinson, *Climate-Vegetation Interactions*, 156 pp., Office for Interdisciplinary Earth Studies, 1986.
- Rouse, J. W., R. H. Haas, J. A. Schell, and D. W. Deering, Monitoring vegetation systems in the Great Plains with ERTS, in *Proceedings: Third ERTS Symposium*, vol. 1, pp. 48-62, 1973.
- Running, S. W. and R. R. Nemani, Relating seasonal patterns of the AVHRR vegetation index to simulated photosynthesis and transpiration of forests in different climates, *Remote Sensing of Environment*, 24, 347-367, 1988.
- Running, S. W., R. R. Nemani, D. L. Peterson, L. E. Band, D. F. Potts, L. L. Pierce, and M. A. Spanner, Mapping regional forest evapotranspiration and photosynthesis by coupling satellite data with ecosystem simulation, *Ecology*, 70, 1090-1101, 1989.
- Running, S. W., D. L. Peterson, M. A. Spanner, and K. B. Teuber, Remote sensing of coniferous leaf area, *Ecology*, 67, 273-276, 1986.
- Singh, S. M., Lowest order correction for solar zenith angle to global vegetation index (GVI) data, *International Journal of Remote Sensing*, 9, 1565-1572, 1988 b.
- Singh, S. M., Simulation of solar zenith angle effect on global vegetation index (GVI) data, *International Journal of Remote Sensing*, 9, 237-248, 1988 a.
- Spanner, M. A., L. L. Pierce, S. W. Running, and D. L. Peterson, The seasonality of AVHRR data of temperate coniferous forests: Relationship with leaf area index, *Remote Sensing of Environment*, 33, 97-112, 1990.
- Townshend, J. R. G. and C. O. Justice, Analysis of the dynamics of African vegetation using the normalized difference vegetation index, *International Journal of Remote Sensing*, 7, 1435-1446, 1986.

- Tucker, C. J., Asymptotic nature of grass canopy spectral reflectance, *Journal of Applied Optics*, 16, 1151-1156, 1976.
- Tucker, C. J., Resolution of grass canopy biomass classes, *Photogrammetric Engineering and Remote Sensing*, 43, 1059-1067, 1977.
- Tucker, C. J., Post senescent grass canopy remote sensing, *Remote Sensing of Environment*, 7, 203-210, 1978.
- Tucker, C. J., A critical review of remote sensing and other methods for non-destructive estimation of standing crop biomass, *Journal of Grass and Forage Science*, 35, 177-182, 1979 b.
- Tucker, C. J., Red and Photographic infrared linear combinations for monitoring vegetation, *Remote Sensing of Environment*, 8, 127-150, 1979 a.
- Tucker, C. J., J. H. Elgin, Jr., J. E. McMurtrey III, and C. J. Fan, Monitoring corn and soybean crop development with hand-held radiometer spectral data, *Remote Sensing of Environment*, 8, 237-248, 1979.
- Tucker, C. J., B. H. Holben, J. H. Elgin, Jr., and J. E. McMurtrey III, Relationship of spectral data to grain yield variation, *Photogrammetric Engineering and Remote Sensing*, 46, 657-666, 1980.
- Tucker, C. J., B. N. Holben, J. H. Elgin, Jr., and J. E. McMurtrey III, Remote sensing of total dry-matter accumulation in winter wheat, *Remote Sensing of Environment*, 11, 171-189, 1981.
- Tucker, C. J., C. O. Justice, and S. D. Prince, Monitoring the grasslands of the Sahel 1984-1985, *International Journal of Remote Sensing*, 7, 1571-1582, 1986.
- Tucker, C. J. and P. J. Sellers, Satellite remote sensing of primary production, *International Journal of Remote Sensing*, 7, 1571-1582, 1986.

- Tucker, C. J., J. R. G. Townshend, and T. E. Goff, African land-cover classification using satellite data, *Science*, 227, 369-375, 1985.
- Tucker, C. J., C. Vanpraet, E. Boerwinkel, and A. Gaston, Satellite remote sensing of total dry matter production in the Senegalese Sahel, *Remote Sensing of Environment*, 13, 461-474, 1983.
- Tucker, C. J., C. L. Vanpraet, M. J. Sharman, and G. Van Ittersum, Satellite remote sensing of total herbaceous biomass production in the Senegalese Sahel: 1980-1984, *Remote Sensing of Environment*, 17, 233-249, 1985.
- Turner, D. P., J. V. Baglio, D. D. Pross, A. Wones, B. McVeety, R. Vong, and D. L. Phillips, Global Climate Change and Isoprene Emissions from Vegetation, (*submitted to Chemosphere*), 1990.
- U.S. Army Corps of Engineers, *GRASS Users and Programmers Manual*, U.S. Army Corps of Engineers, Construction Engineering Research Laboratory, Champagne, IL, 1988.
- Wardley, N. W. and P. J. Curran, The estimation of green-leaf-area index from remotely sensed airborne multispectral scanner data, *International Journal of Remote Sensing*, 5, 671-679, 1984.
- Webb, W. L., W. K. Lauenroth, S. R. Szarek, and R. S. Kinerson, Primary production and abiotic controls in forests, grasslands, and desert ecosystems in the United States., *Ecology*, 64, 134-151, 1983.
- Whittaker, R. H., Net production relations of shrubs in the Great Smoky Mountains, *Ecology*, 43, 357-377, 1962.
- Whittaker, R. H., Forest dimensions and production in the Great Smoky Mountains, *Ecology*, 47, 103-121, 1966.

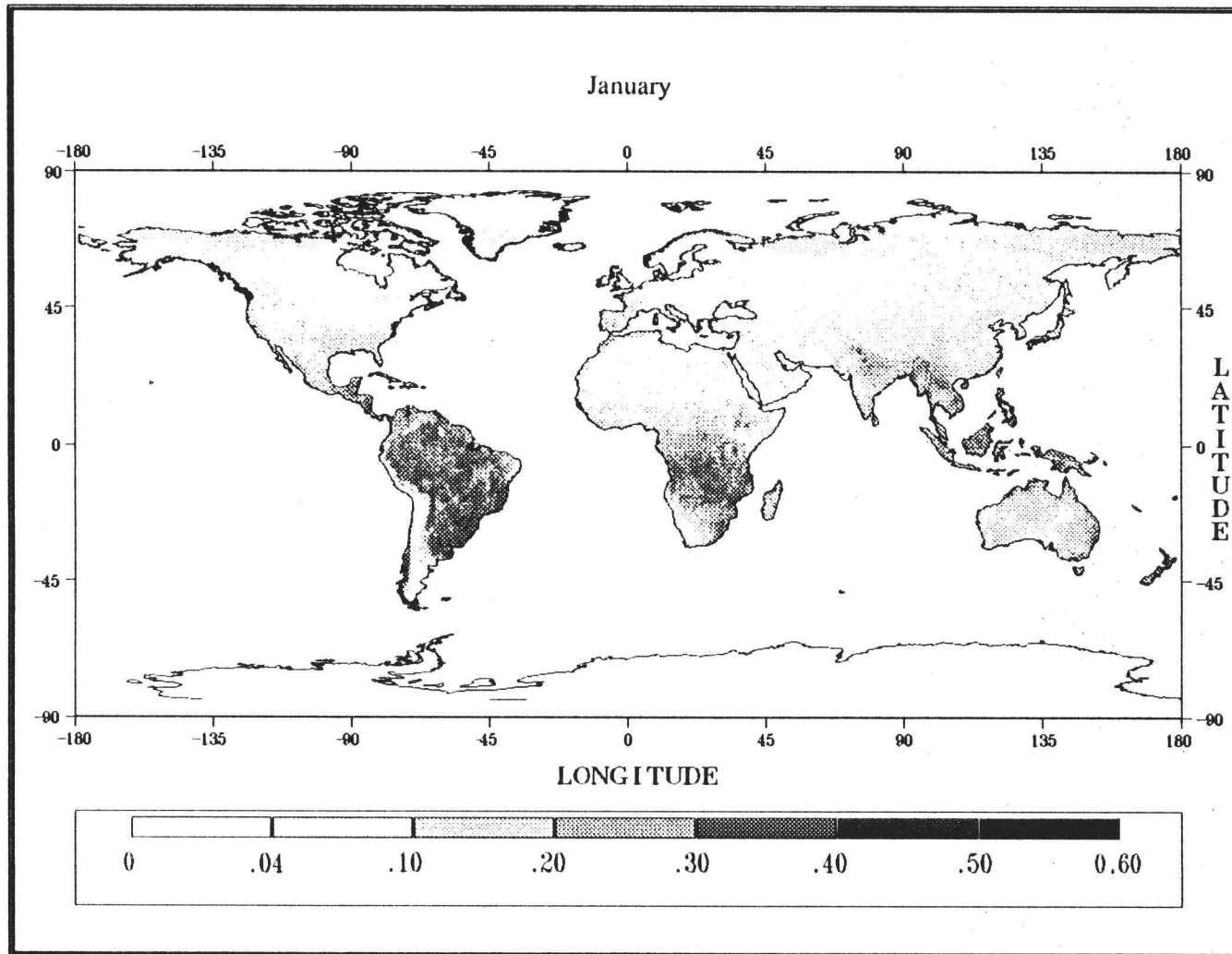
- Whittaker, R. H., *Communities and Ecosystems, 2nd Edition*, 385 pp., MacMillan Publishing Co., New York, NY, 1975.
- Whittaker, R. H. and W. A. Niering, Vegetation of the Santa Catalina Mountains, Arizona V. Biomass, production, and diversity along the elevation gradient, *Ecology*, *56*, 771-790, 1975.
- Whittaker, R. H. and G. M. Woodwell, Structure, production, and diversity of the oak-pine forest at Brookhaven, New York, *Journal of Ecology*, *57*, 157-174, 1969.
- Wiegand, C. L., A. J. Richardson, and E. T. Kanemasu, Leaf area index estimates for wheat from Landsat and their implications for evapotranspiration and crop modeling, *Agronomy Journal*, *71*, 336-342, 1979.
- Woolley, J. T., Reflectance and transmittance of light by leaves, *Plant Physiology*, *47*, 656-662, 1971.

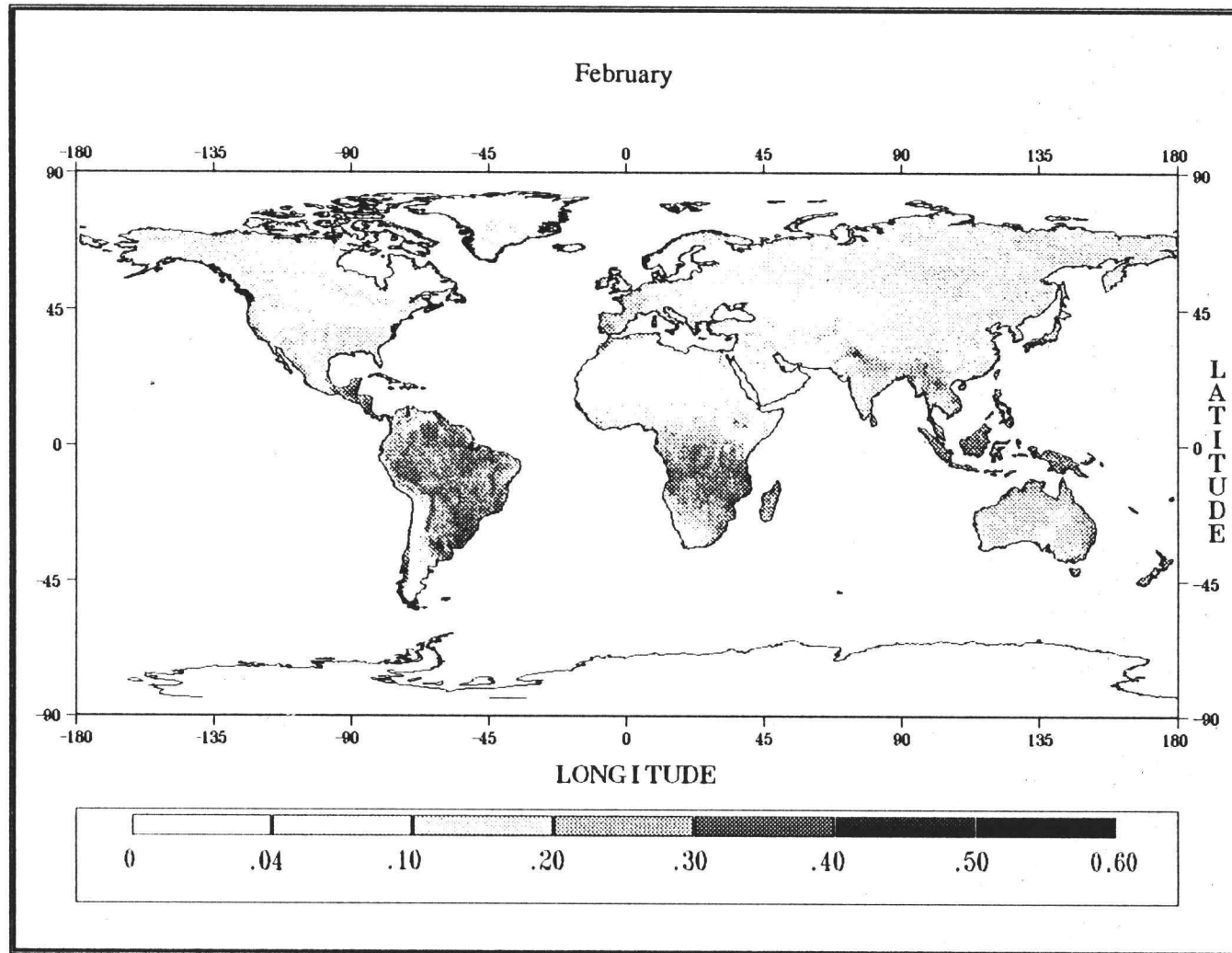
## APPENDICES

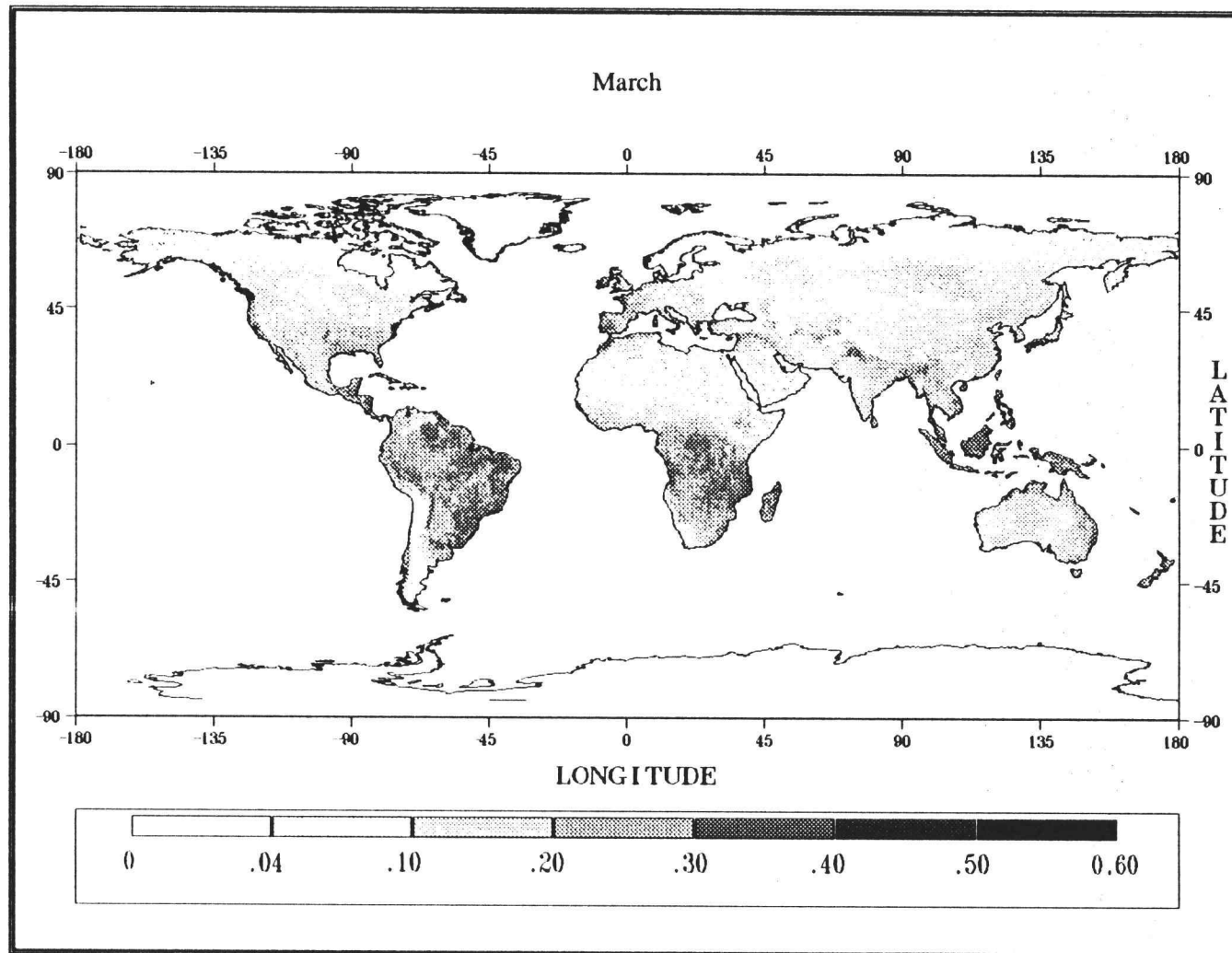


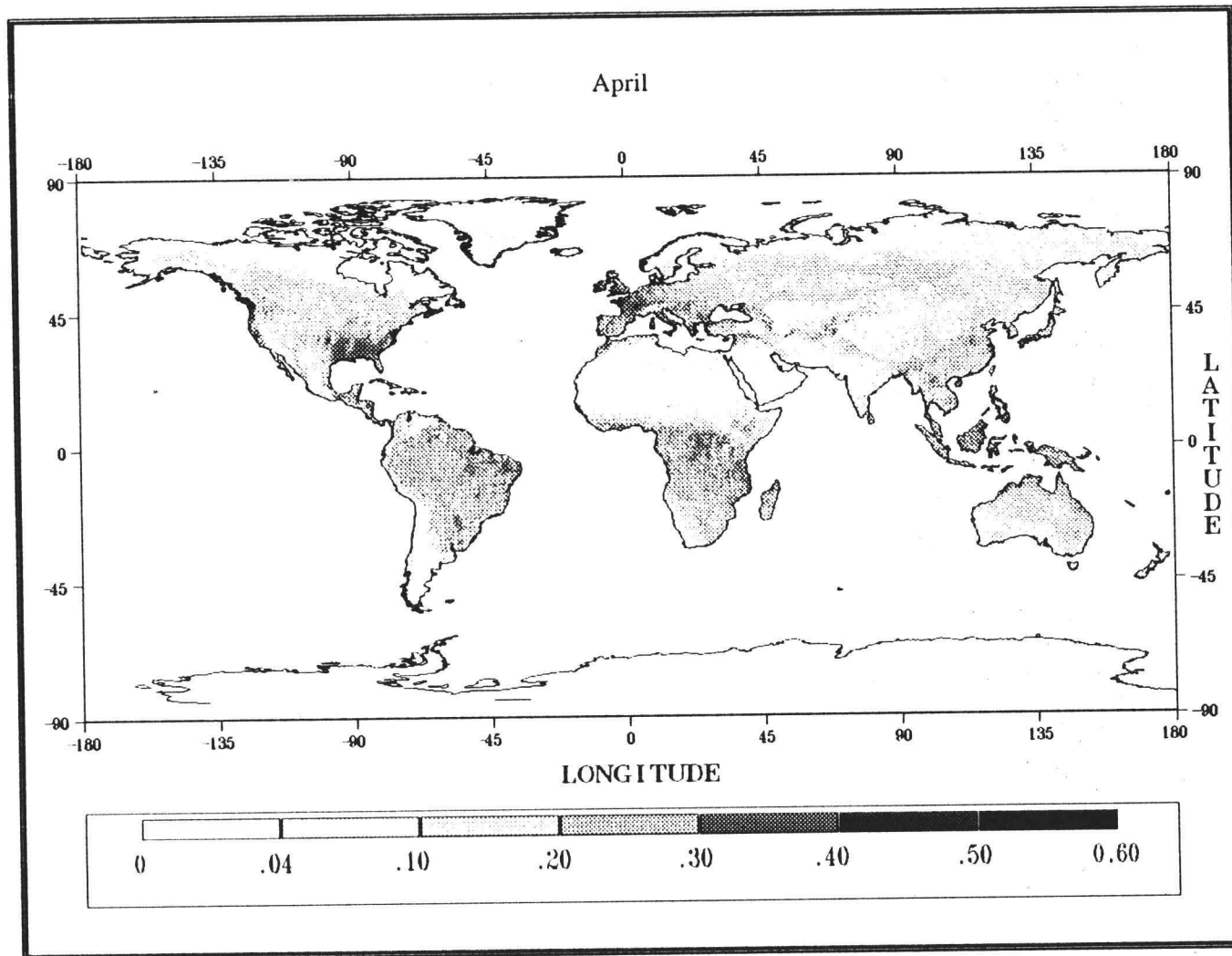
## APPENDIX A

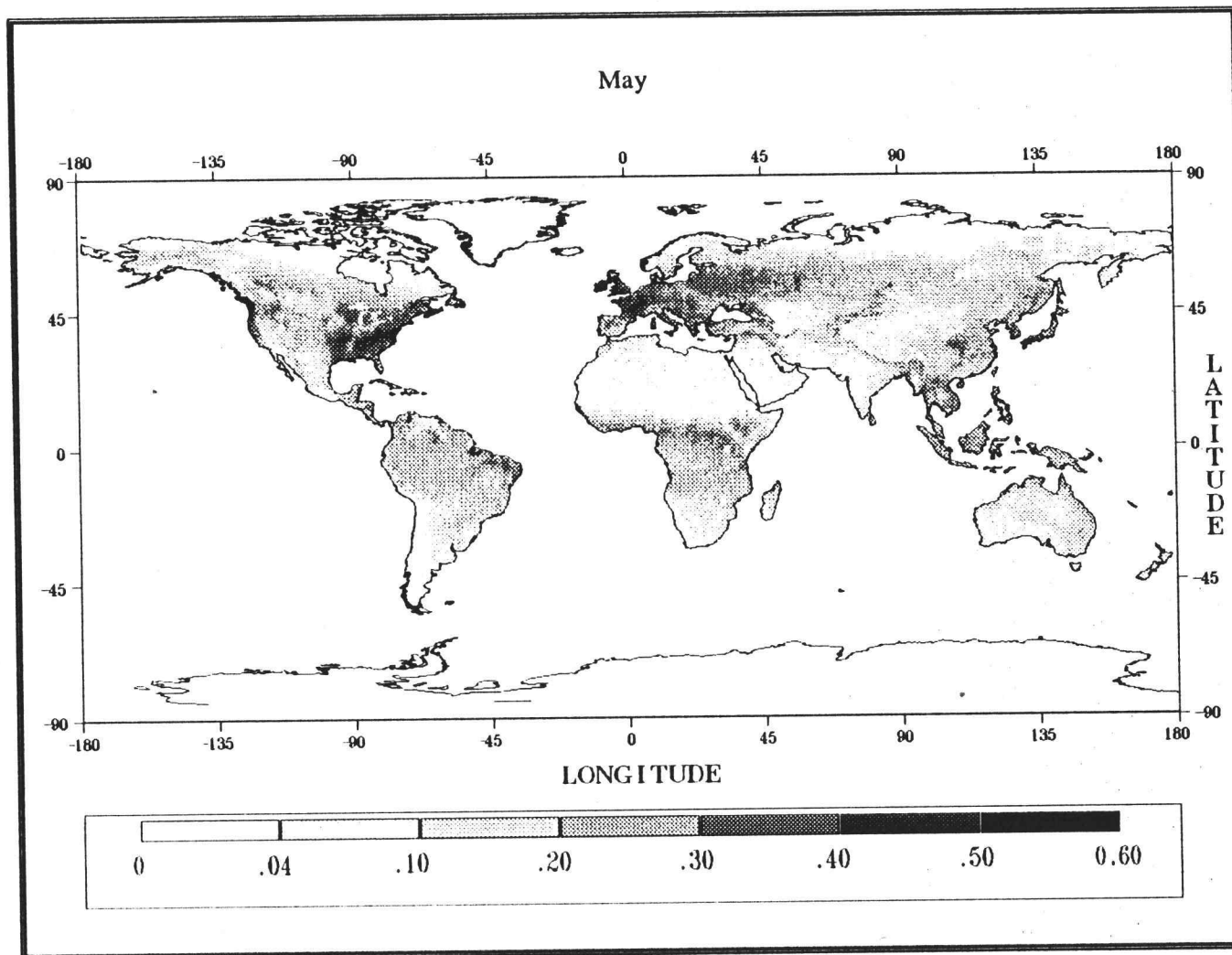
### Monthly Images of GVI, January through December

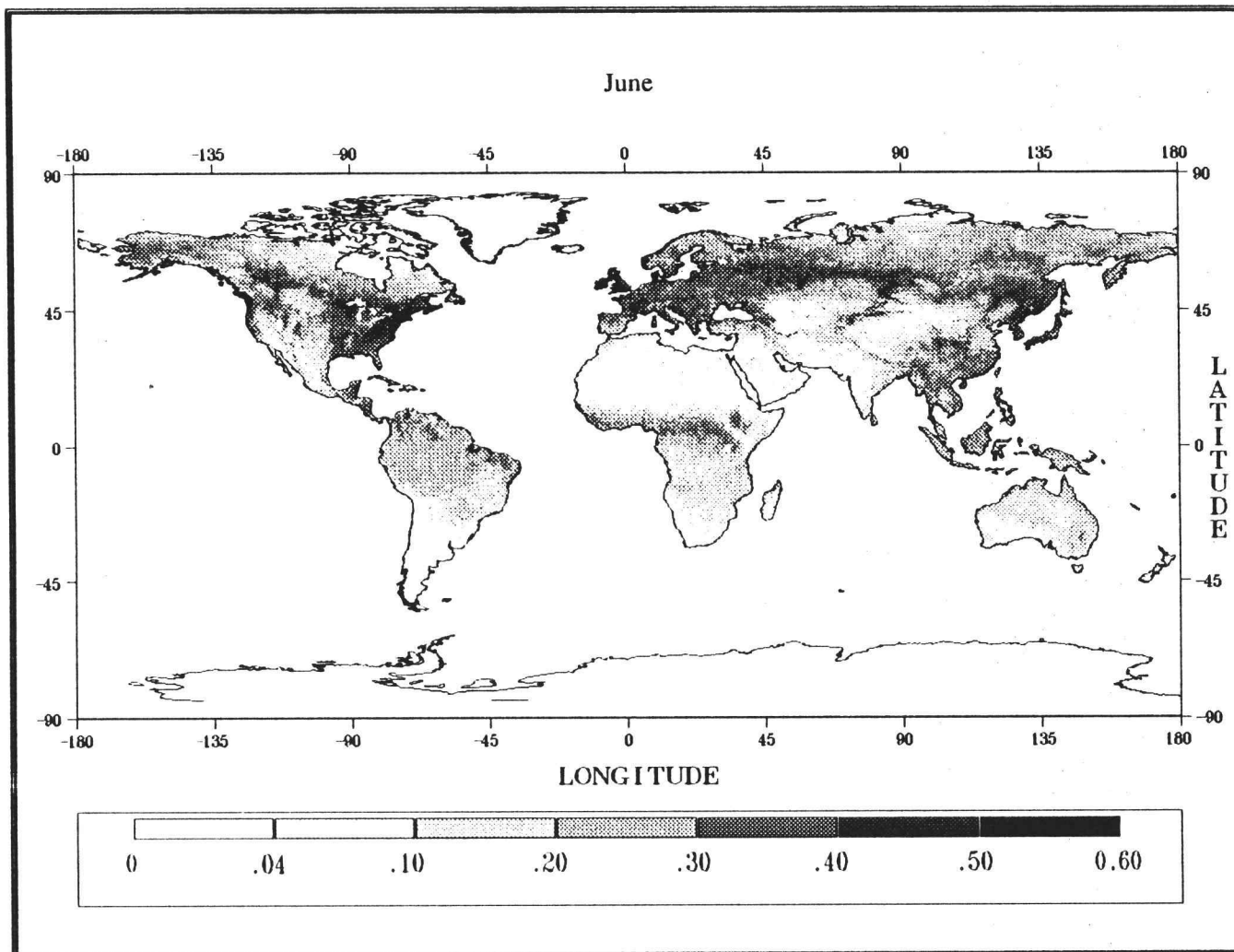


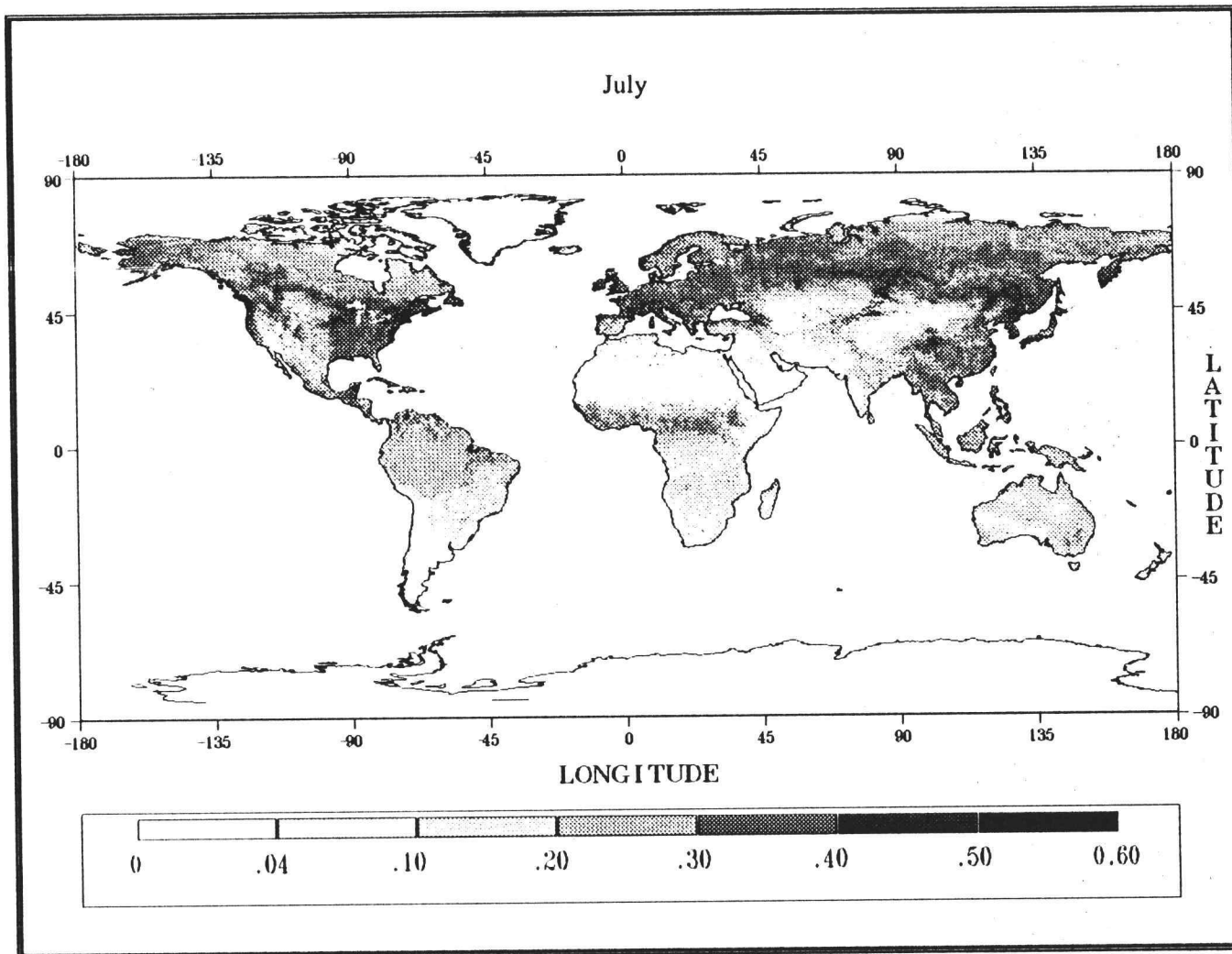




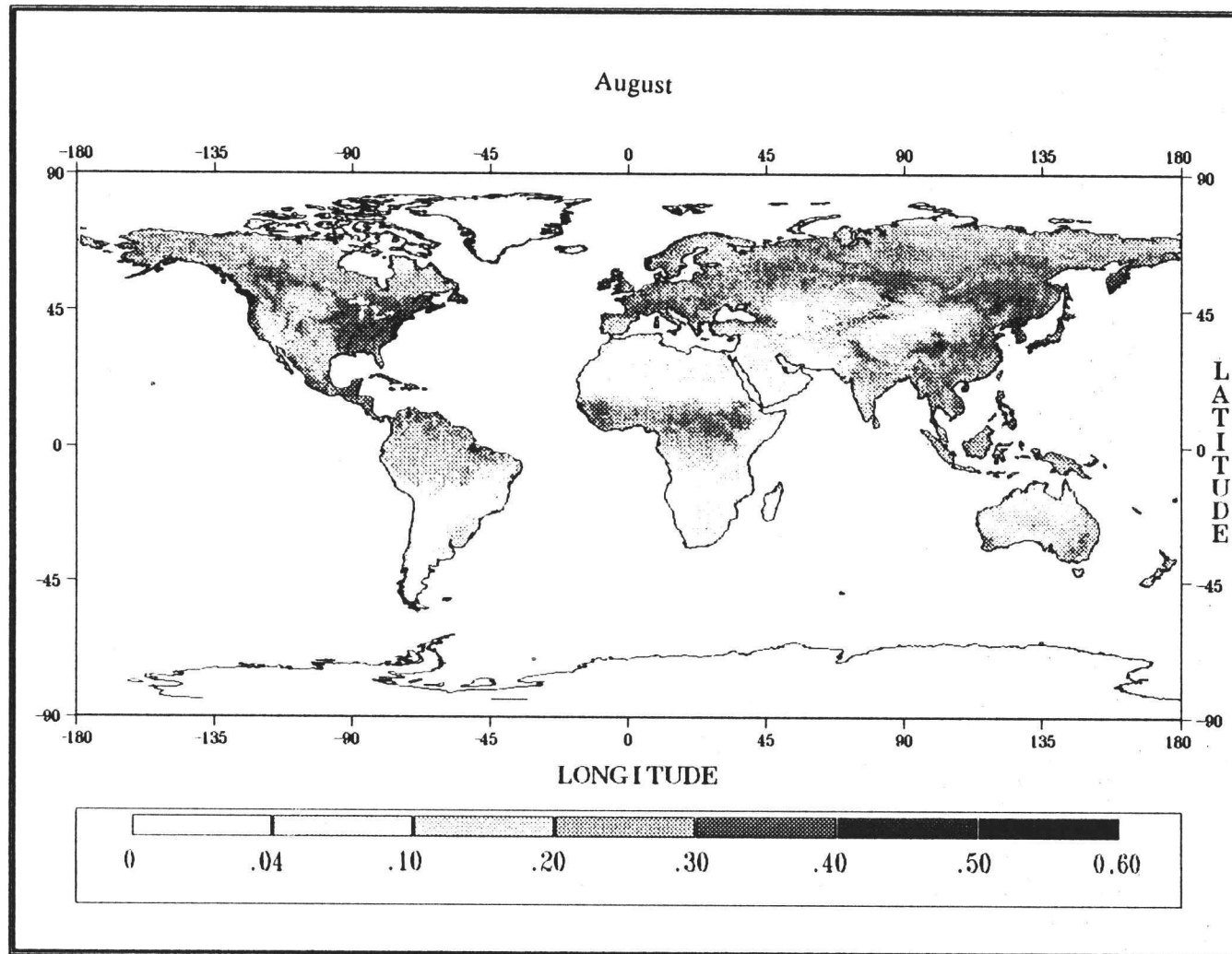


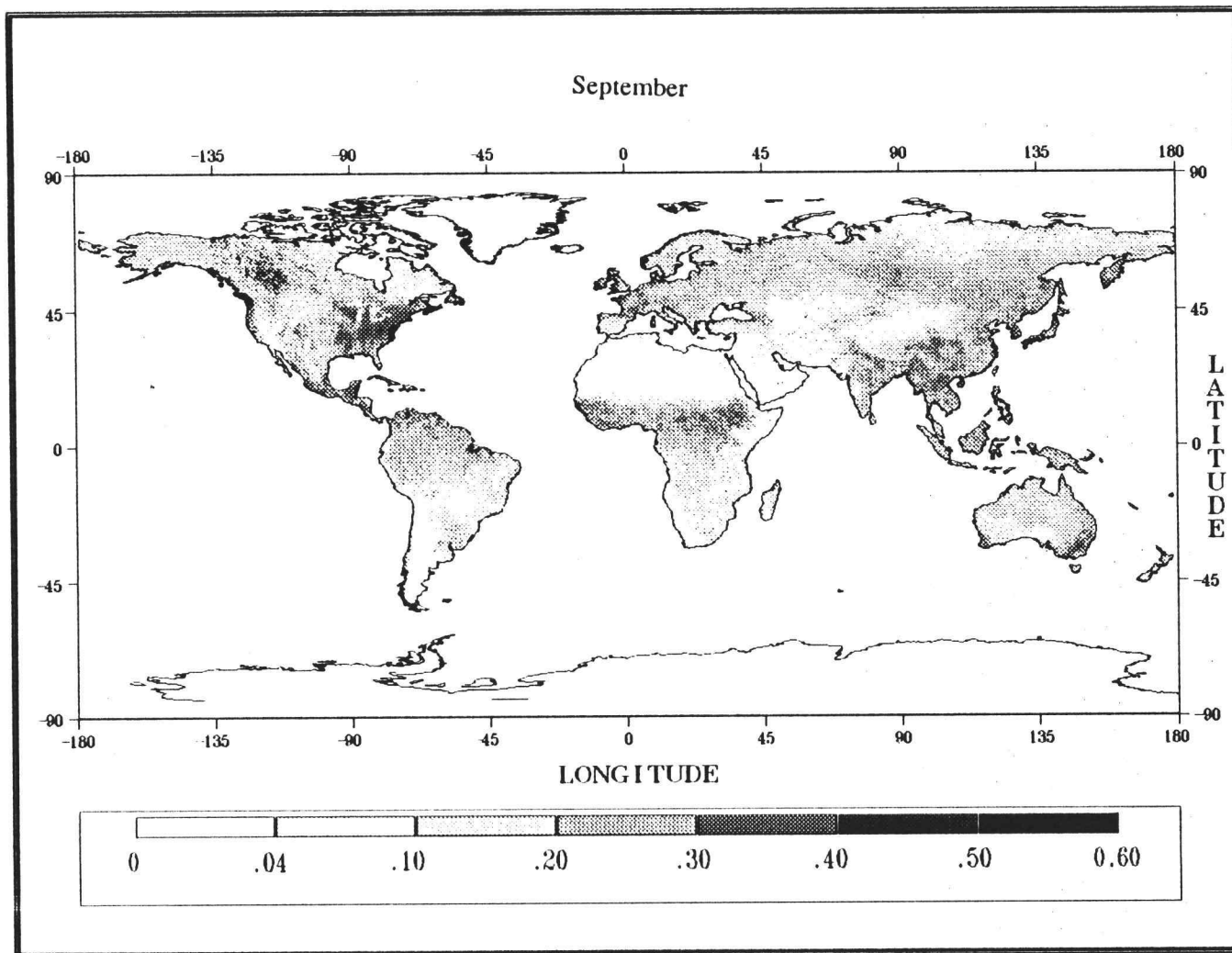


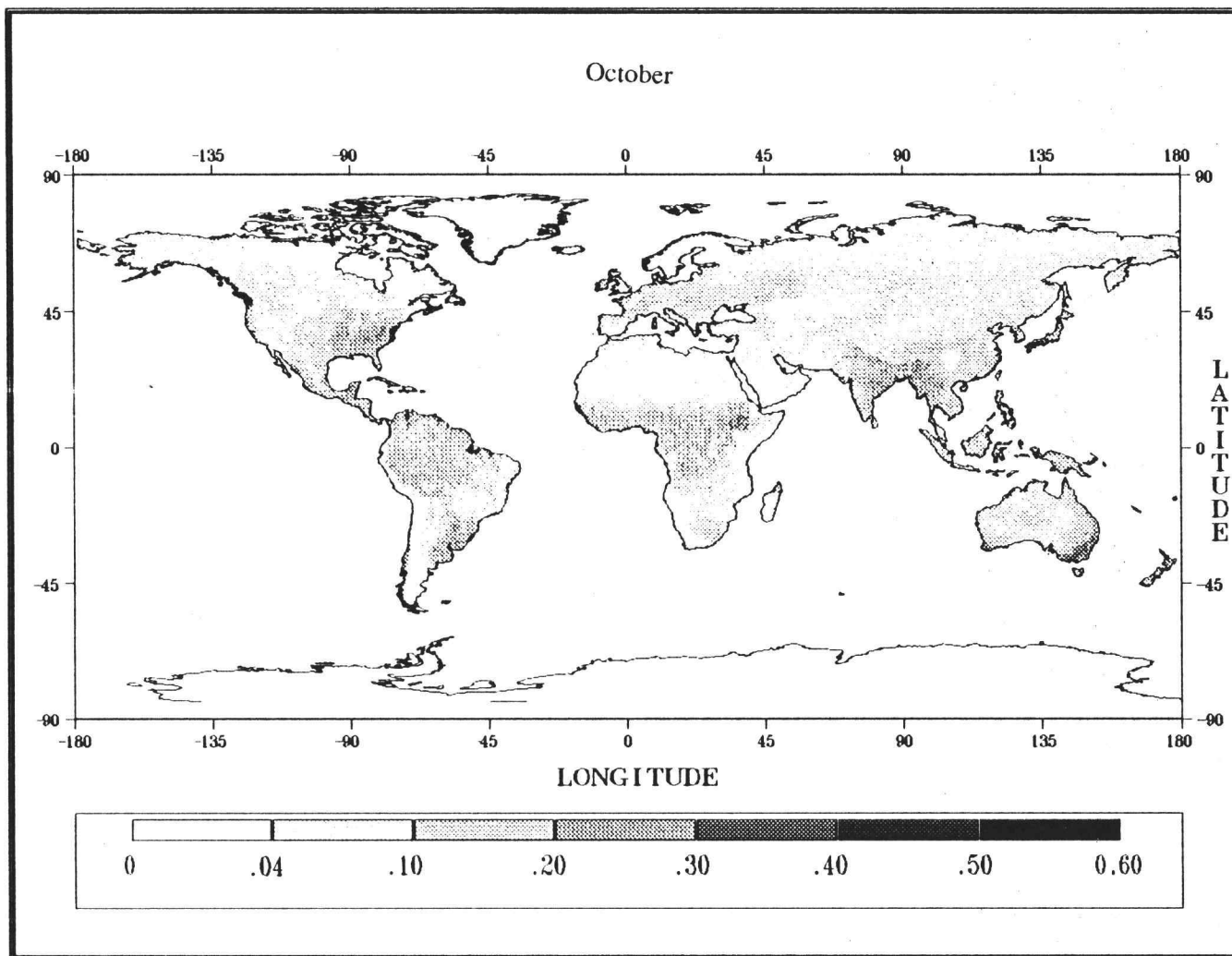


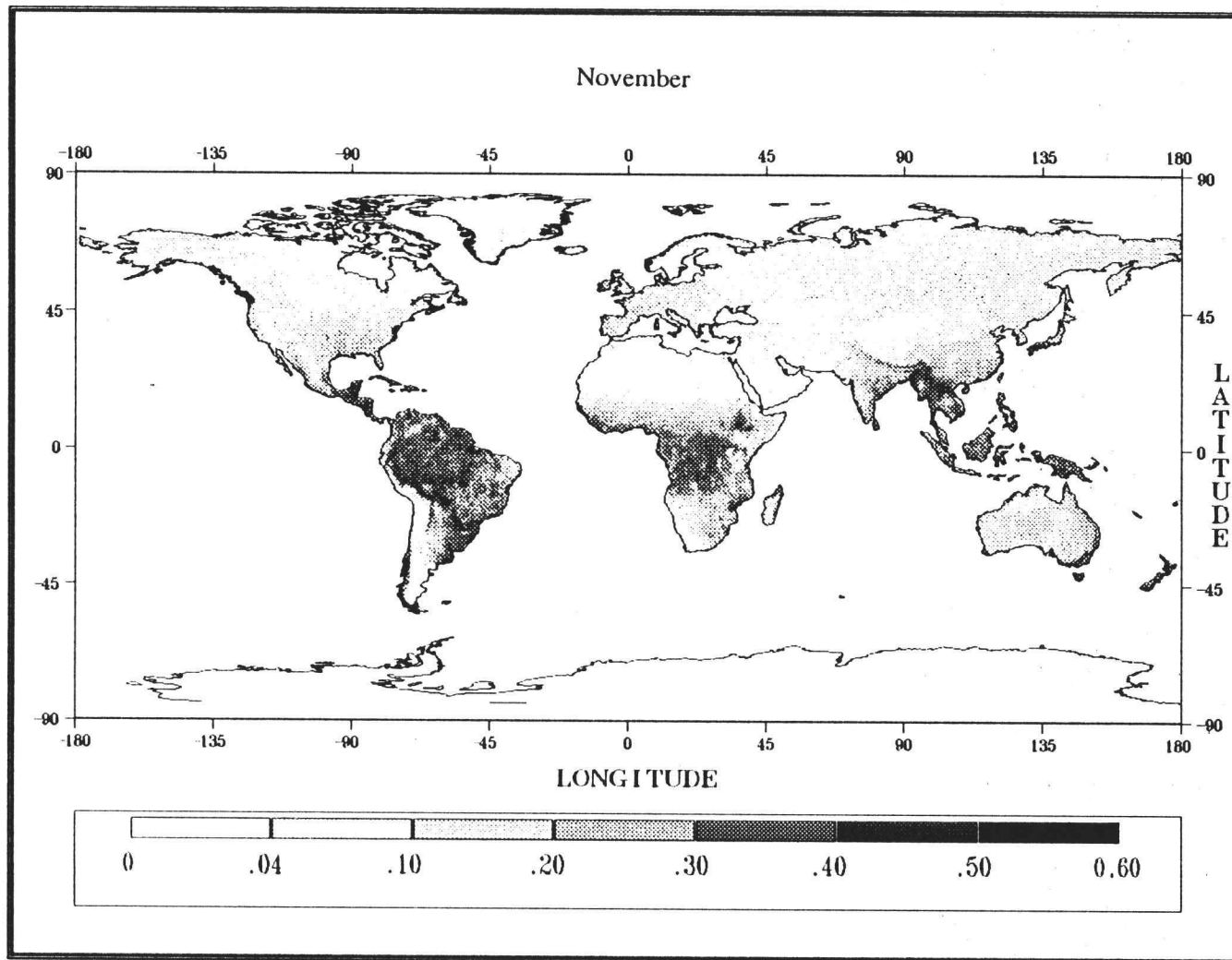


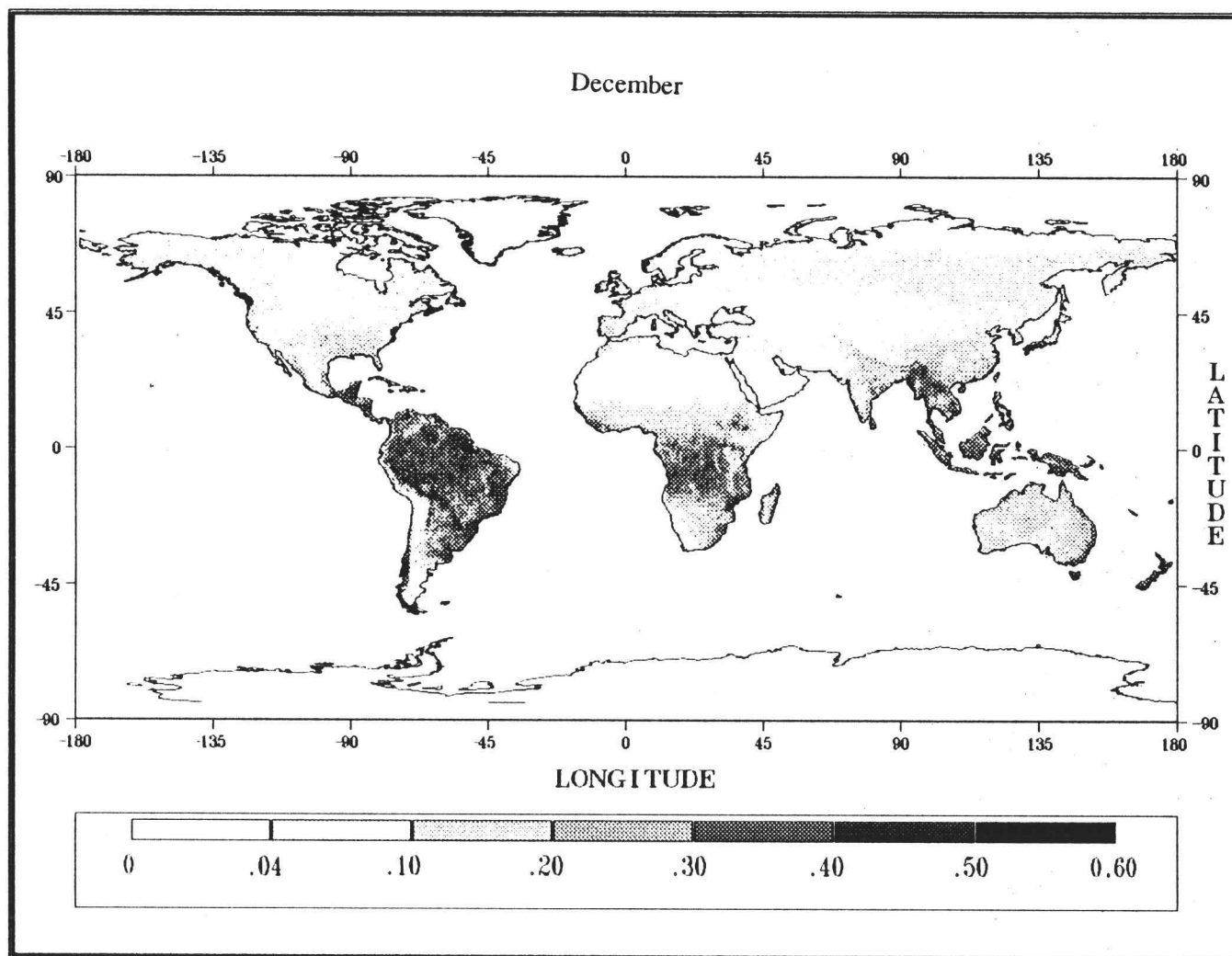












## APPENDIX B

Derivation of FBD-GVI relationship

Original equation expressed generically:

$$Y = a \ln \frac{X}{b} \quad (1)$$

where:

$$Y = \text{NDVI}$$

$$X = \text{FBD}$$

$a, b$  = biome specific constants

Equation 1 must now be manipulated to bring  $X$  (FBD) to the outside. The following equations show the steps of this process.

Divide both sides by  $a$ .

$$\frac{Y}{a} = \ln \frac{X}{b} \quad (2)$$

Exponentiate the equation.

$$\exp \frac{Y}{a} = \frac{X}{b} \quad (3)$$

Multiply both sides by  $b$ .

$$X = a \exp \frac{Y}{b} \quad (4)$$

Variable Substitution and further algebraic manipulation.

Set up the equations in order to simultaneously solve for  $a$  and  $b$ .

(the equations are manipulated with the X and Y variables for ease)

$$X = a \exp \frac{Y}{b} \quad (5)$$

remove the exponent

$$\ln X = \ln \left\{ a \exp \frac{Y}{b} \right\} \quad (6)$$

final equation

$$\ln X = \ln a + \frac{Y}{b} \quad (7)$$

Substitute in the known model variables.

$$\ln F_{max} = \ln a + \frac{N_{max}}{b} \quad (8)$$

$$\ln F_{min} = \ln a + \frac{N_{min}}{b} \quad (9)$$

where:

$F_{min}$  = FBD minimum value per biome

$F_{max}$  = FBD maximum value per biome

$N_{min}$  = GVI minimum value per biome

$N_{max}$  = GVI maximum value per biome

$a, b$  = biome specific constants

Solve for for  $b$ .

$$\ln F_{max} = \ln a + \frac{N_{max}}{b} \quad (10)$$

$$\ln F_{min} = \ln a + \frac{N_{min}}{b} \quad (11)$$

Subtract equation 11 from equation 10

$$\ln \left\{ \frac{F_{max}}{F_{min}} \right\} = \frac{N_{max} - N_{min}}{b} \quad (12)$$

$$b = \frac{N_{max} - N_{min}}{\ln F_{max} / F_{min}}$$

Solve for  $a$  in terms of  $b$ . (leave  $b$  as the variable " $b$ ").

$$\ln F_{max} = \ln a \frac{N_{max}}{b} \quad (14)$$

$$\ln a = \ln F_{max} - \ln b \quad (15)$$

expontiate

$$a = F_{max} \frac{-N_{max}}{b} \quad (16)$$

The components of the model are now ready to be solved with the data presented in the methods section of this manuscript.



## APPENDIX C

### 1) Table of biome specific variables and constants

Biome	Fmax	Fmin	Nmax	Nmin	B	A
NonpolarDesert	0.05	0.01	33	5	0.0077137	19.2614
PolarDesert	0.10	0.01	17	4	0.0031623	3.47438
Tundra	0.05	0.01	37	6	0.0073951	19.8827
SouthernTemperateBLF	0.80	0.20	45	8	0.14938	27.4112
Grassland	0.5	0.05	42	9	0.024885	14.3317
Shrubland	0.5	0.10	39	4	0.081248	19.2614
Farms/Towns	0.5	0.1	42	8	0.064472	20.5041
NonpaddyIrrigatedDryland	0.5	0.1	37	4	0.082277	20.5041
Forest/Fields/Woods	0.8	0.1	45	10	0.05202	16.8314
NorthernTemperateBLF	0.6	0.3	50	8	0.18899	43.2809
CoolConiferHardwood	1.0	0.3	46	7	0.20549	29.0704
TropicalMontane	0.7	0.3	45	15	0.1964	35.4067
Wetlands/Hinterlands/Shore	0.5	0.1	40	7	0.072478	21.7467
DryForestandWoodland	0.5	0.1	42	10	0.060474	19.8827
Semi-aridWoodland	0.3	0.1	33	6	0.073060	25.4867
WarmConiferForest	1.0	0.1	41	12	0.030303	11.726
Paddyland	0.5	0.1	38	10	0.056282	17.3974
Taiga	1.5	0.3	40	20	0.060	12.4267
TropicalSeas.HumidBLF	0.8	0.3	45	22	0.1174	23.4495
Trop/Subt.HumidFrst	1.3	0.3	44	20	0.088397	16.3673
CoolConiferForest	2.0	0.5	45	17	0.21549	20.1977

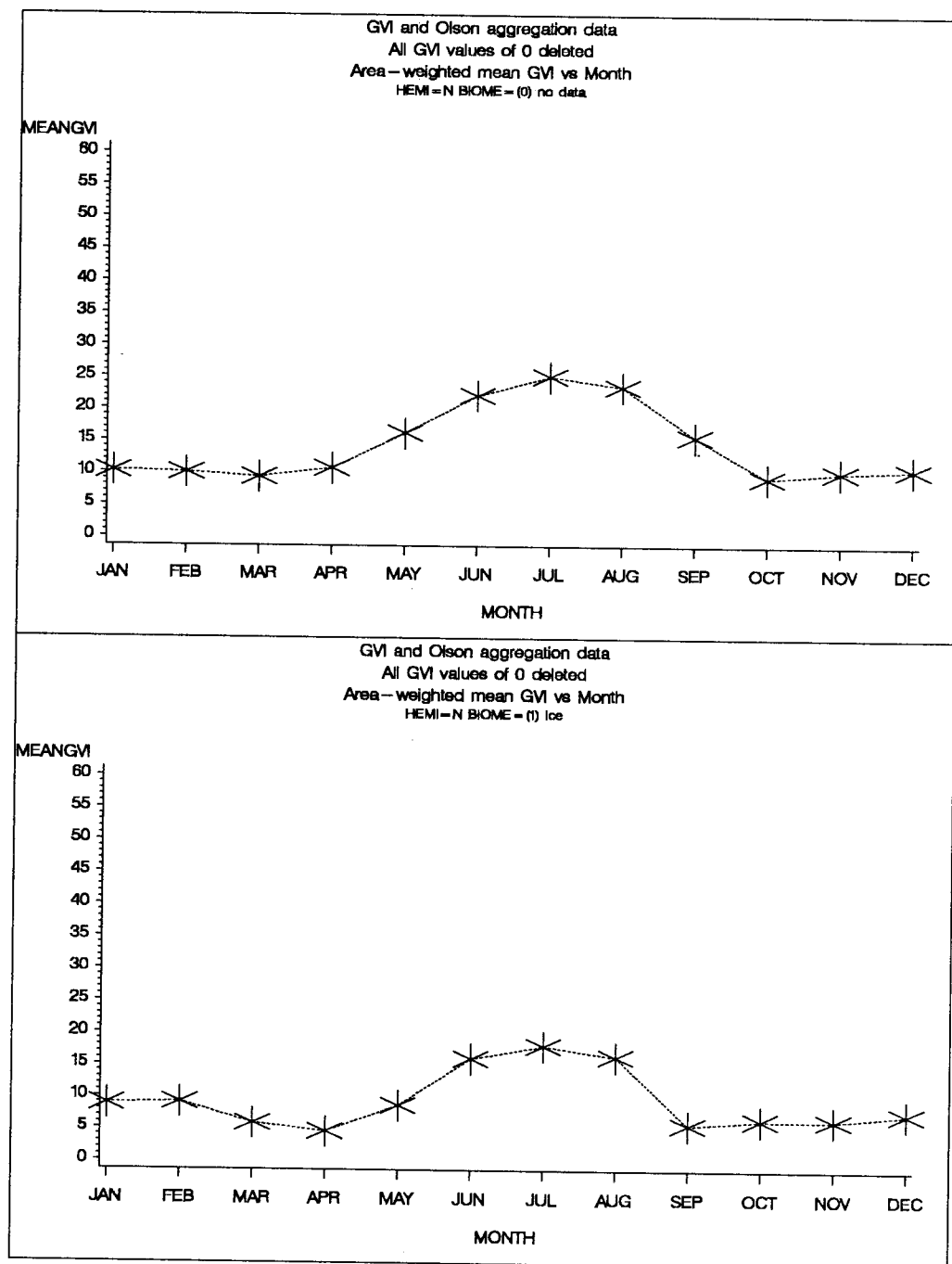
## APPENDIX D

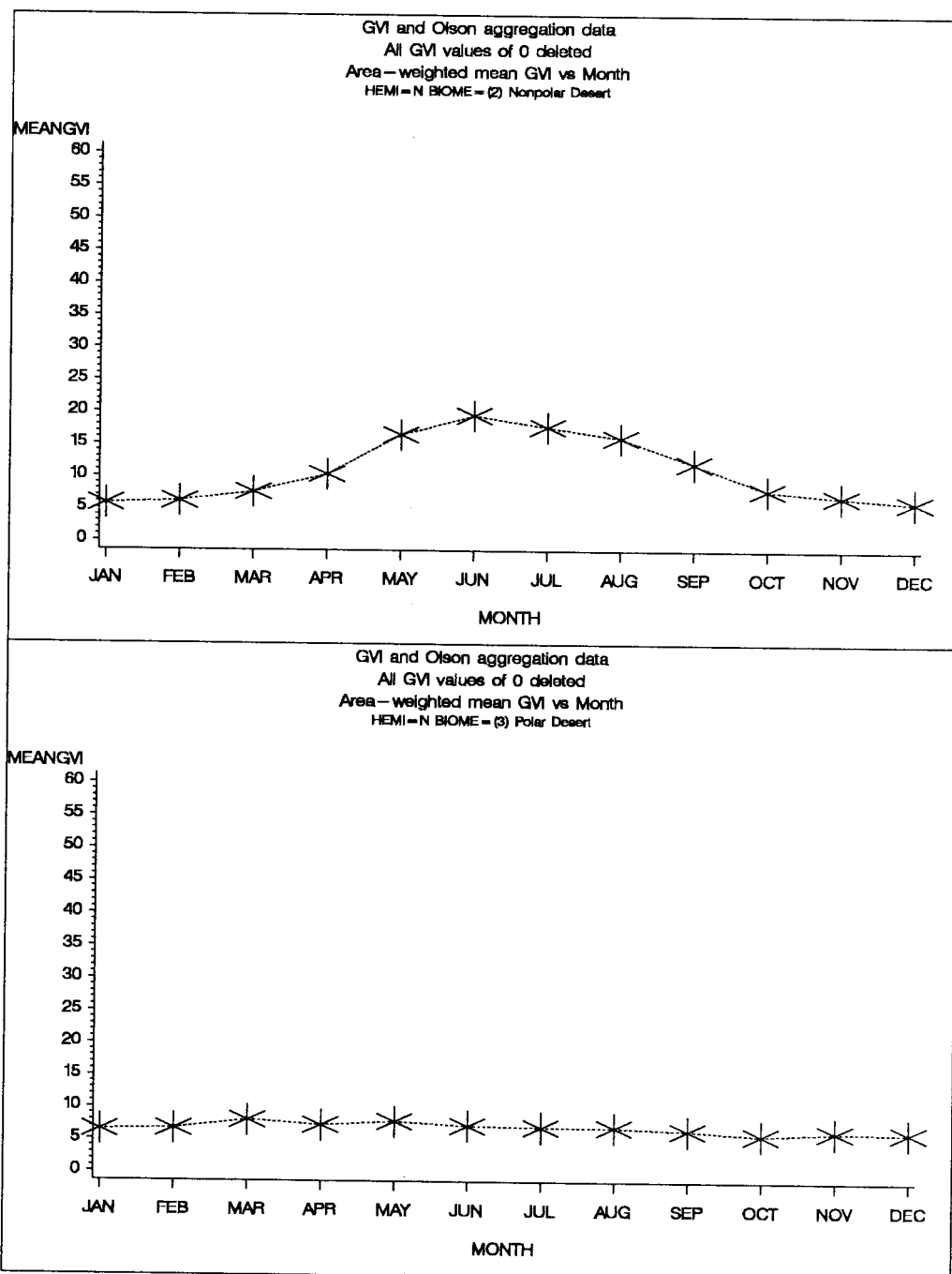
1) Table of Olson categories by number used in the aggregation.

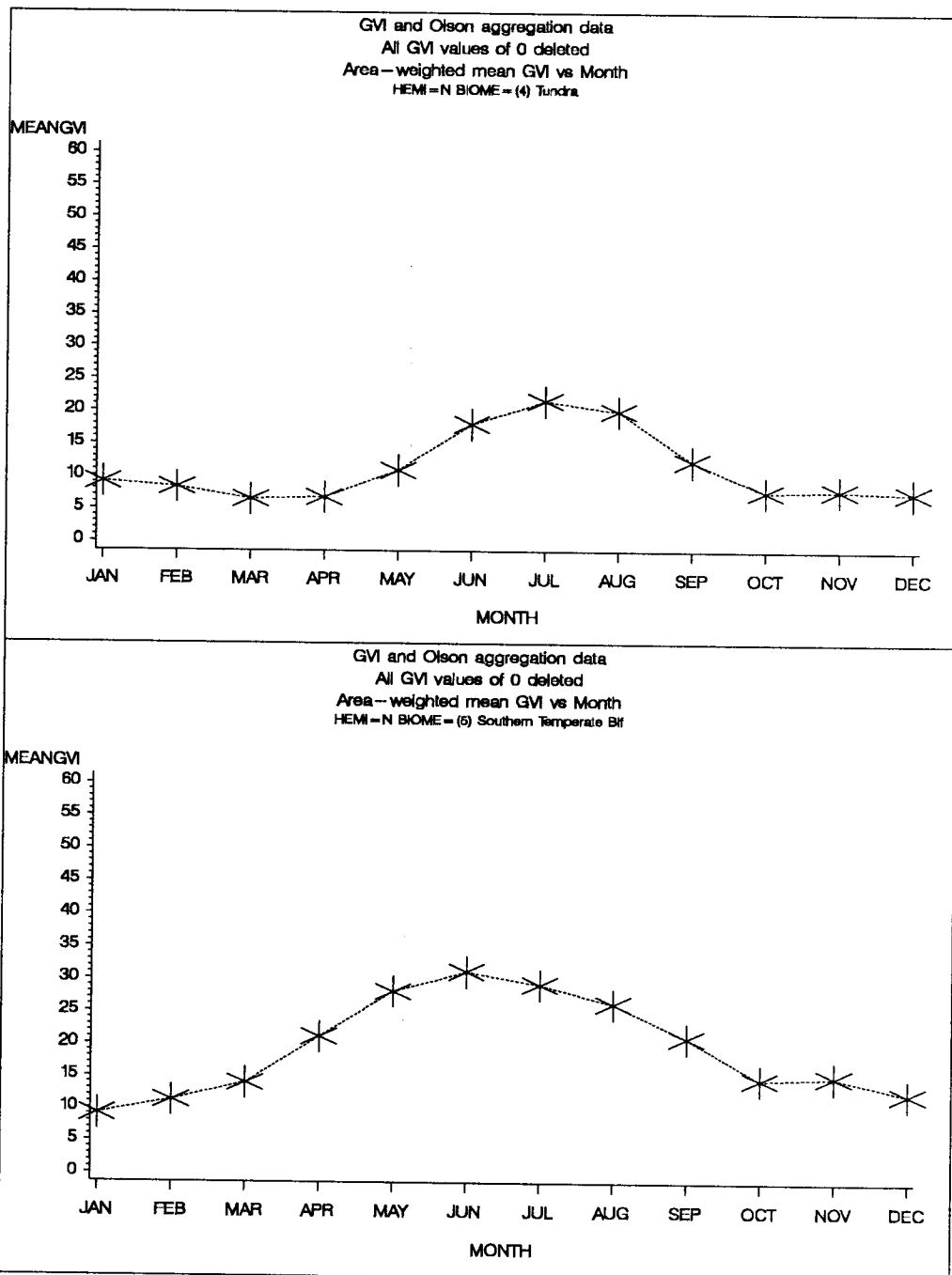
Biome	Olson Categories
NonpolarDesert	49 52 69 71
PolarDesert	50 51
Tundra	42 53 54 63
SouthernTemperateBLF	26
Grassland	40 64
Shrubland	41
Farms/Towns	30 31
NonpaddyIrrigatedDryland	37 38 39
Forest/Fields/Woods	55 56 57 58
NorthernTemperateBLF	25
CoolConiferHardwood	23 24
TropicalMontane	28
Wetlands/Hinterlands/Shore	44 45 65 66 67 68 72
DryForestandWoodland	32 43
Semi-aridWoodland	46 47 48 59
WarmConiferForest	27
Paddyland	36
Taiga	20 21 60 61 62
TropicalSeas.HumidBLF	29
Trop/Subt.HumidFrst	33 73
CoolConiferForest	22

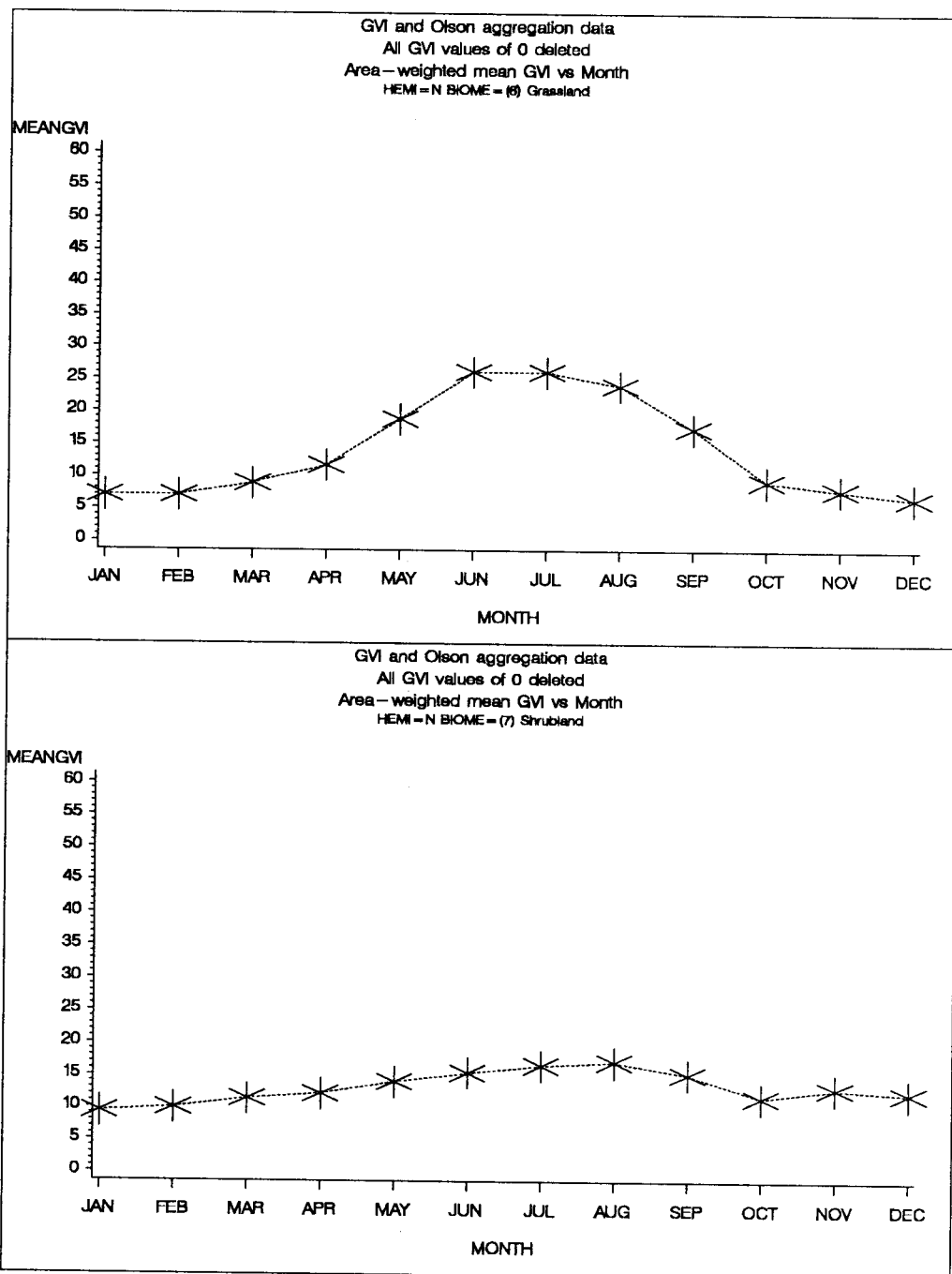
## **APPENDIX E**

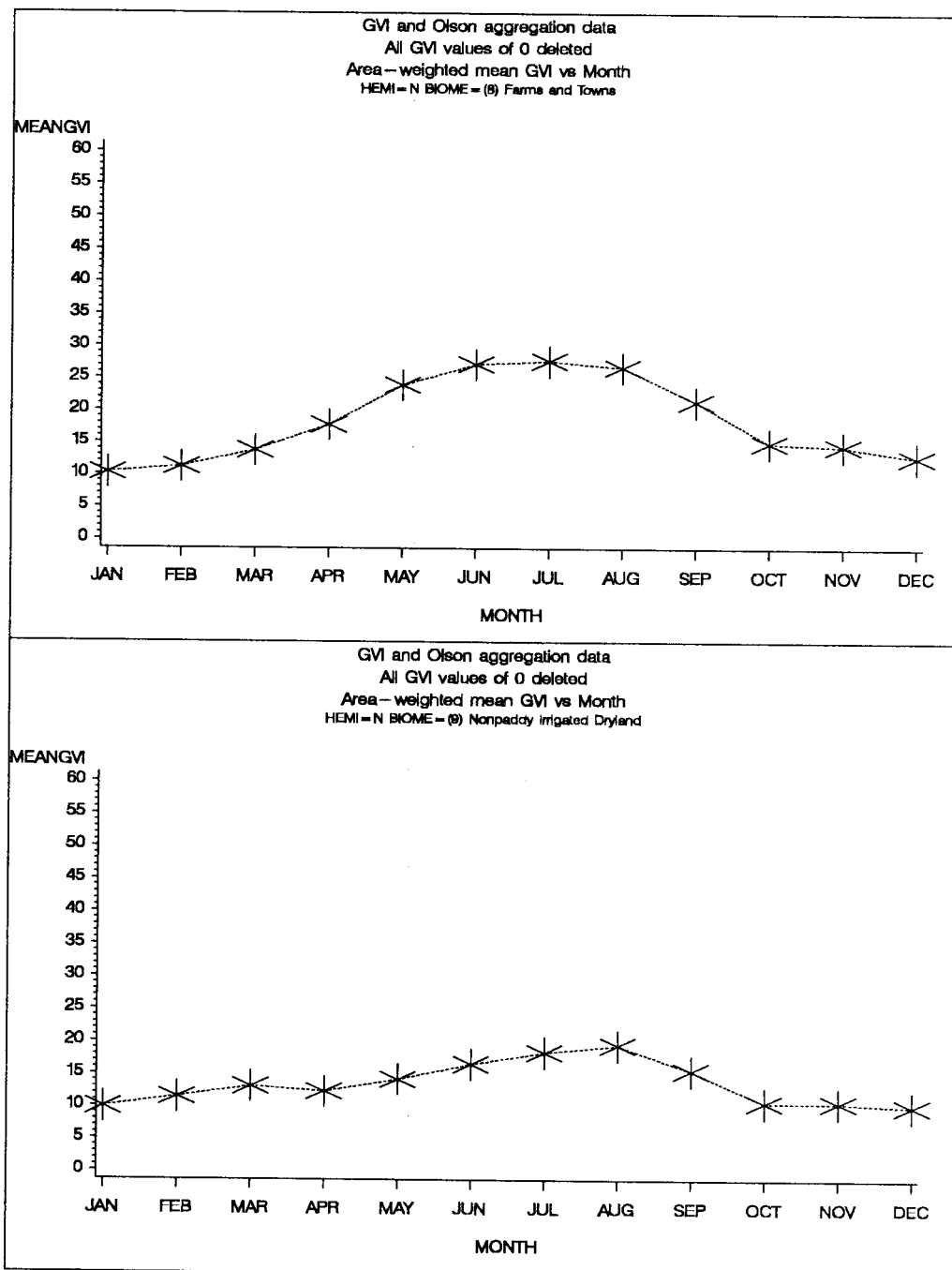
### **Temporal Profiles for Each Biome**



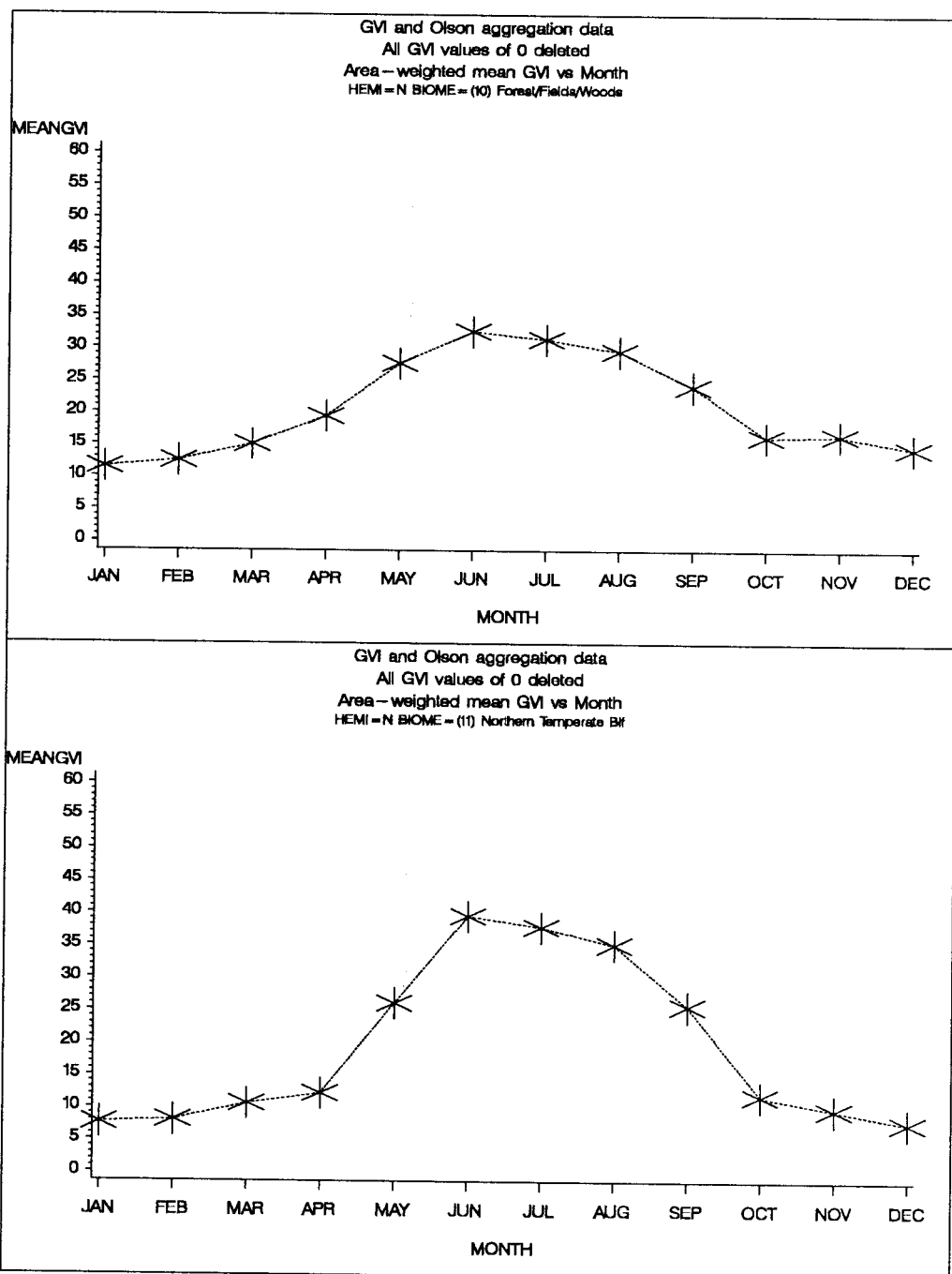


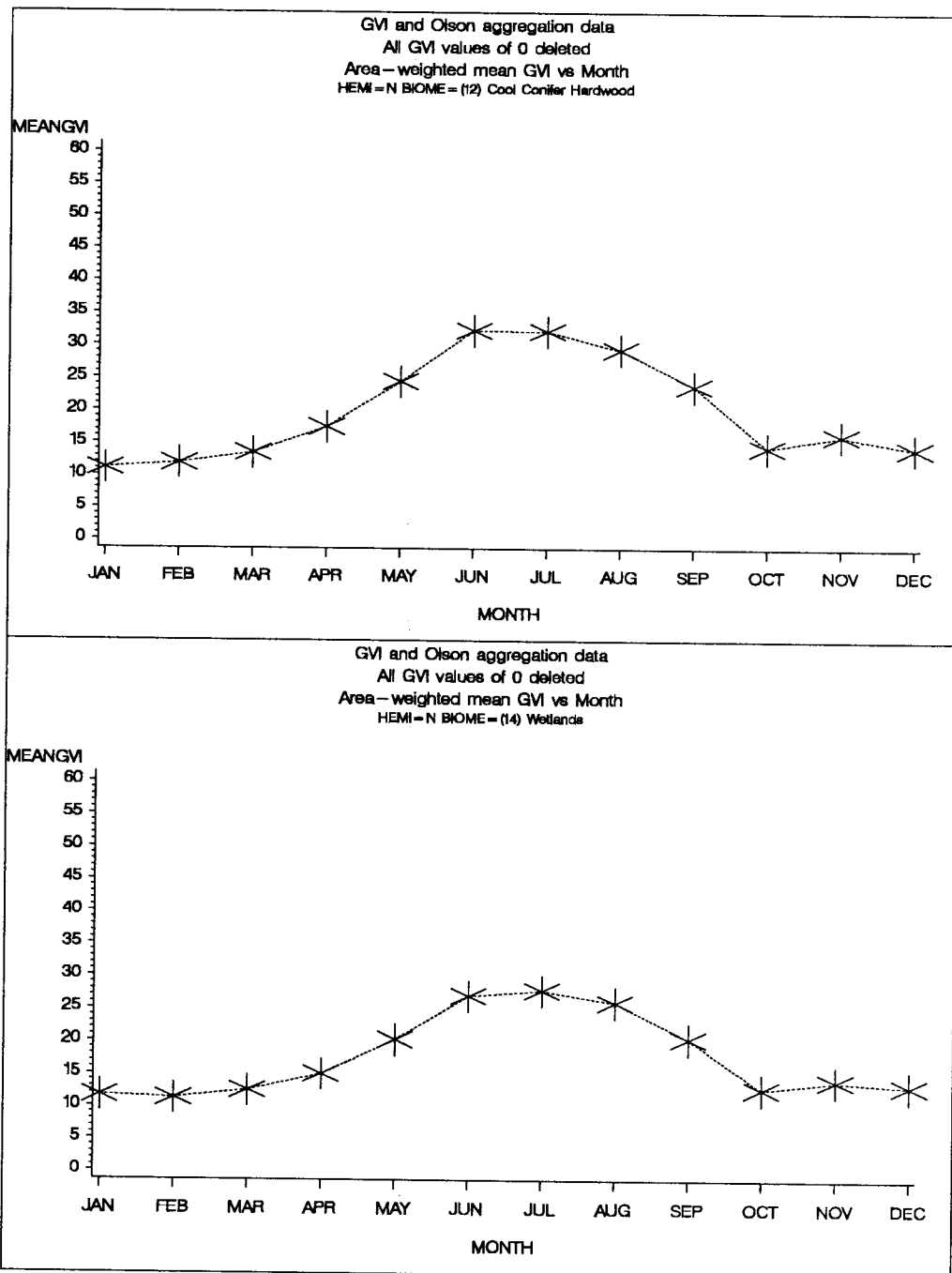


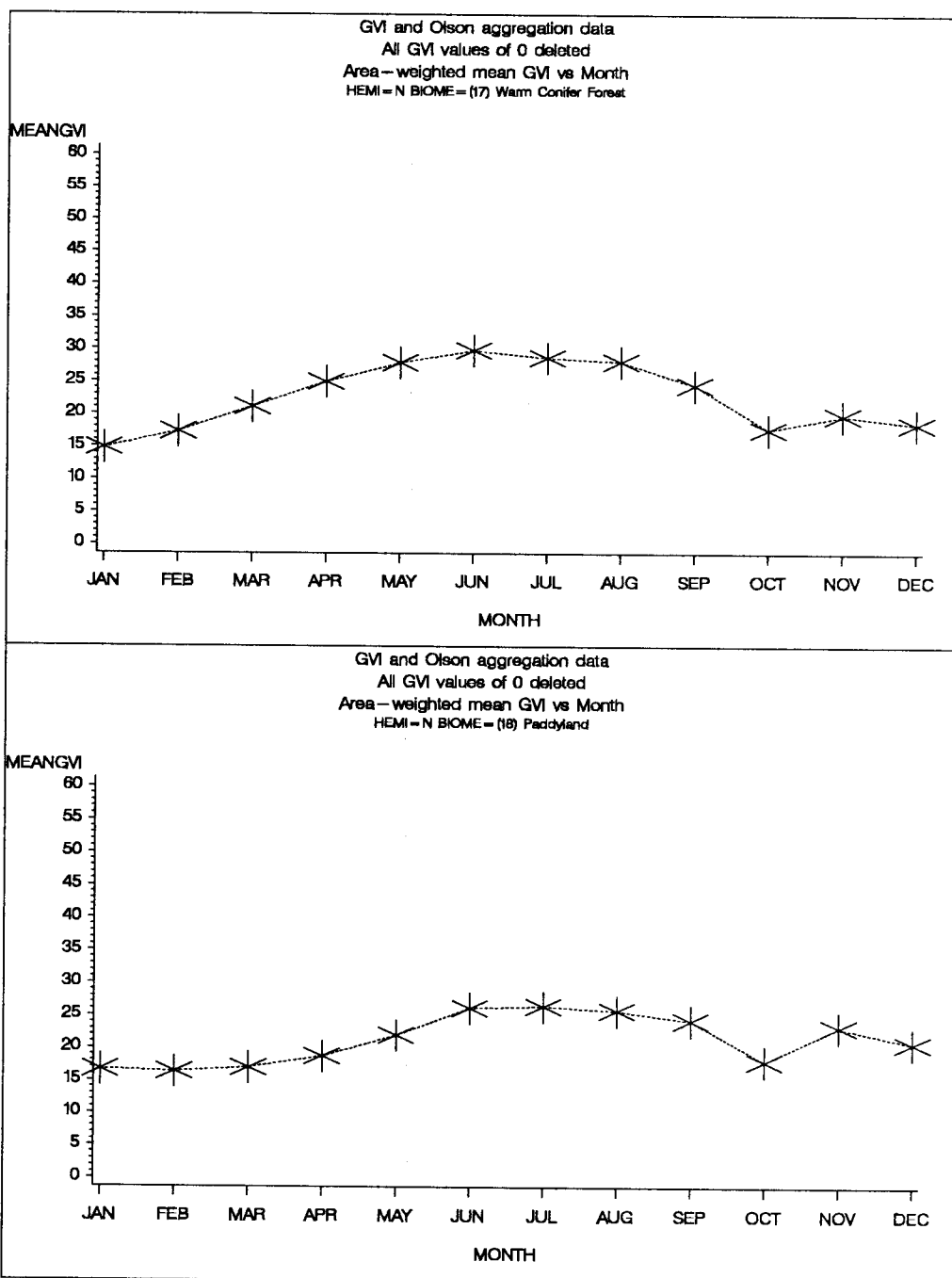


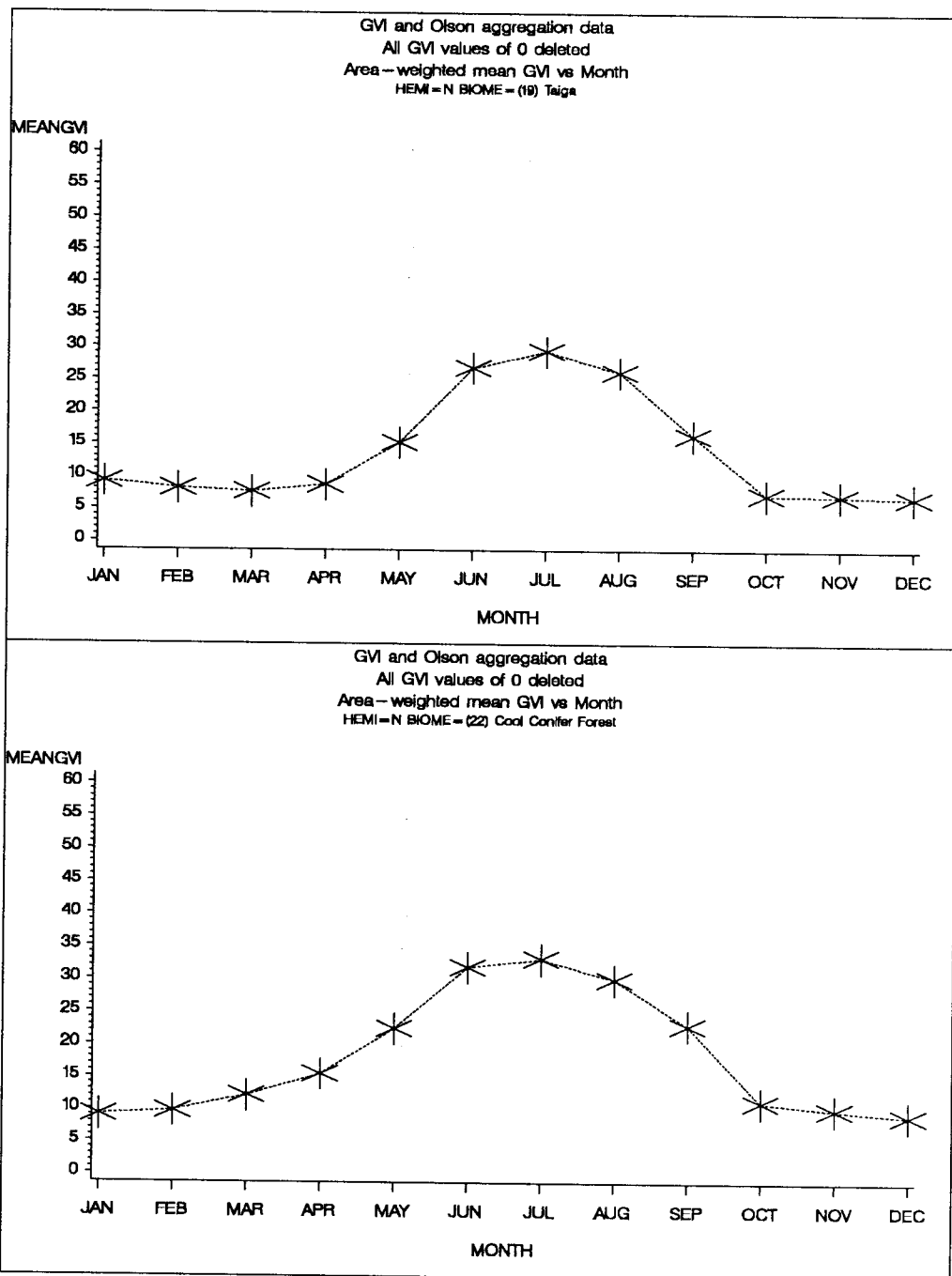


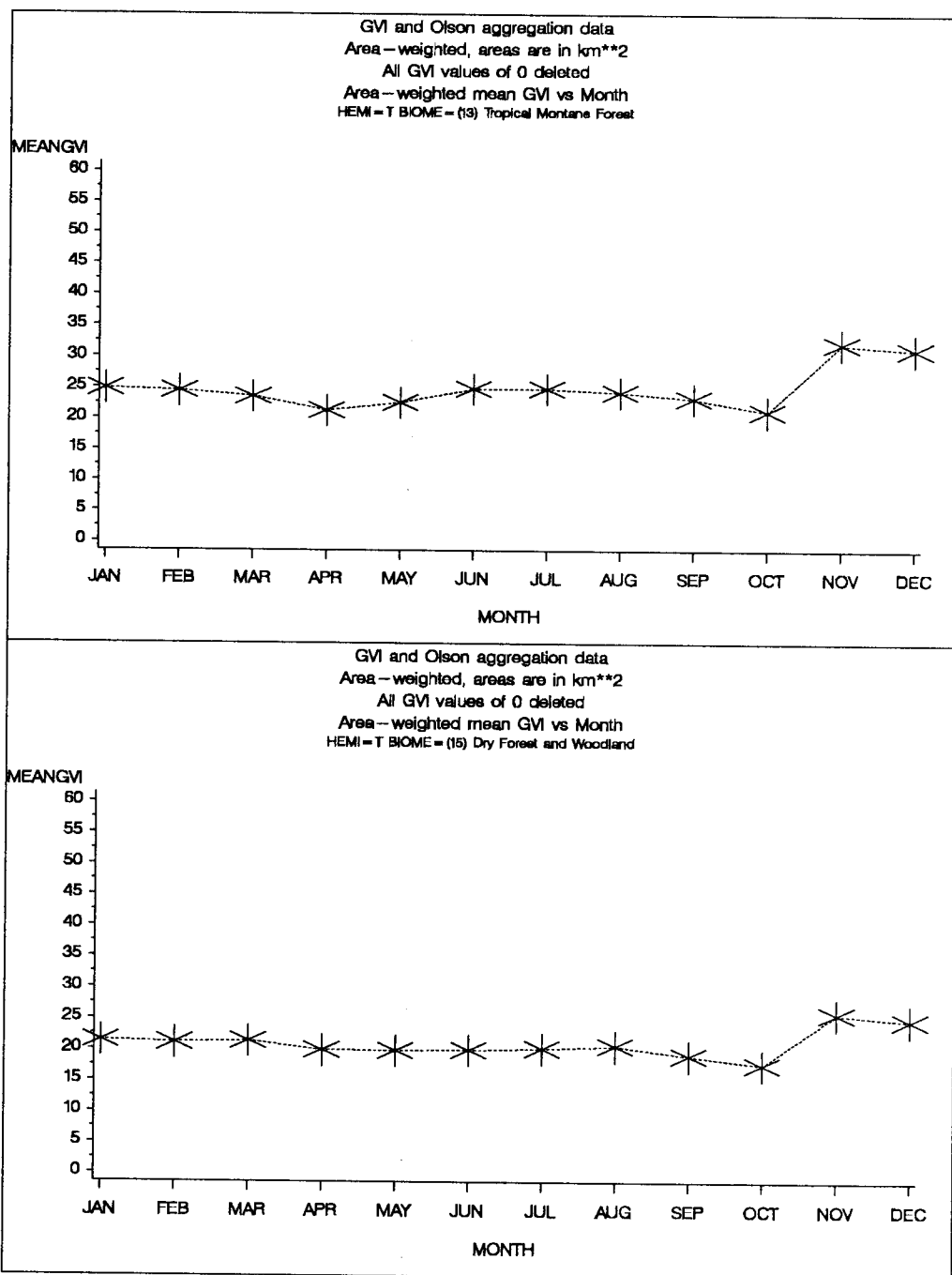


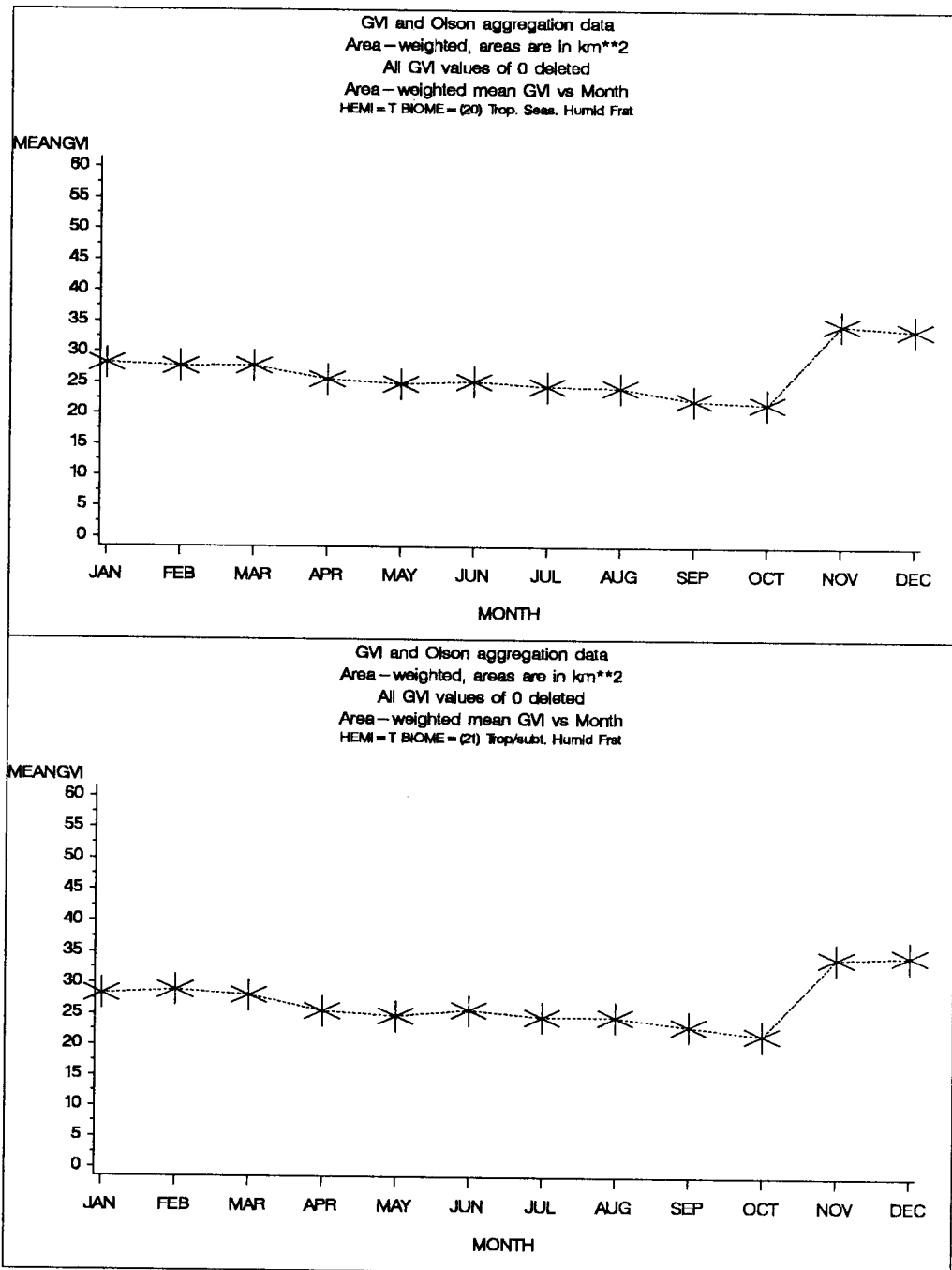


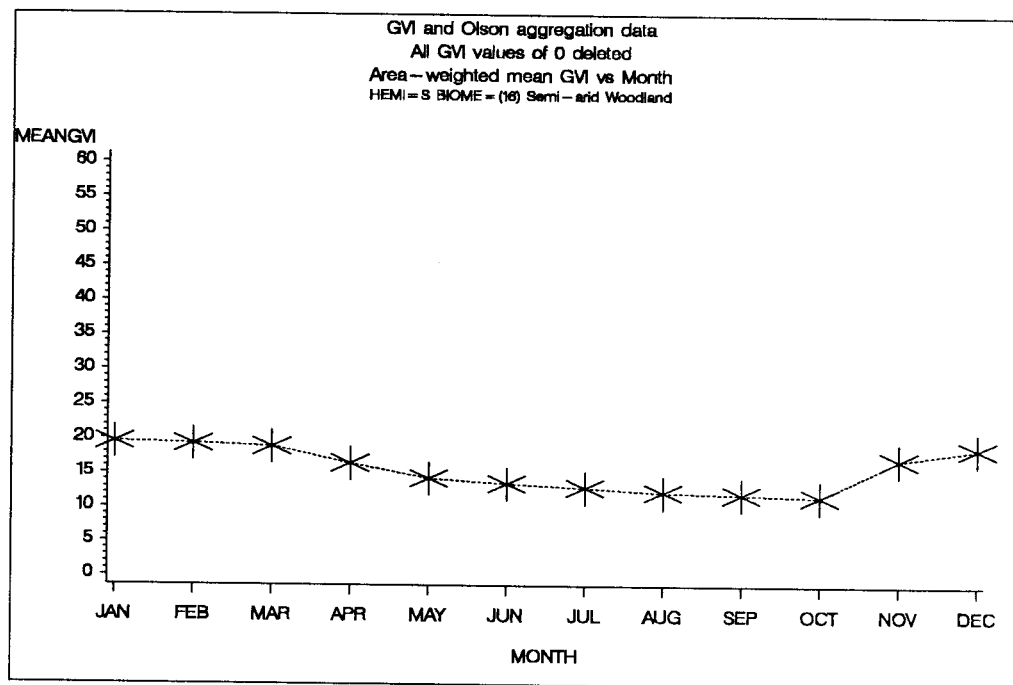








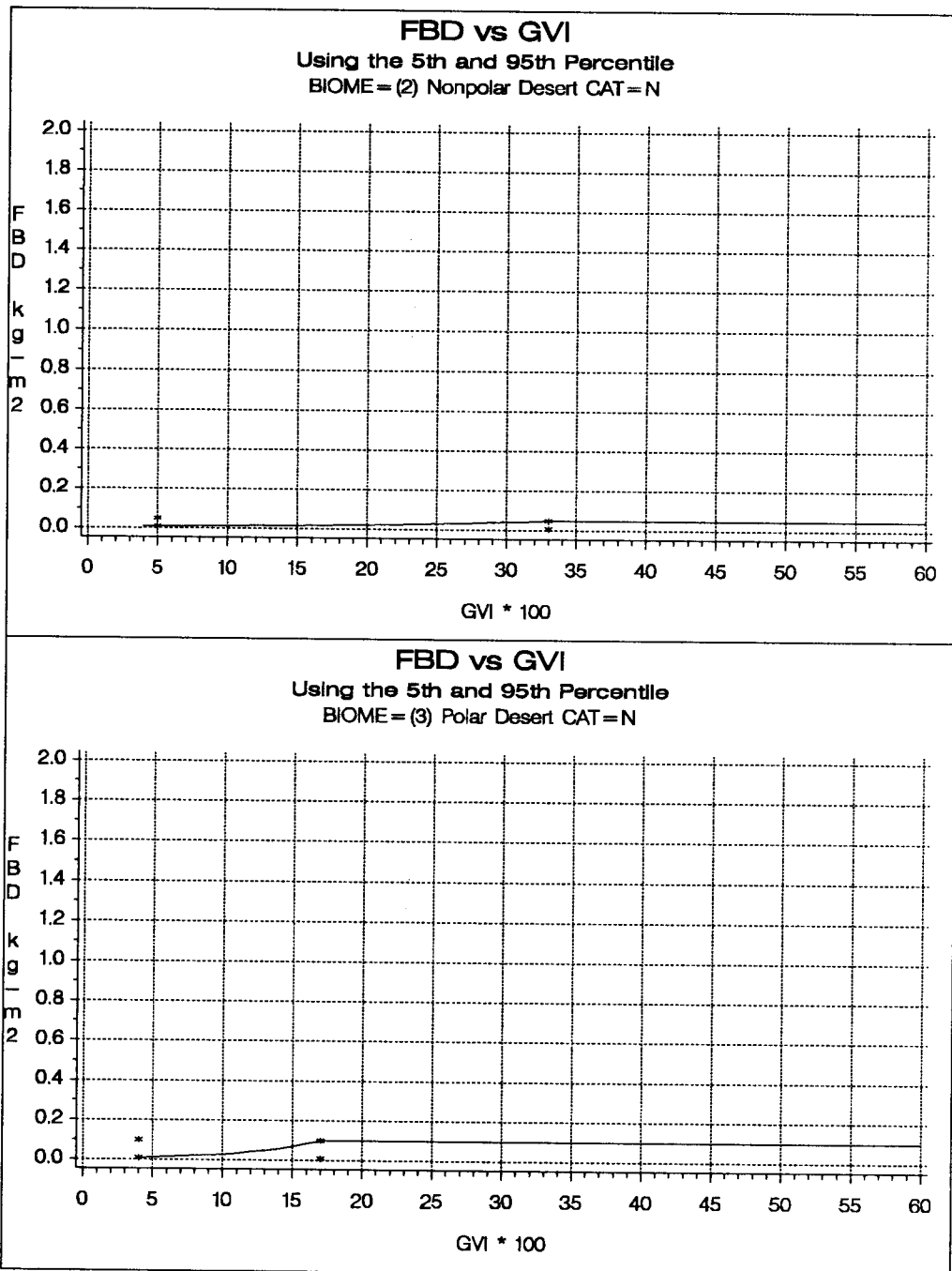


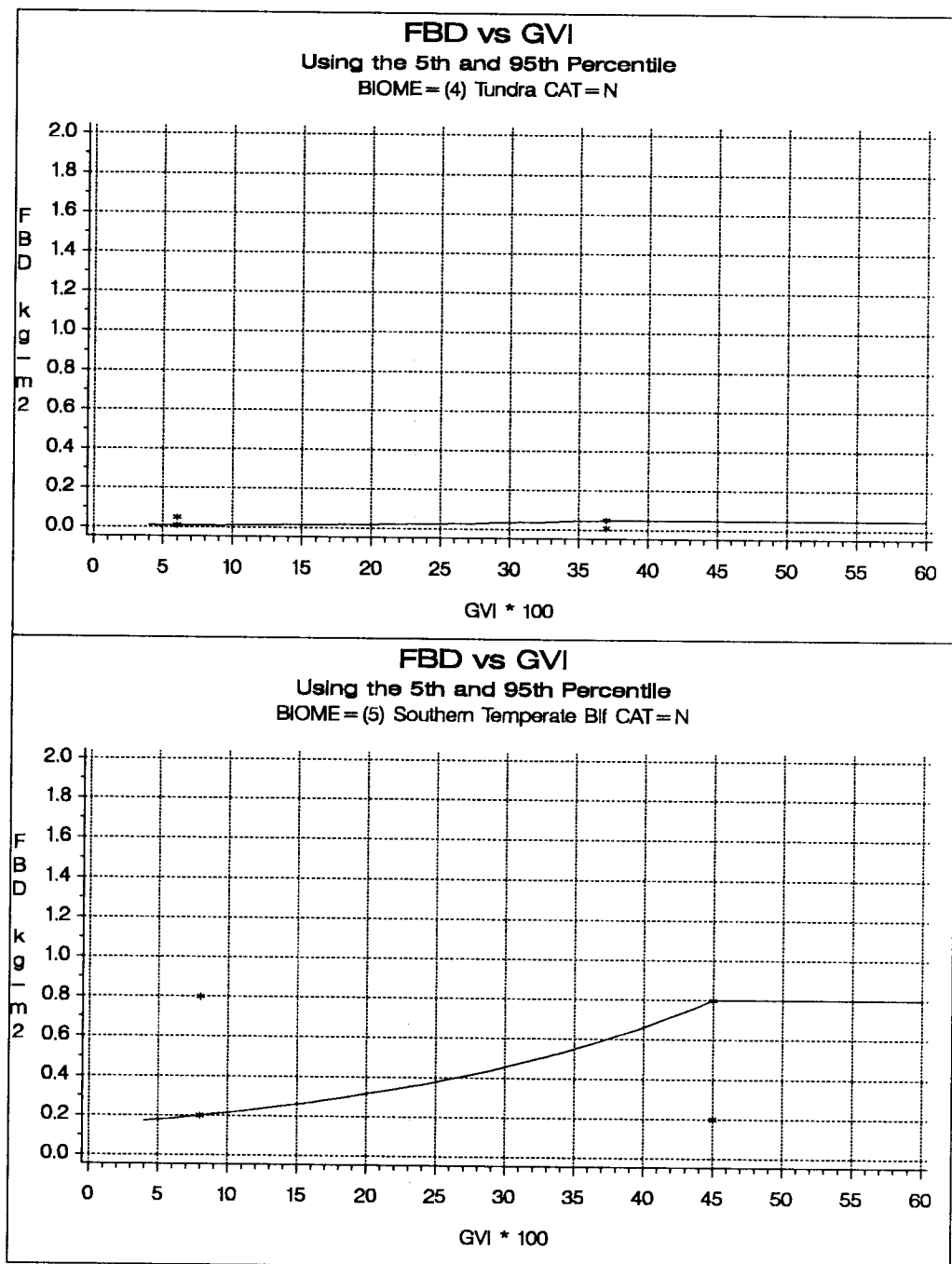


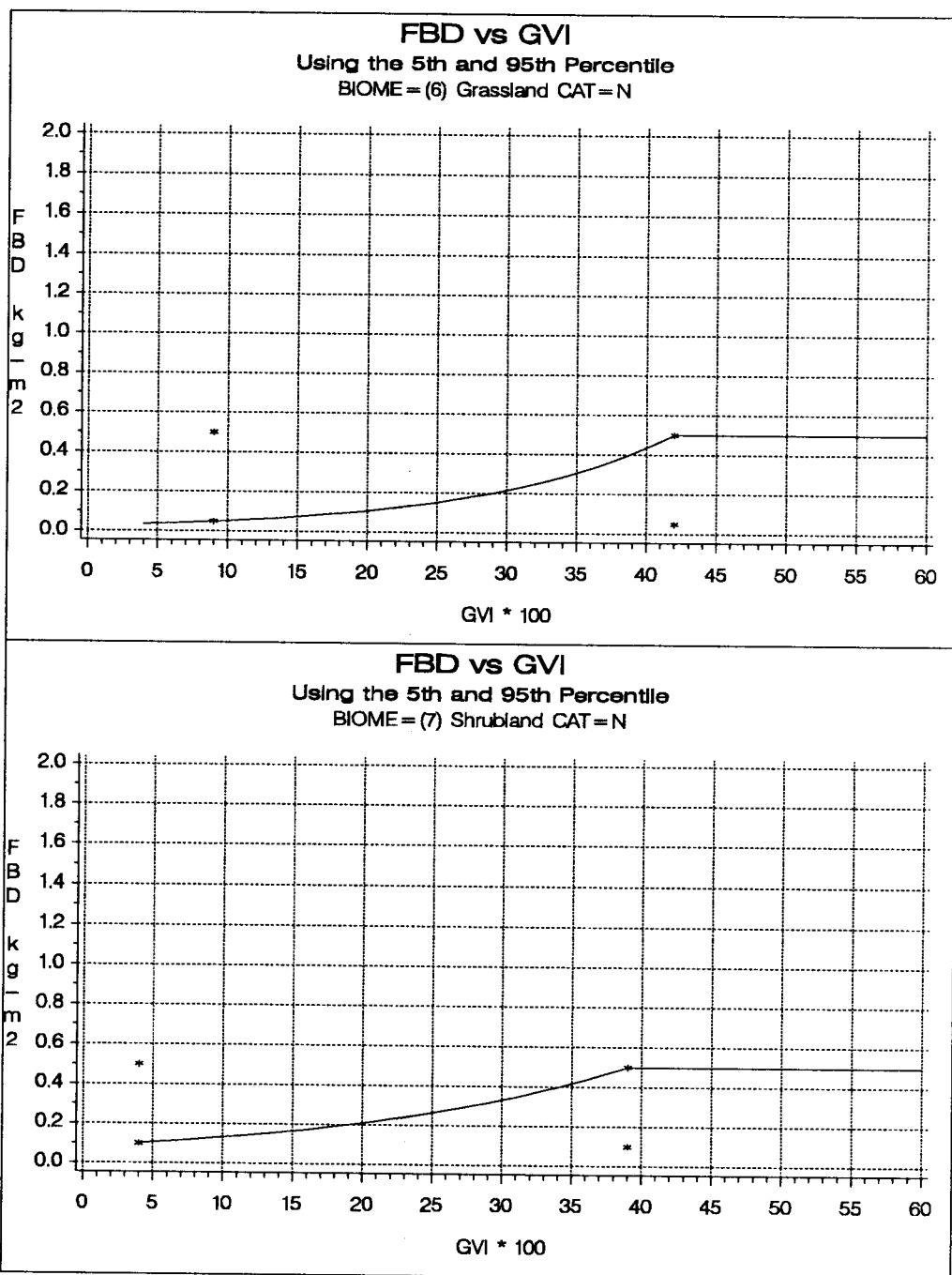
## **APPENDIX F**

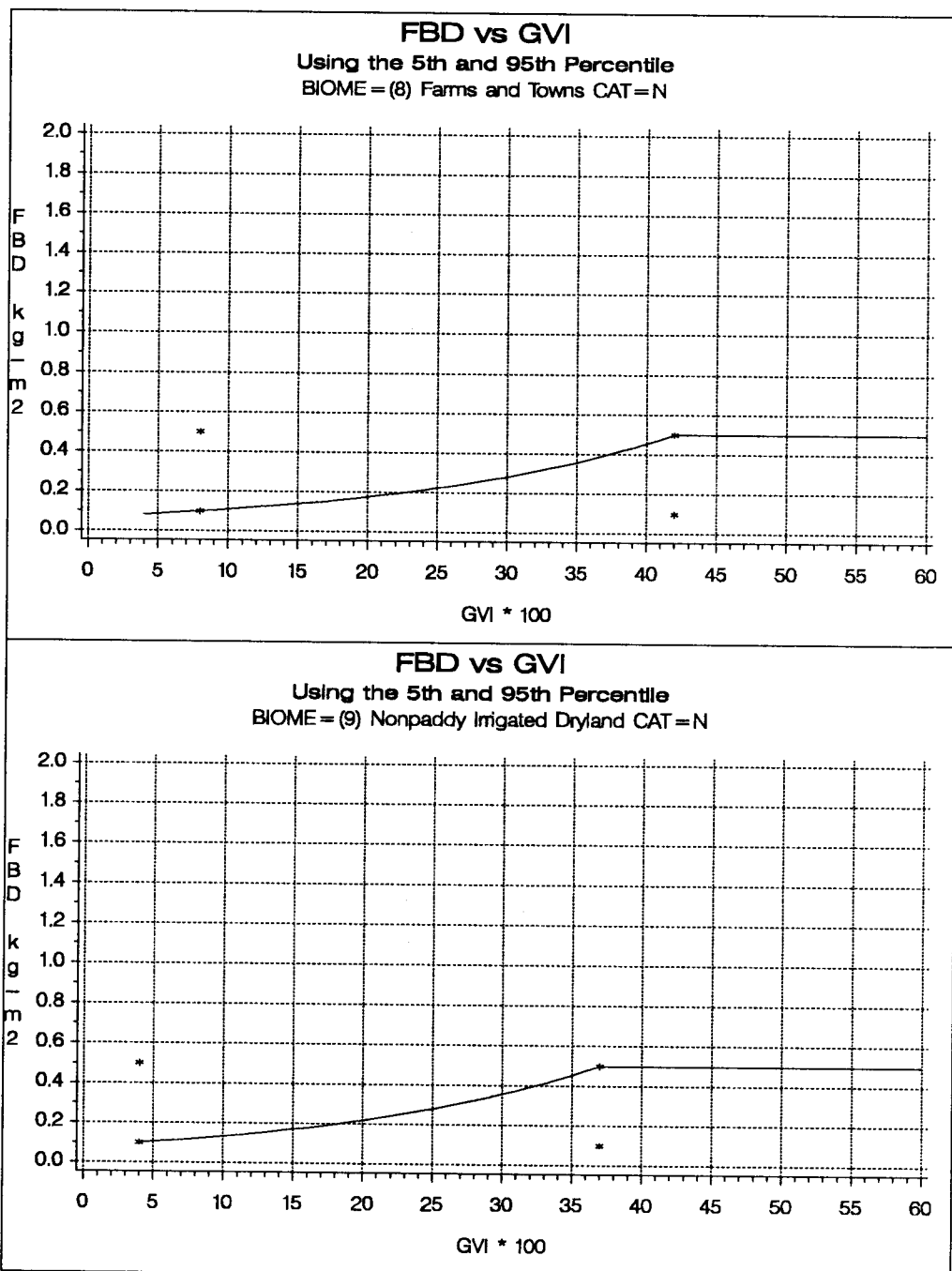
### **Calibration Curves for Each Biome**

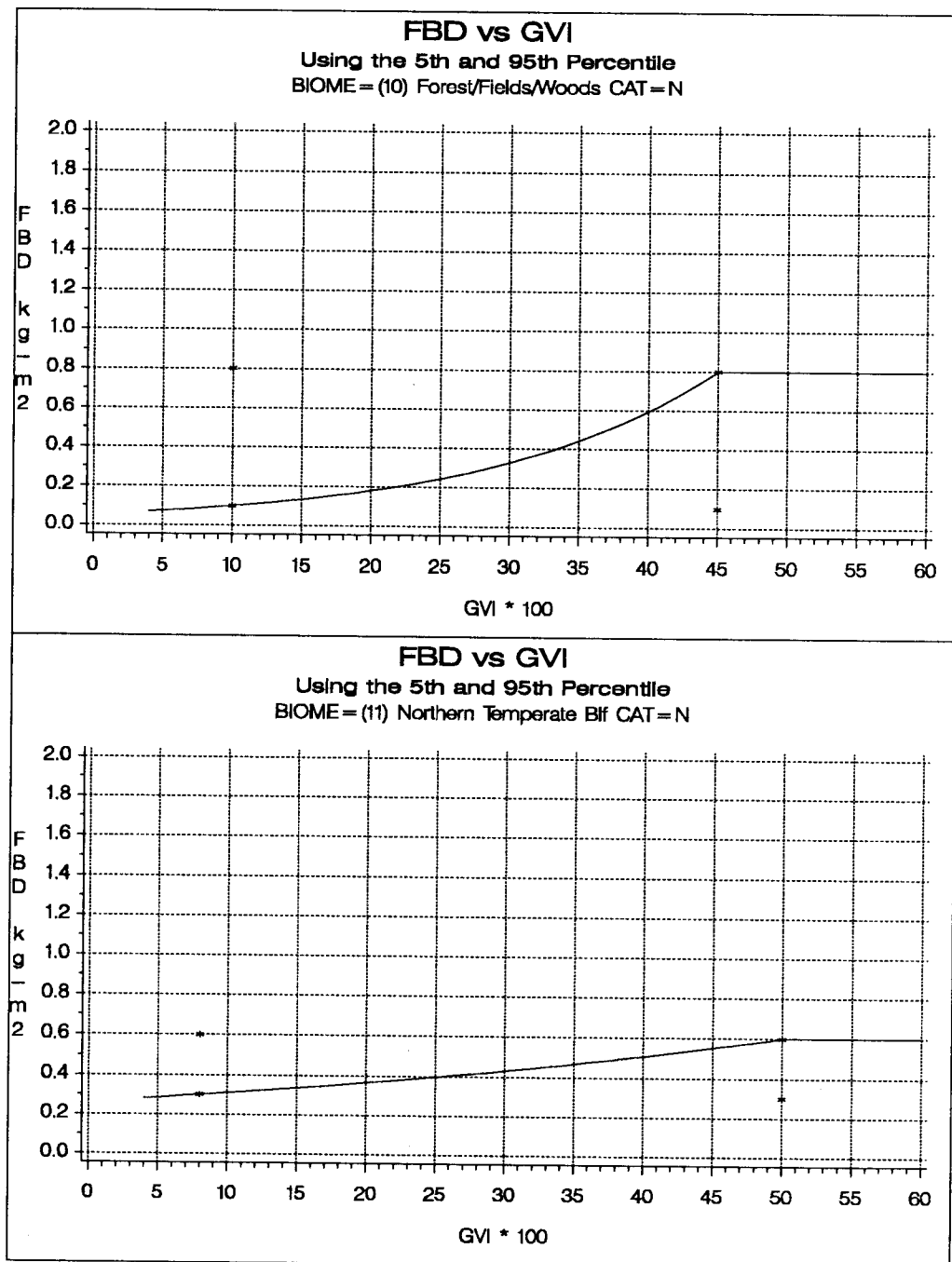


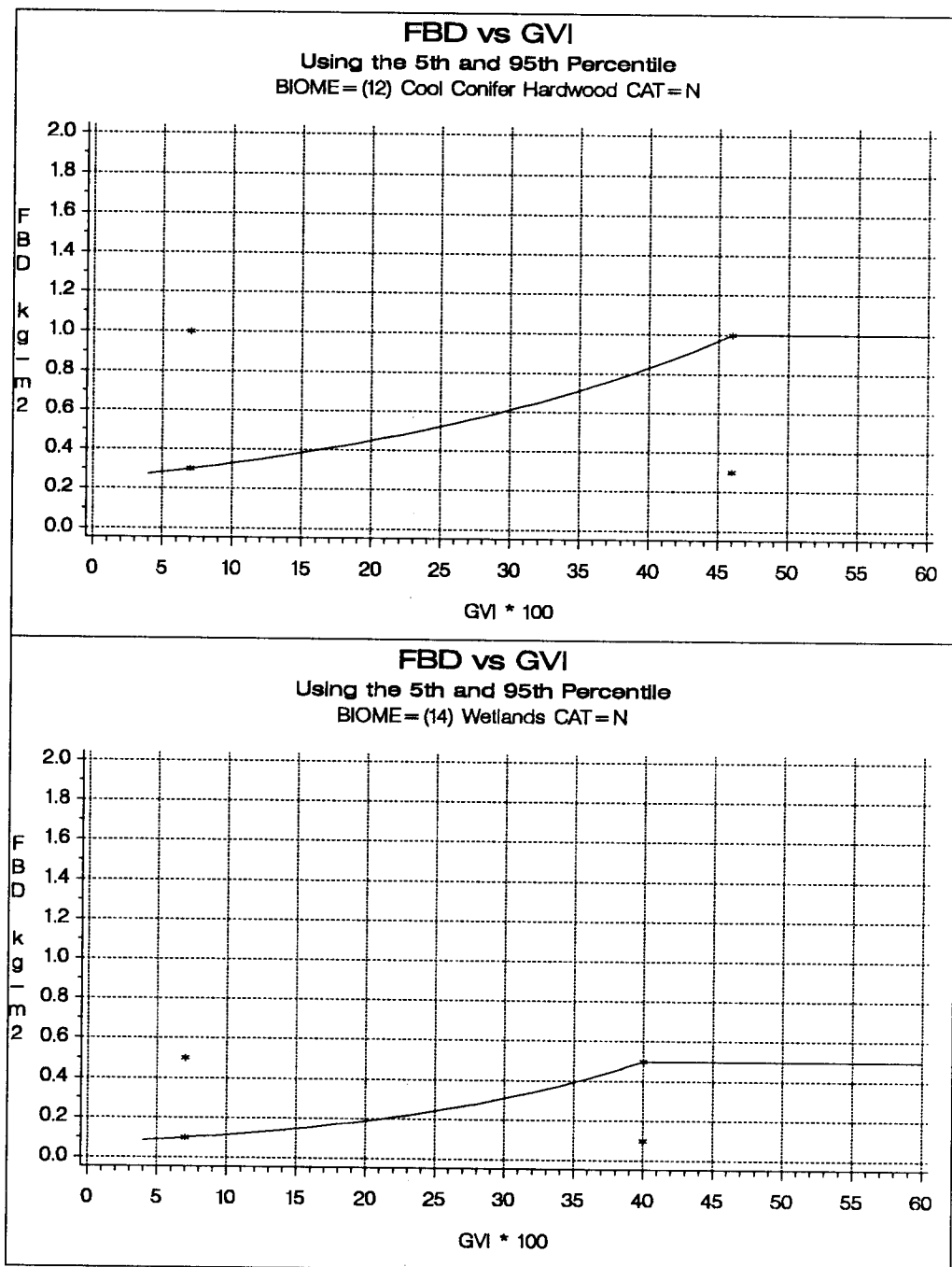


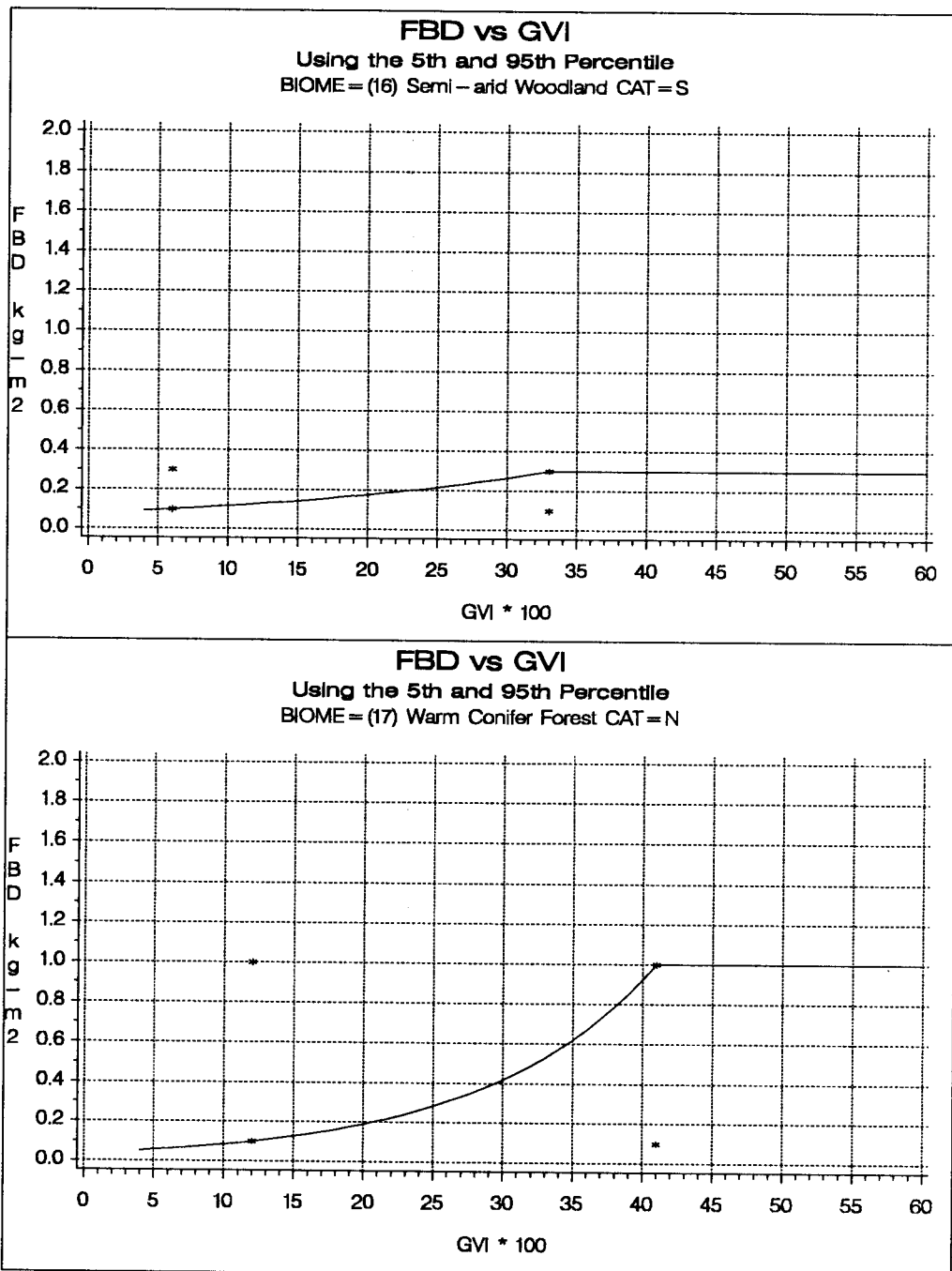


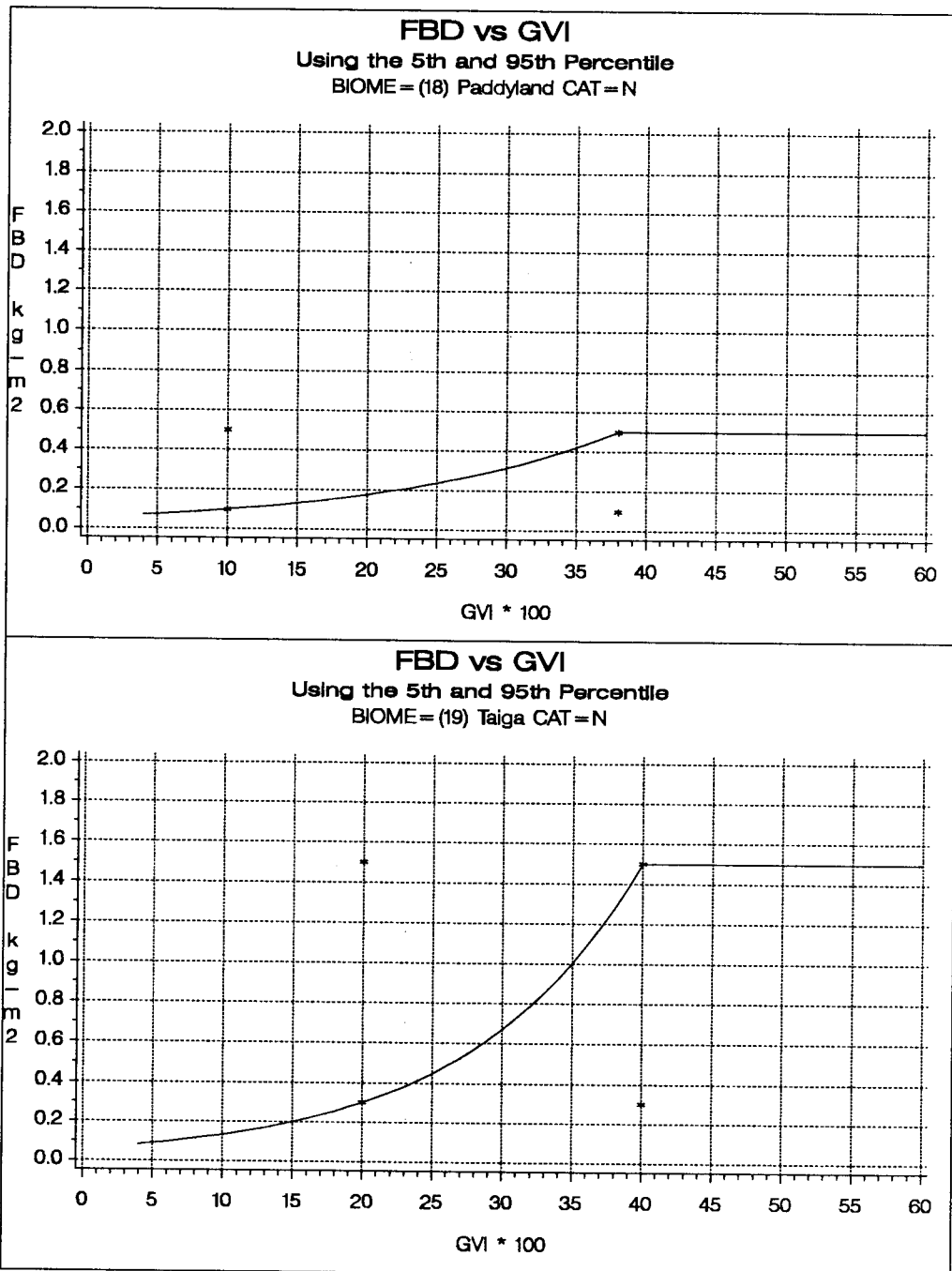




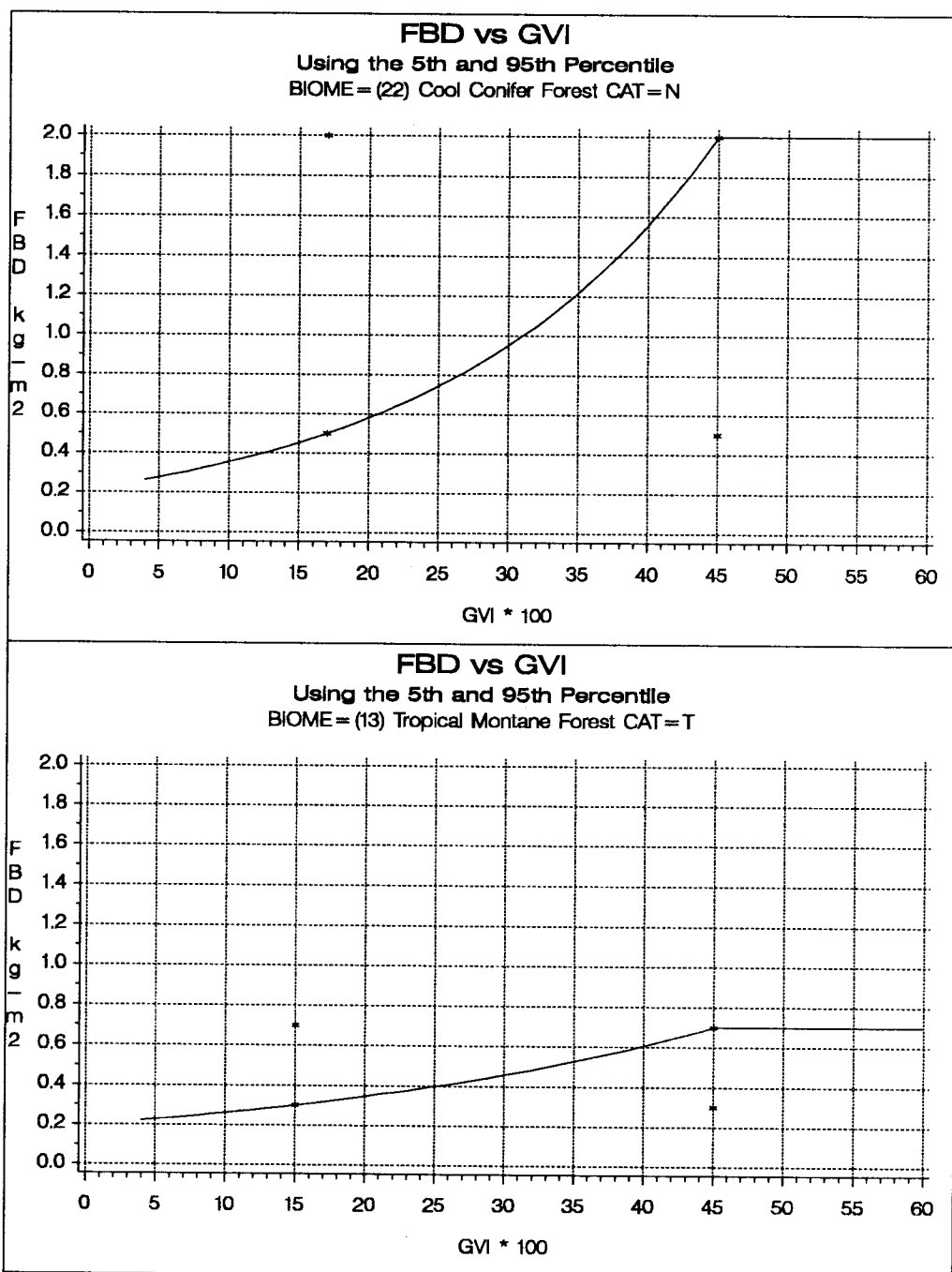


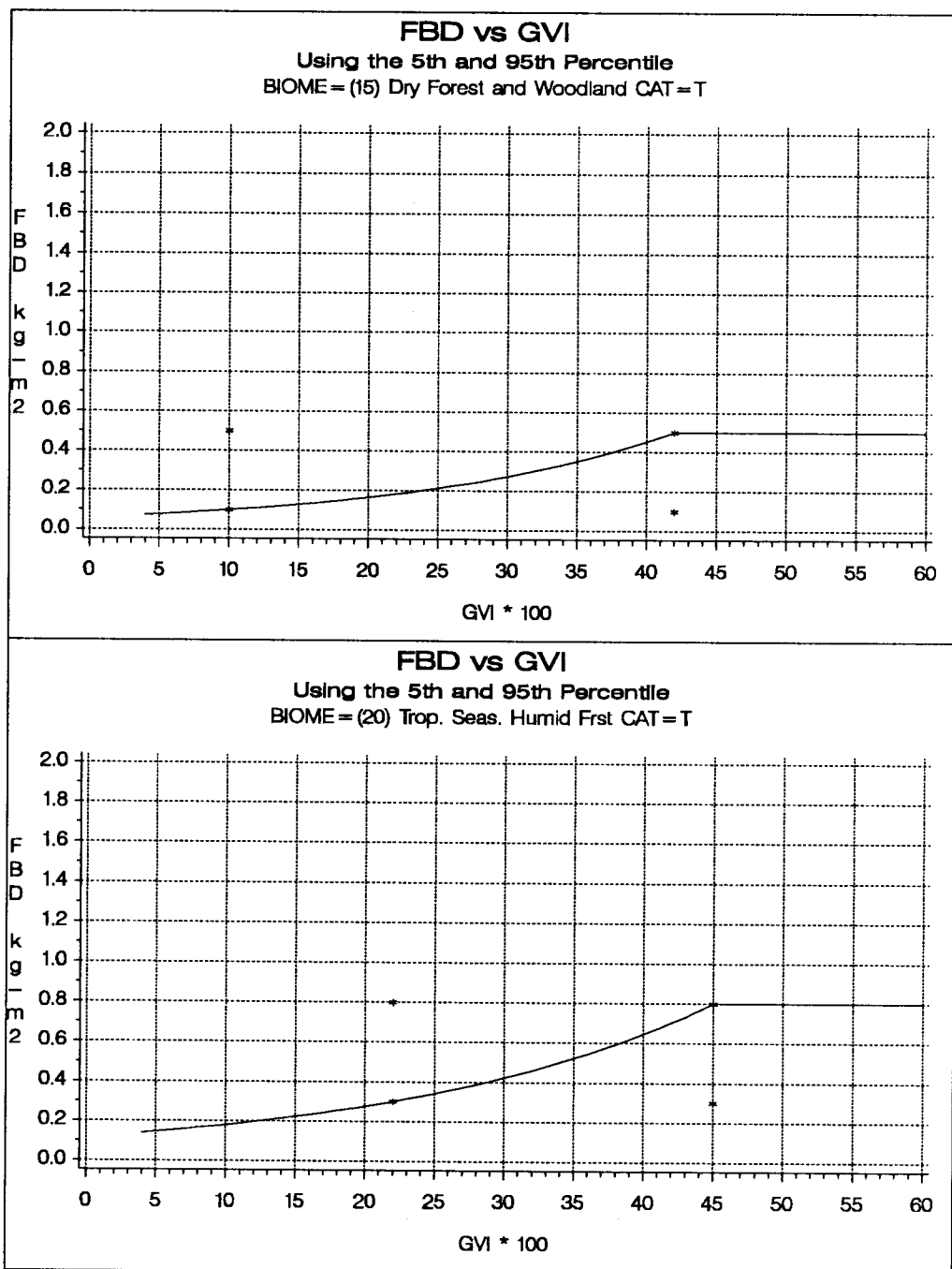


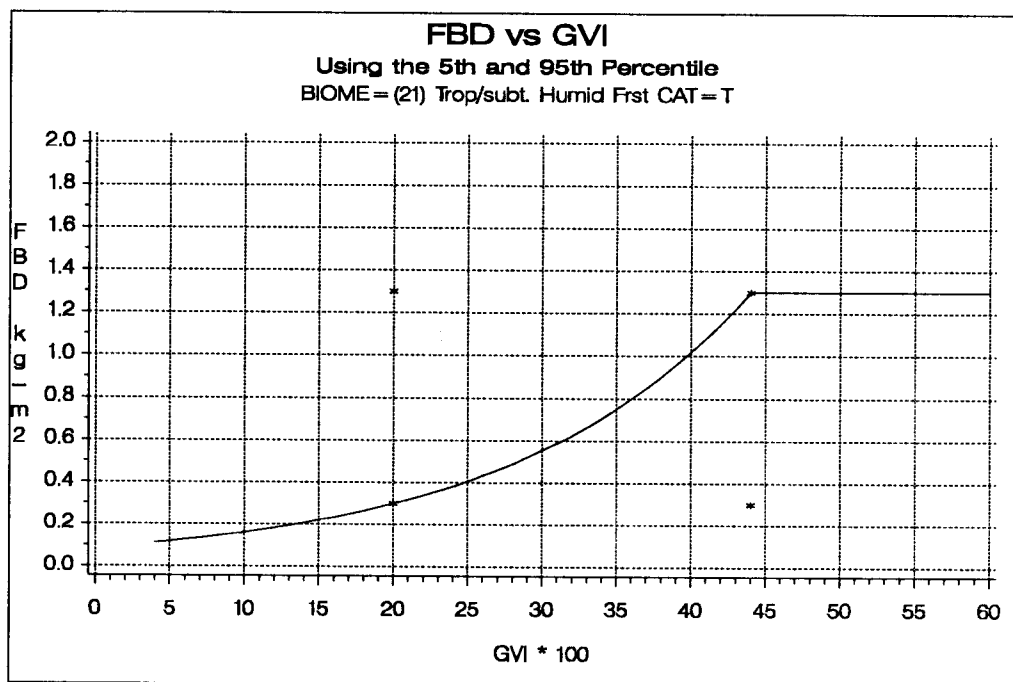






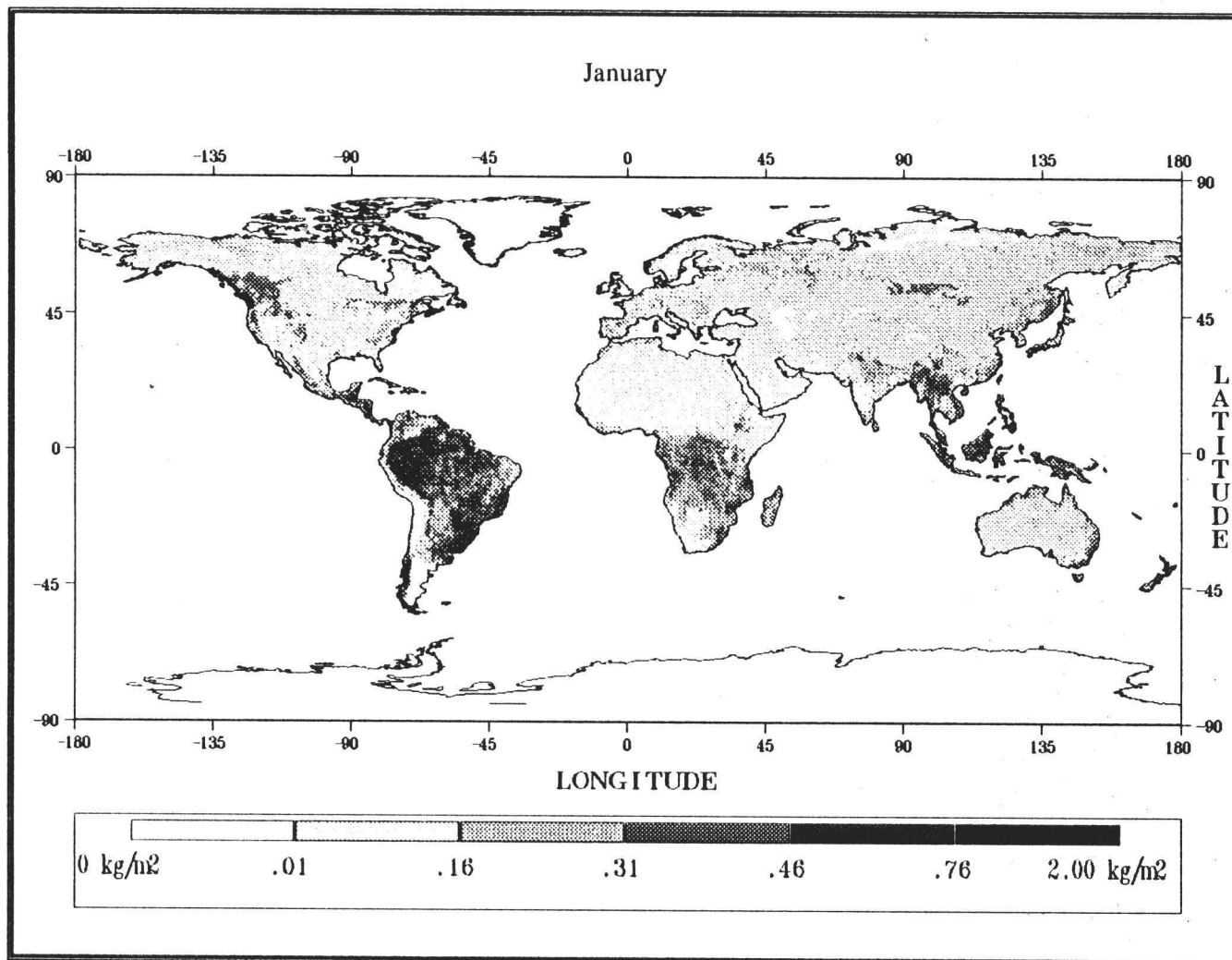


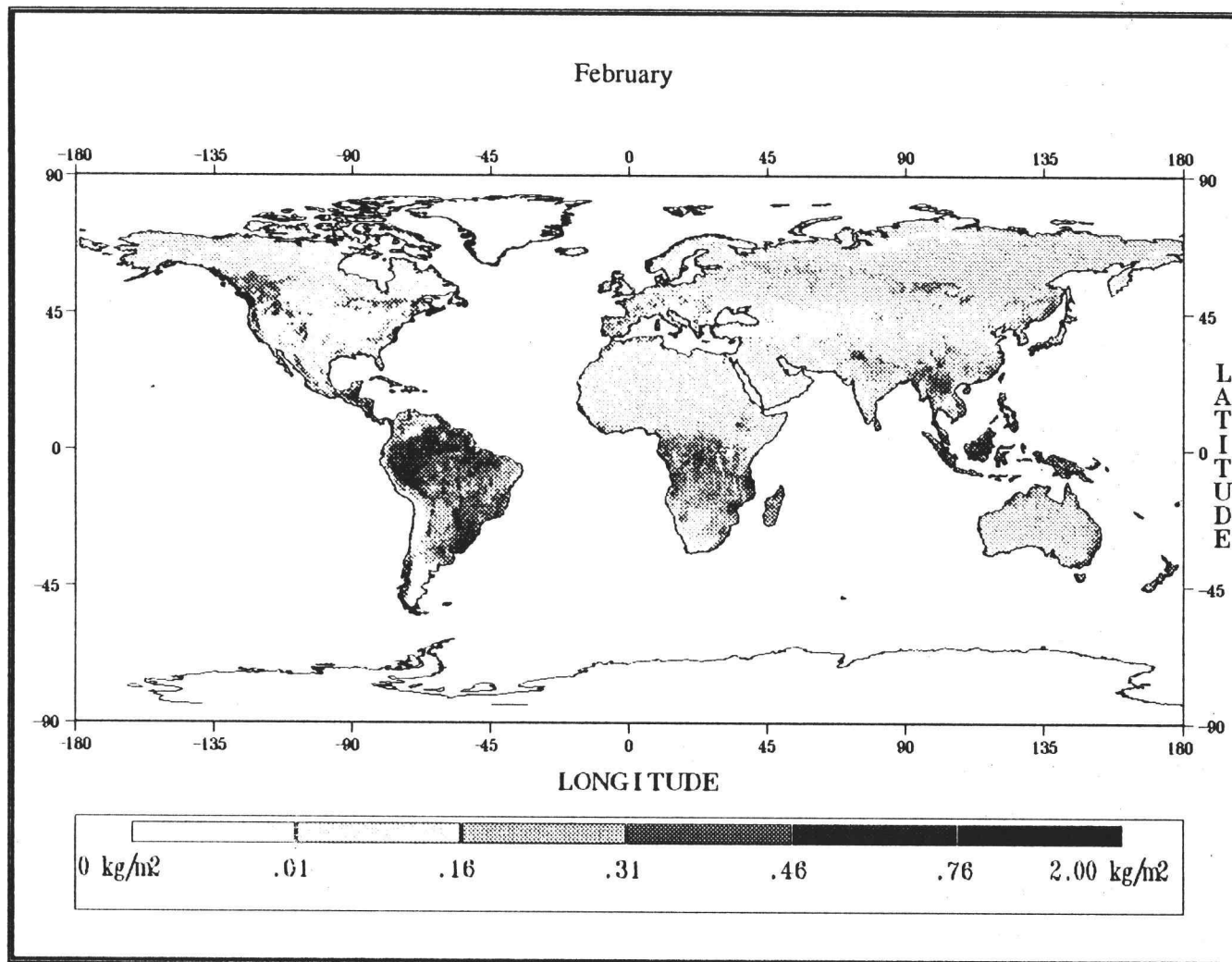


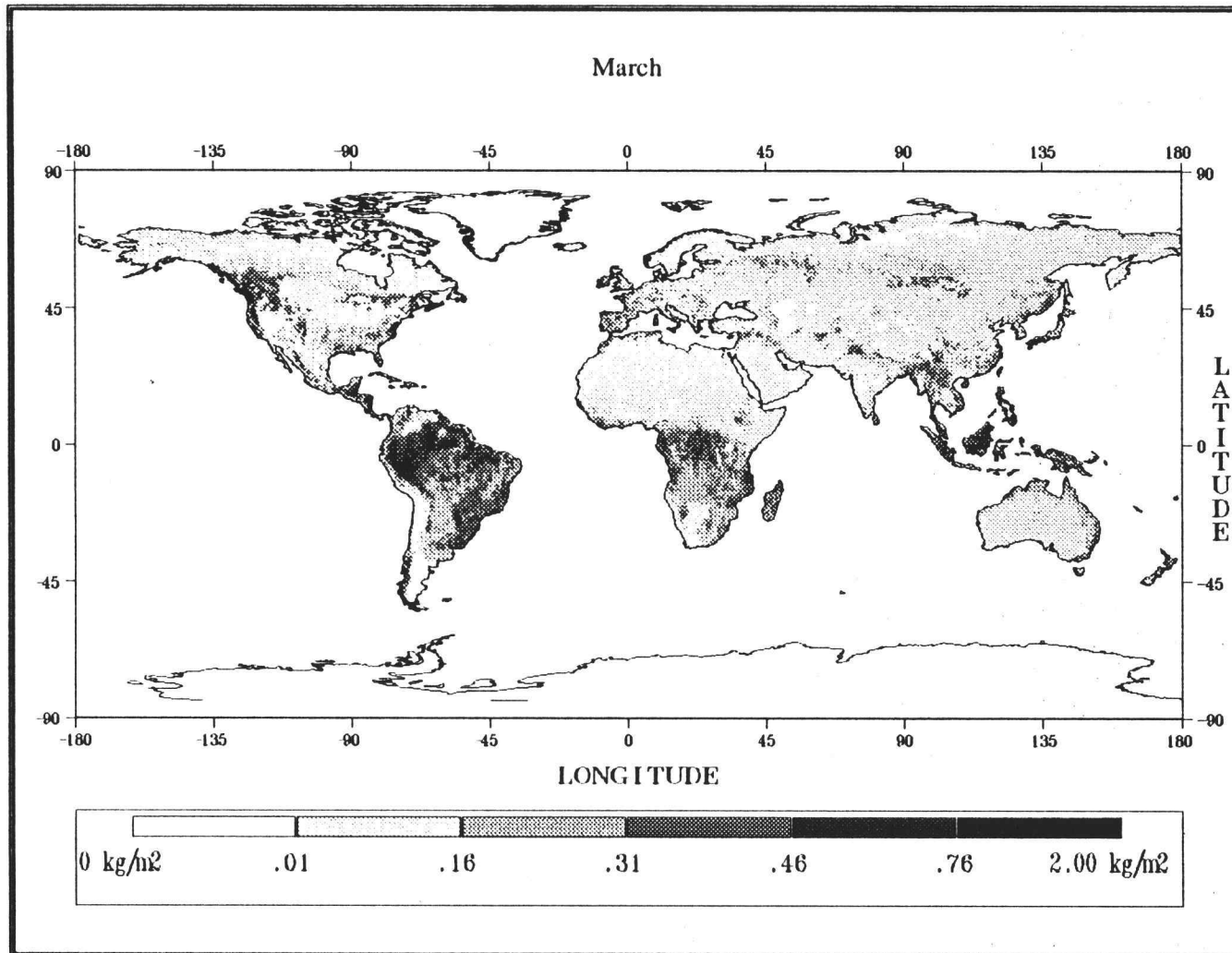


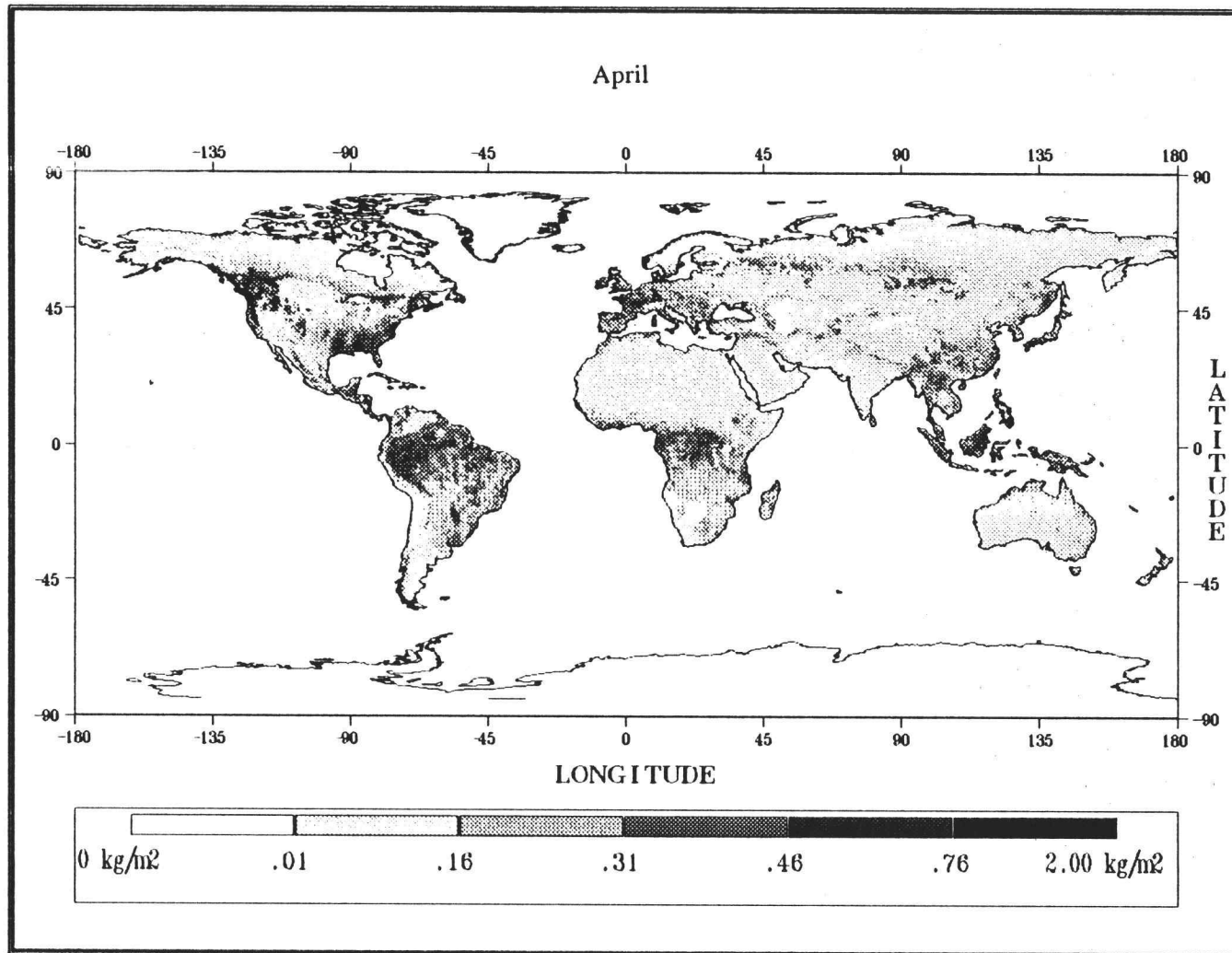
**APPENDIX G**

Monthly FBD Surfaces, January through December

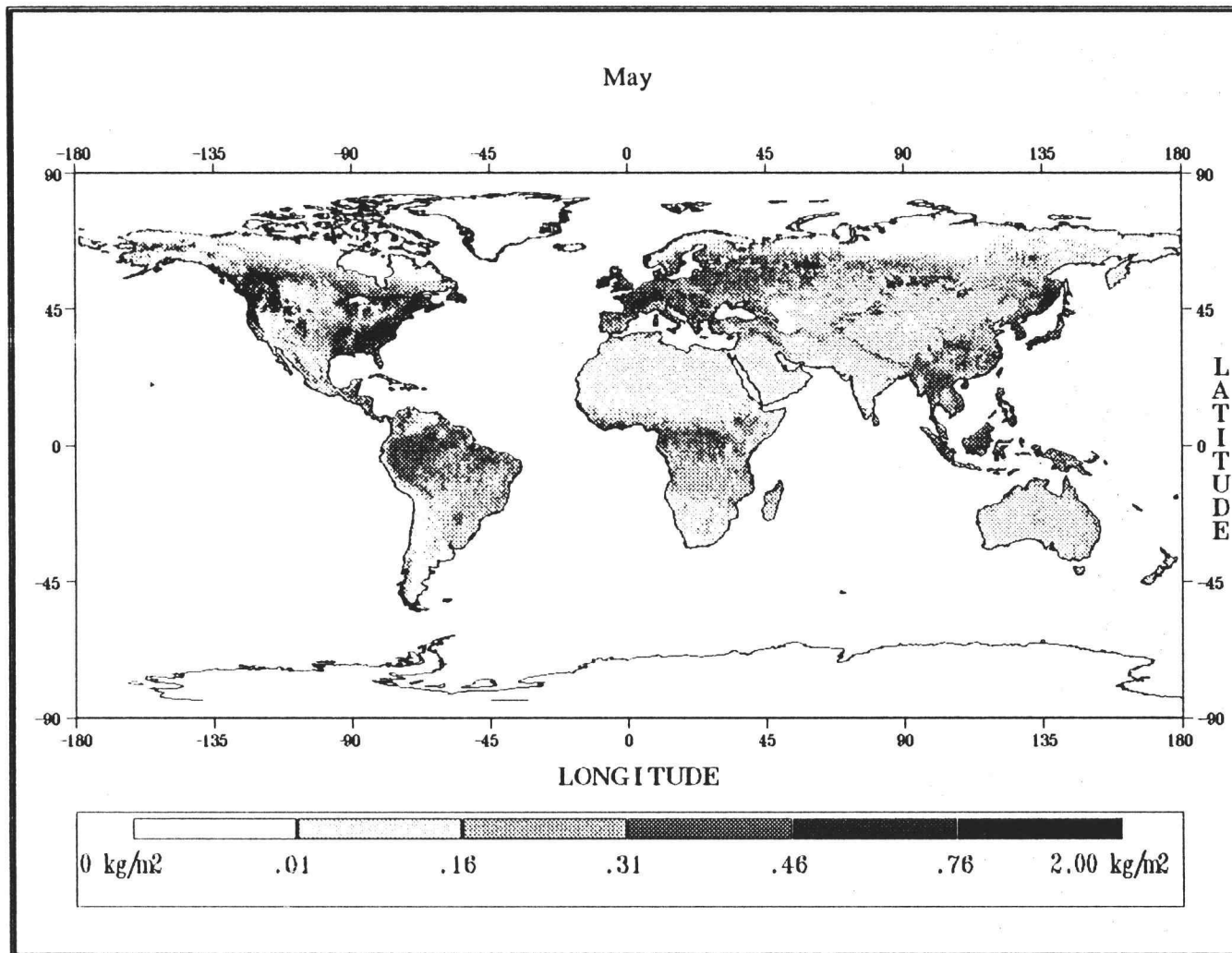


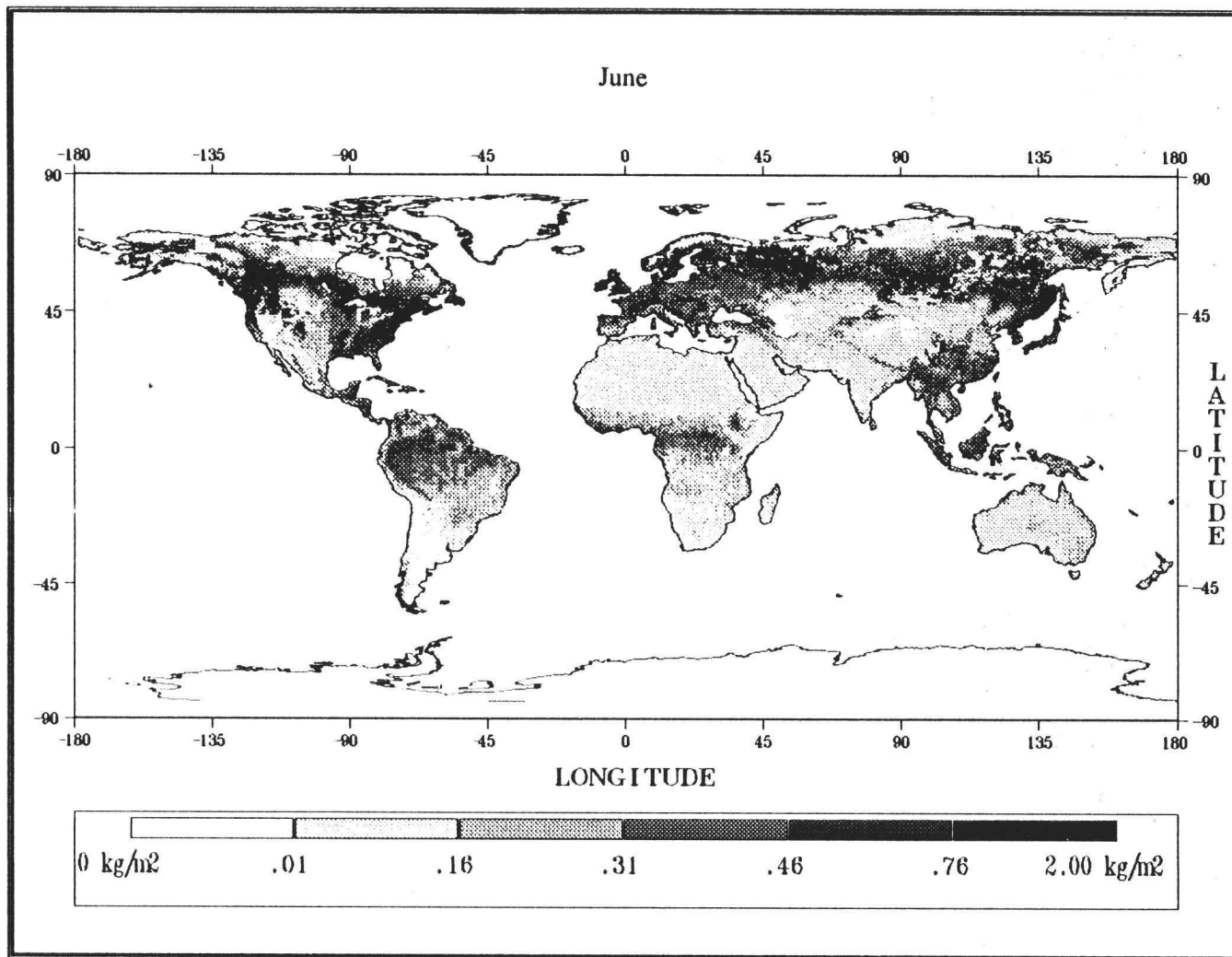


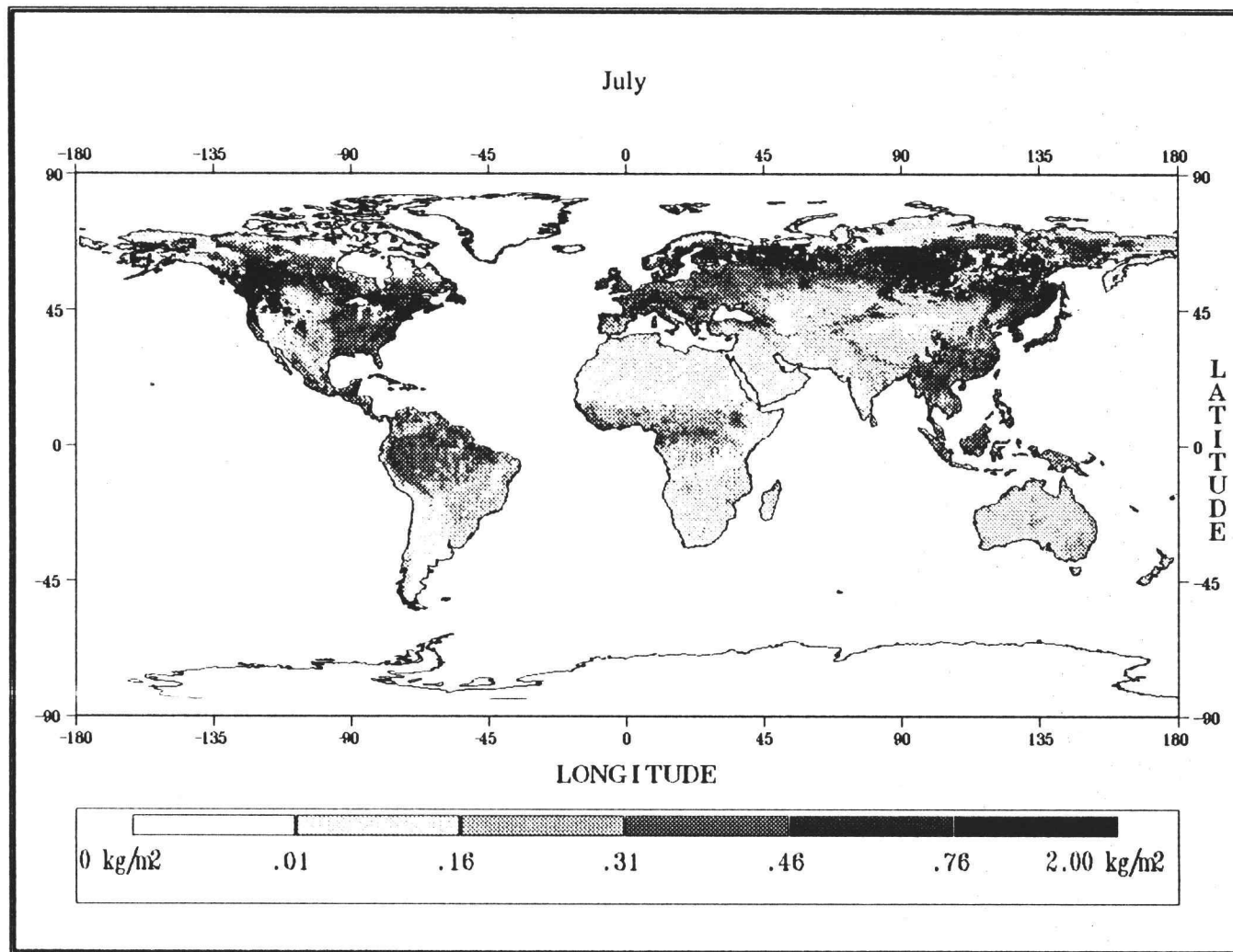


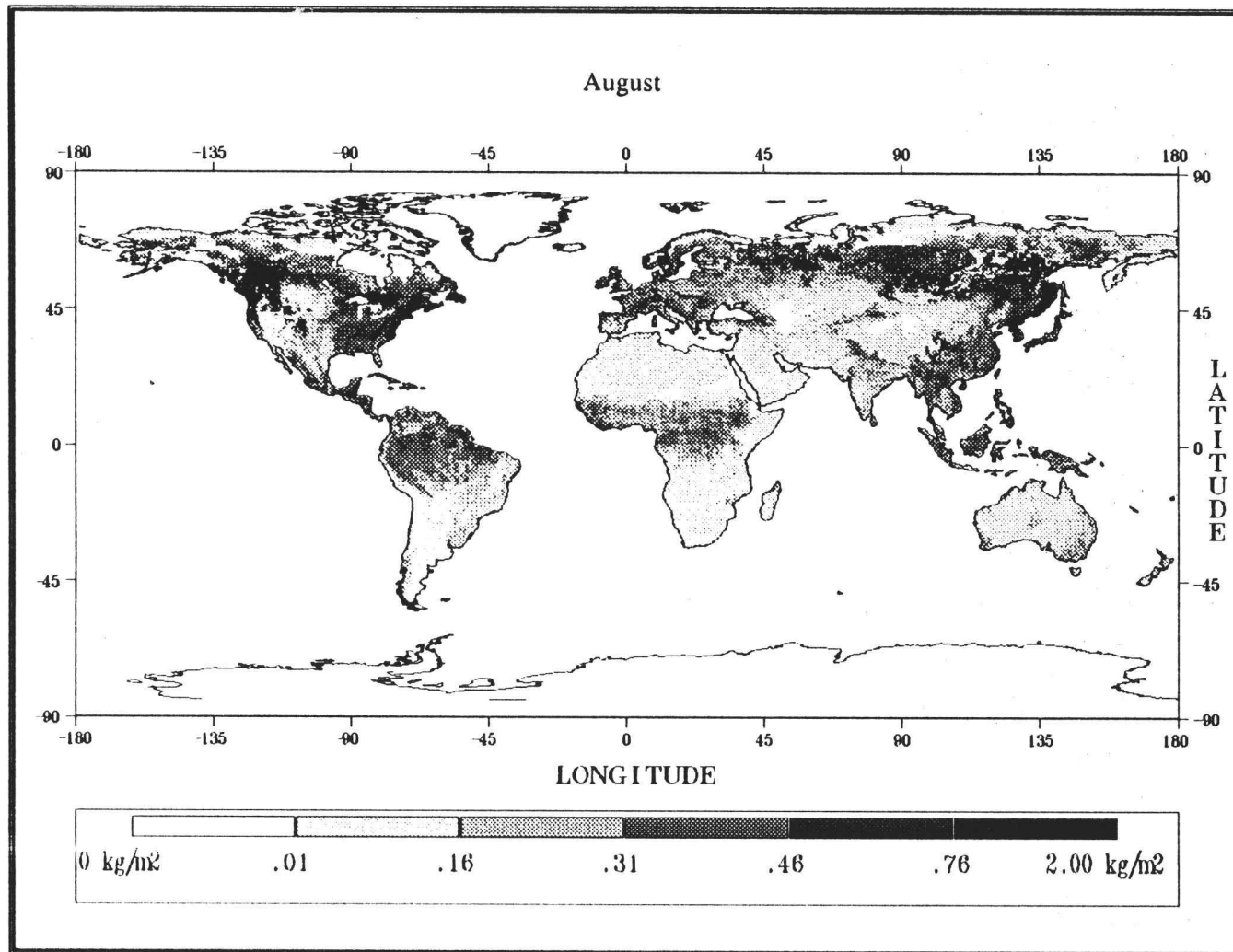


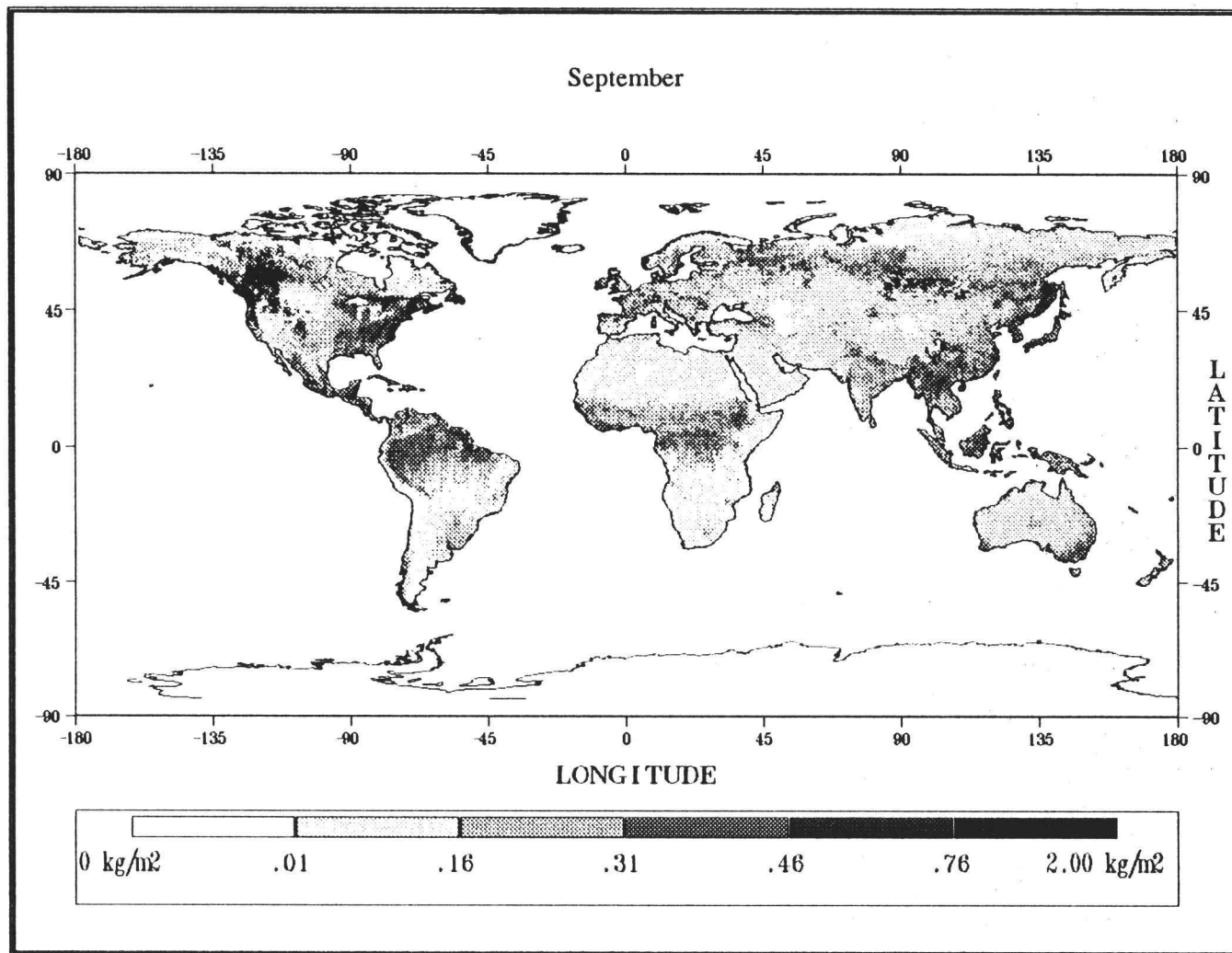


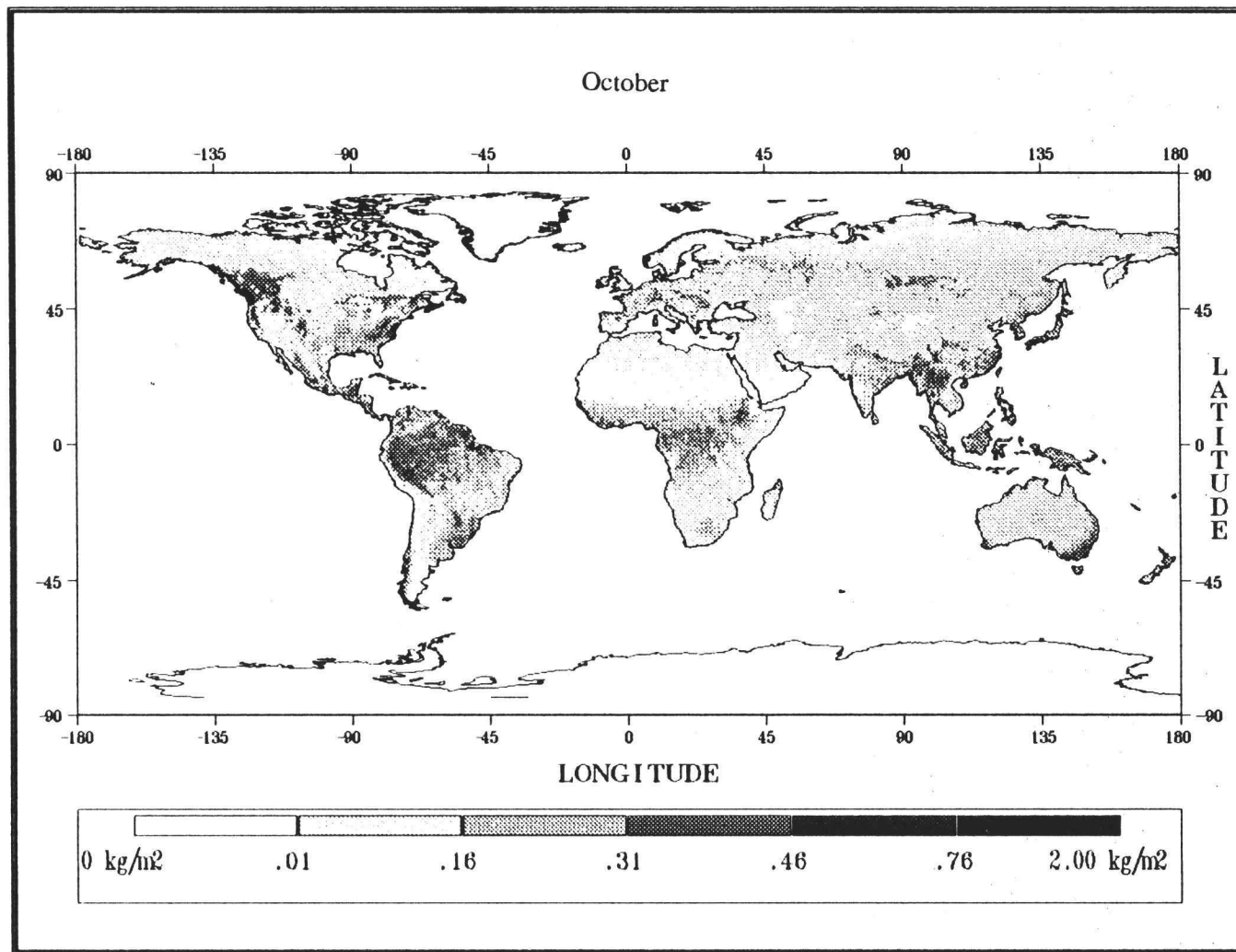


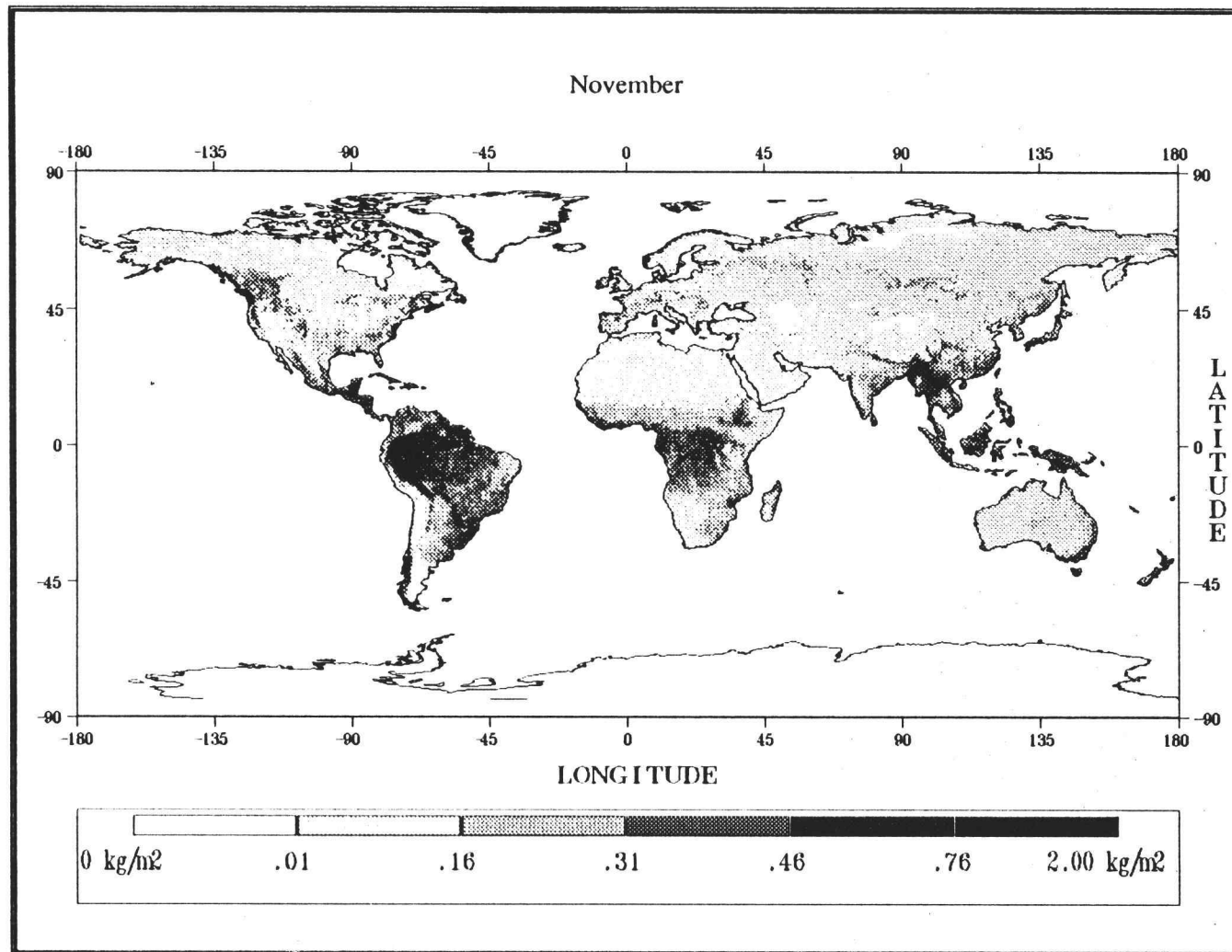


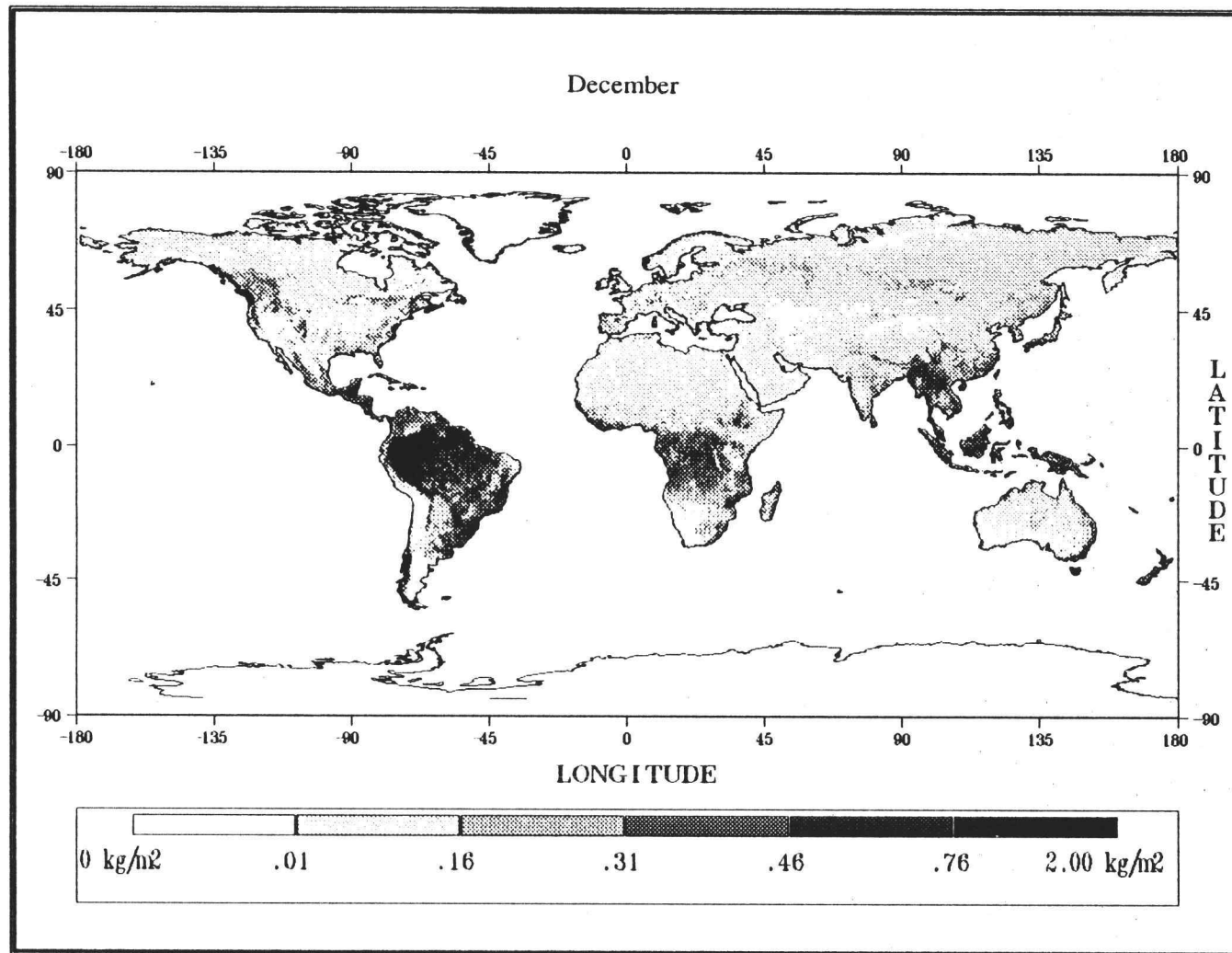








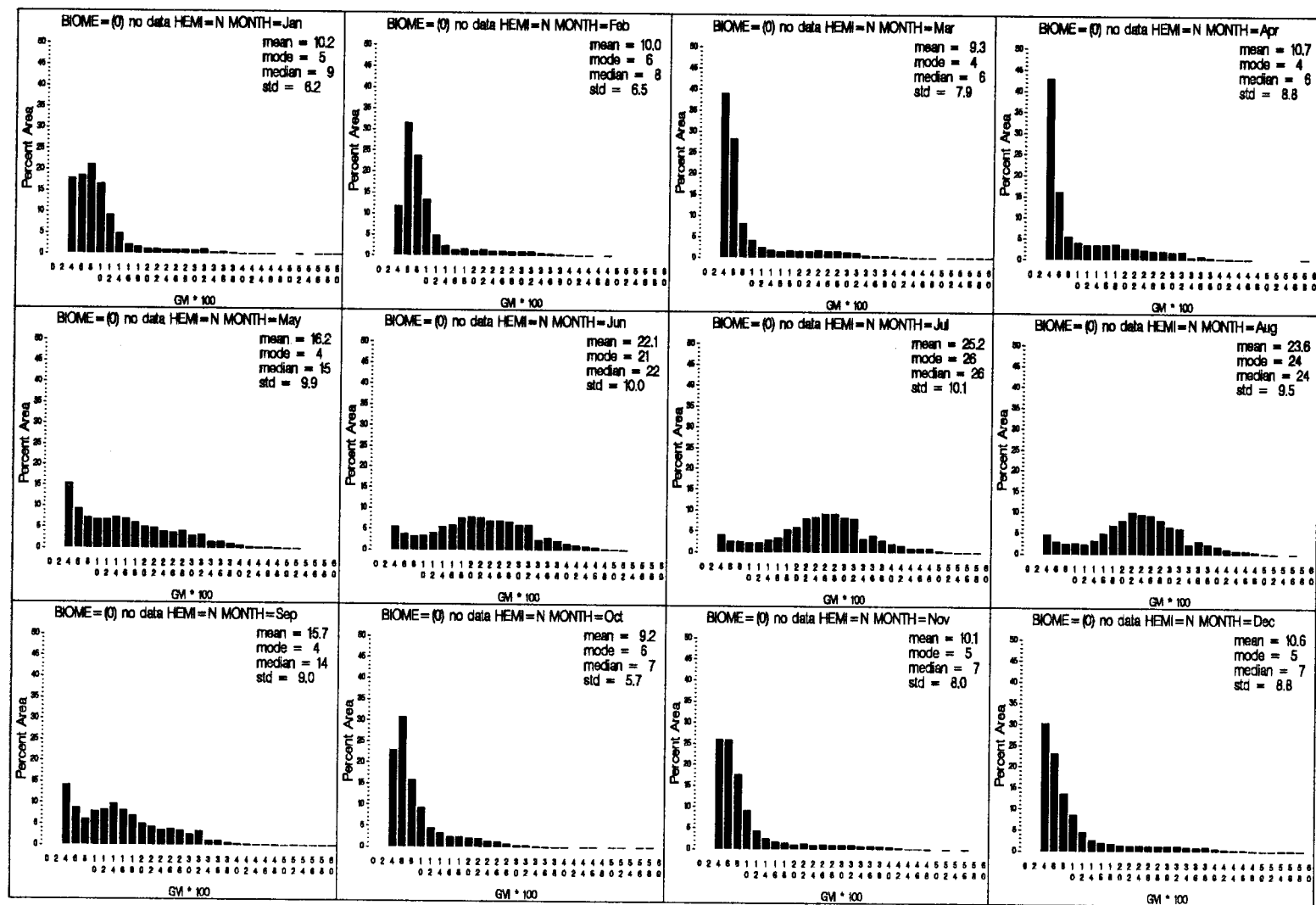


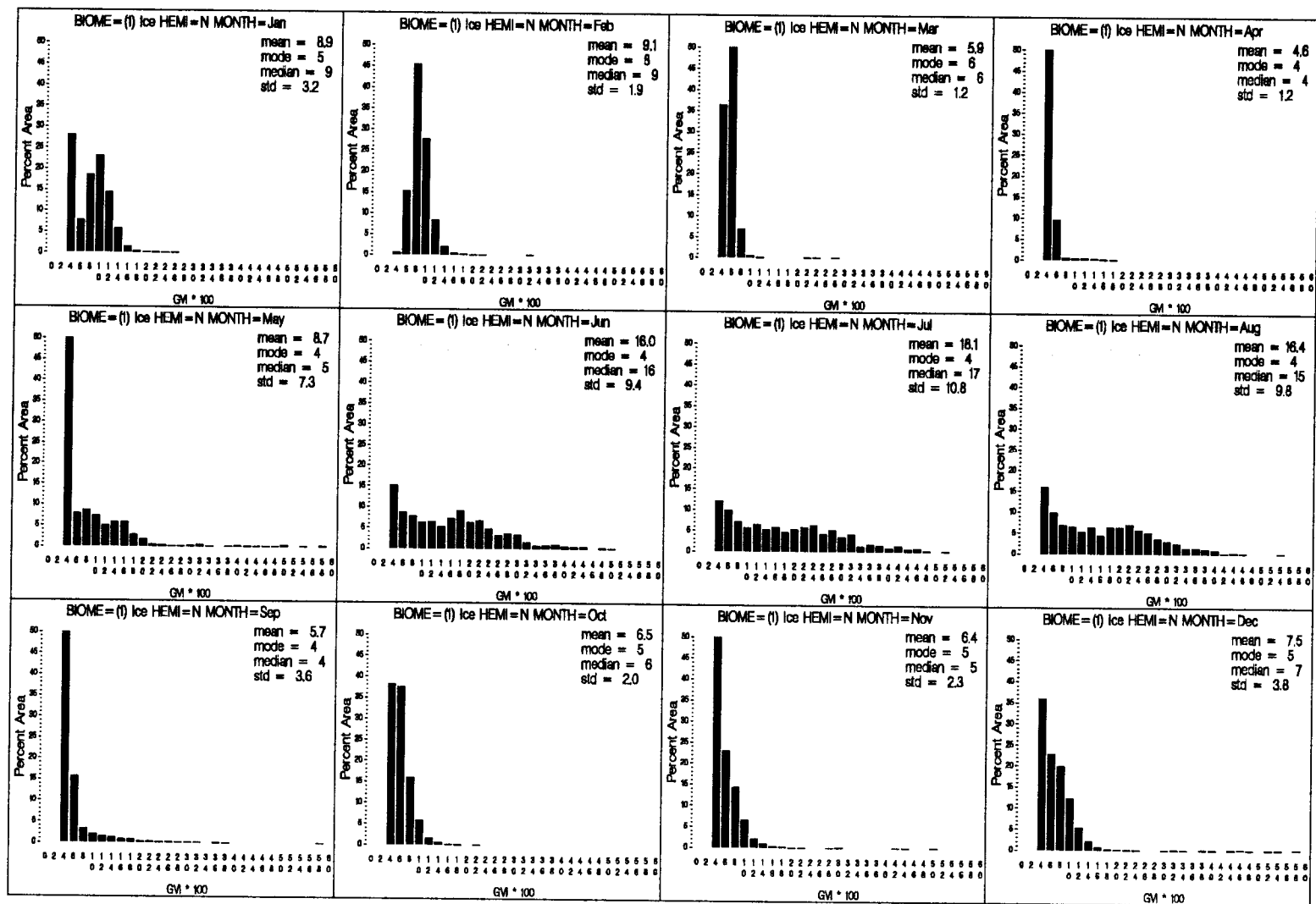


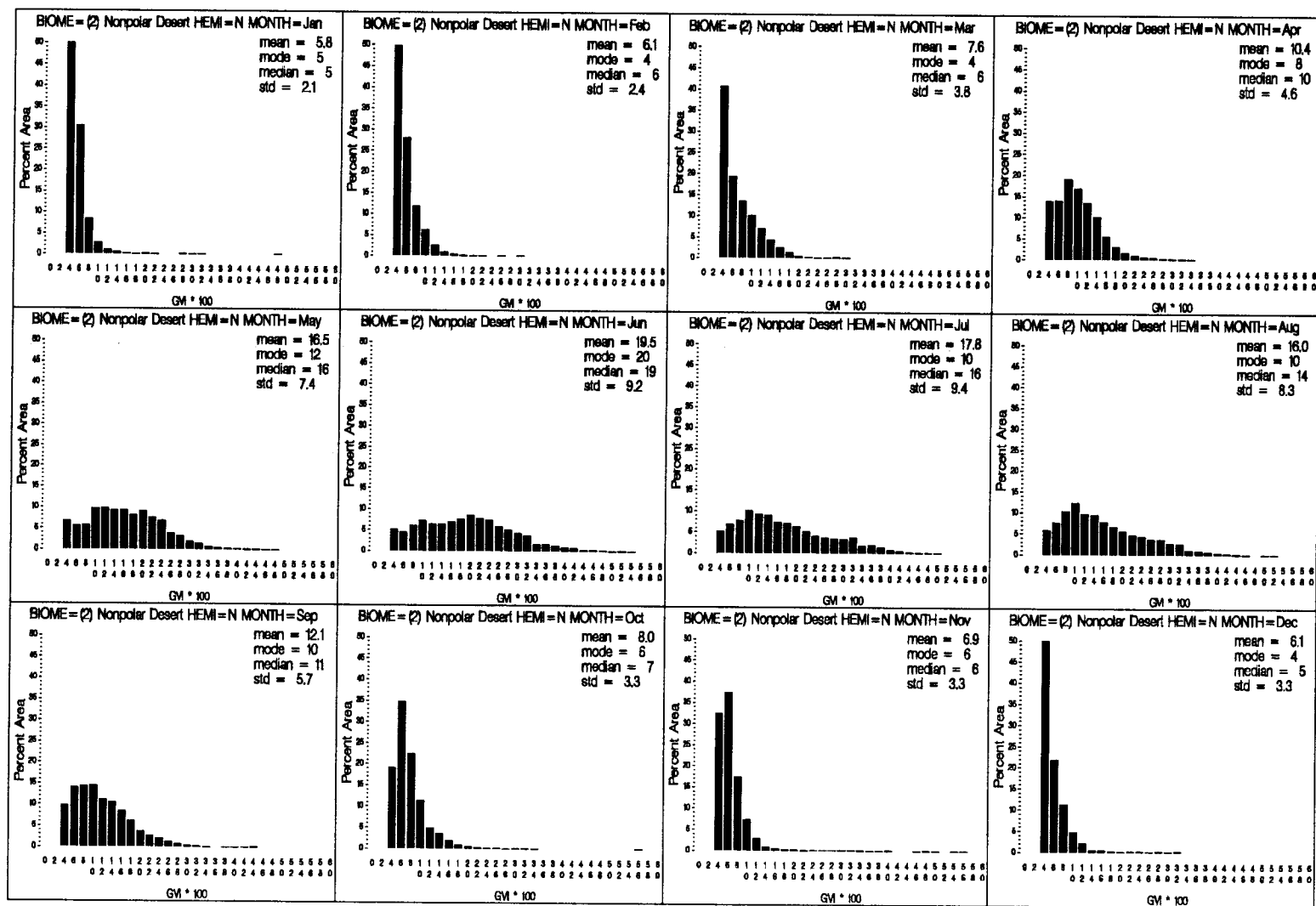


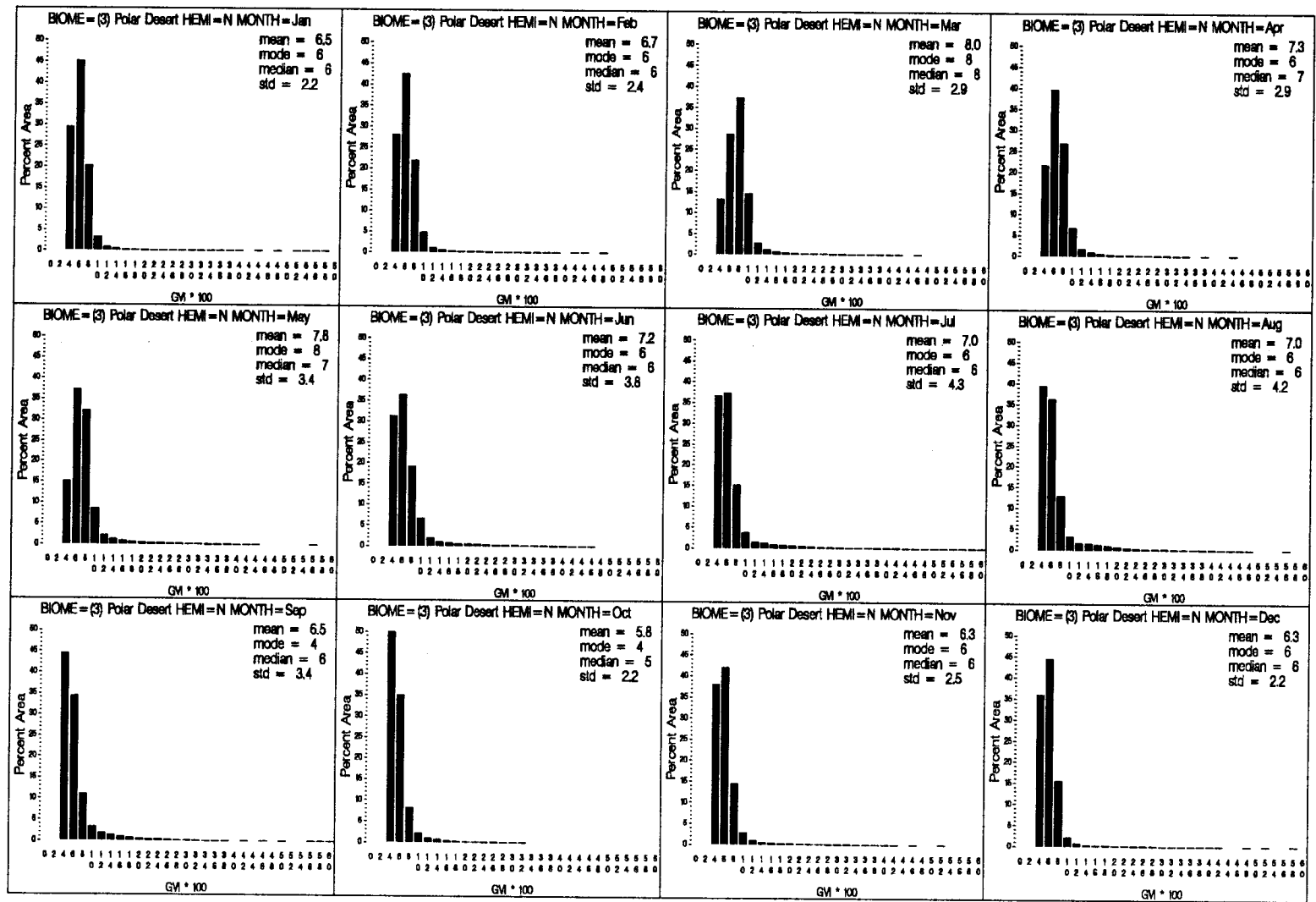
## **APPENDIX H**

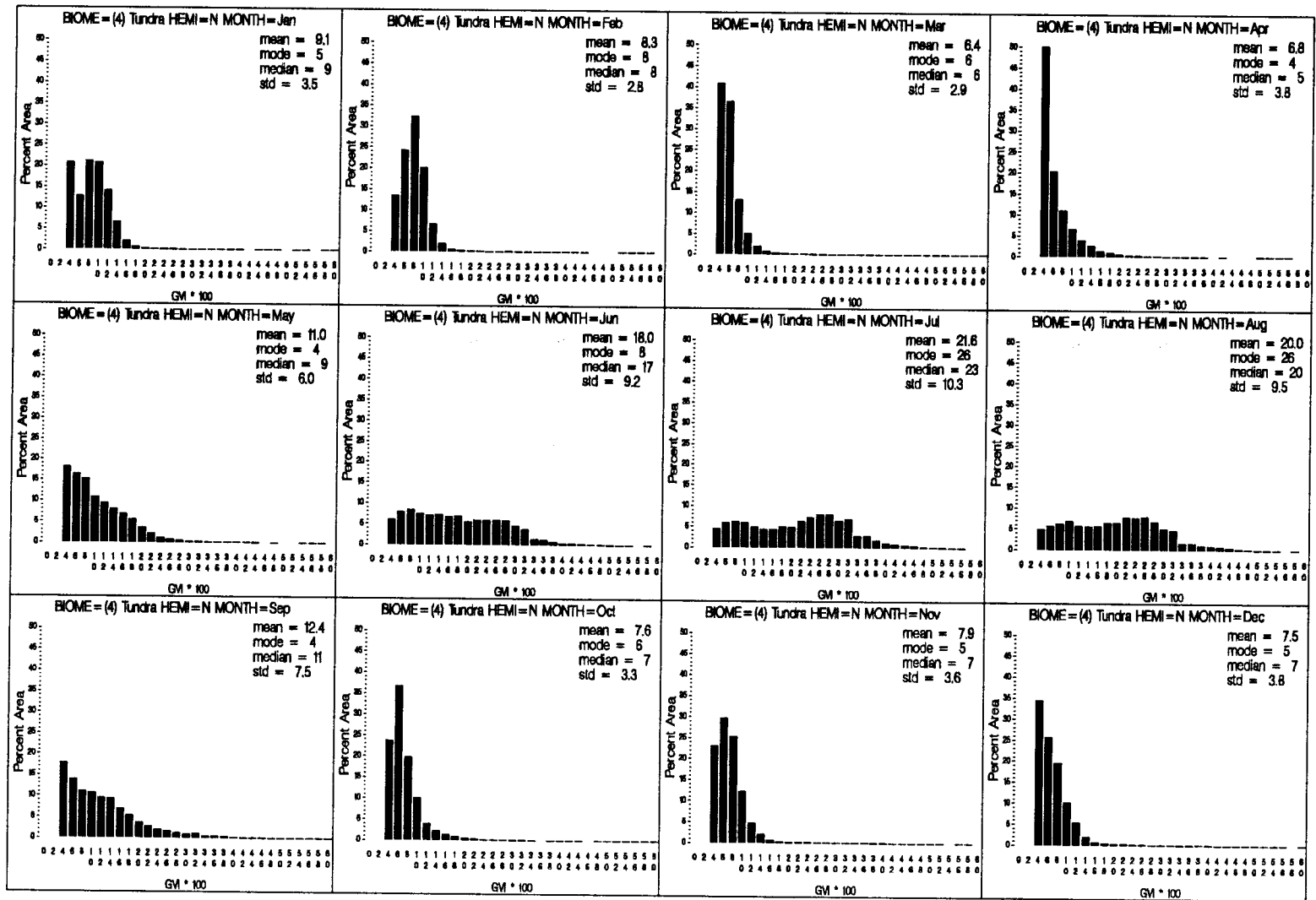
### **Monthly Histograms of GVI per Biome**

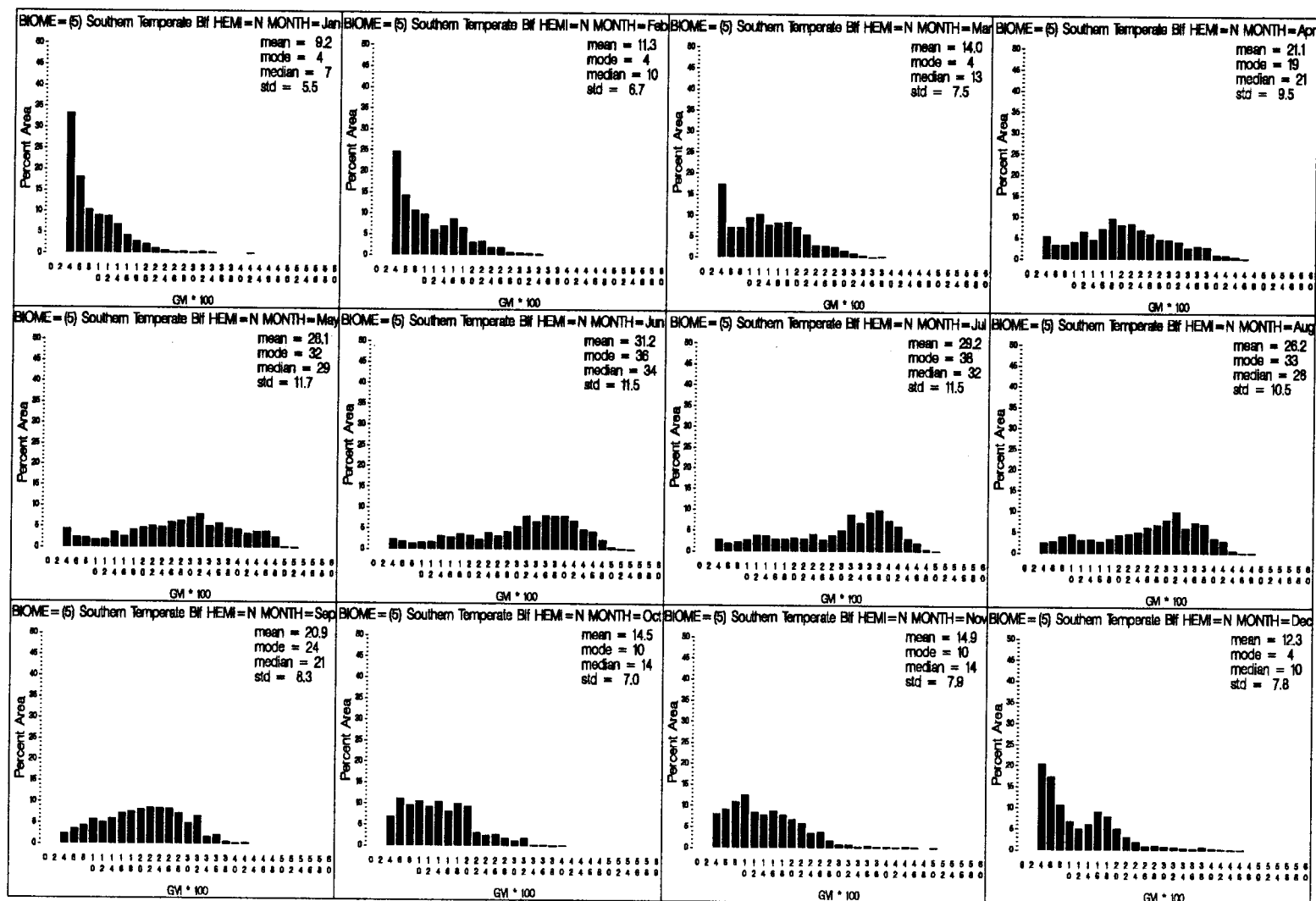


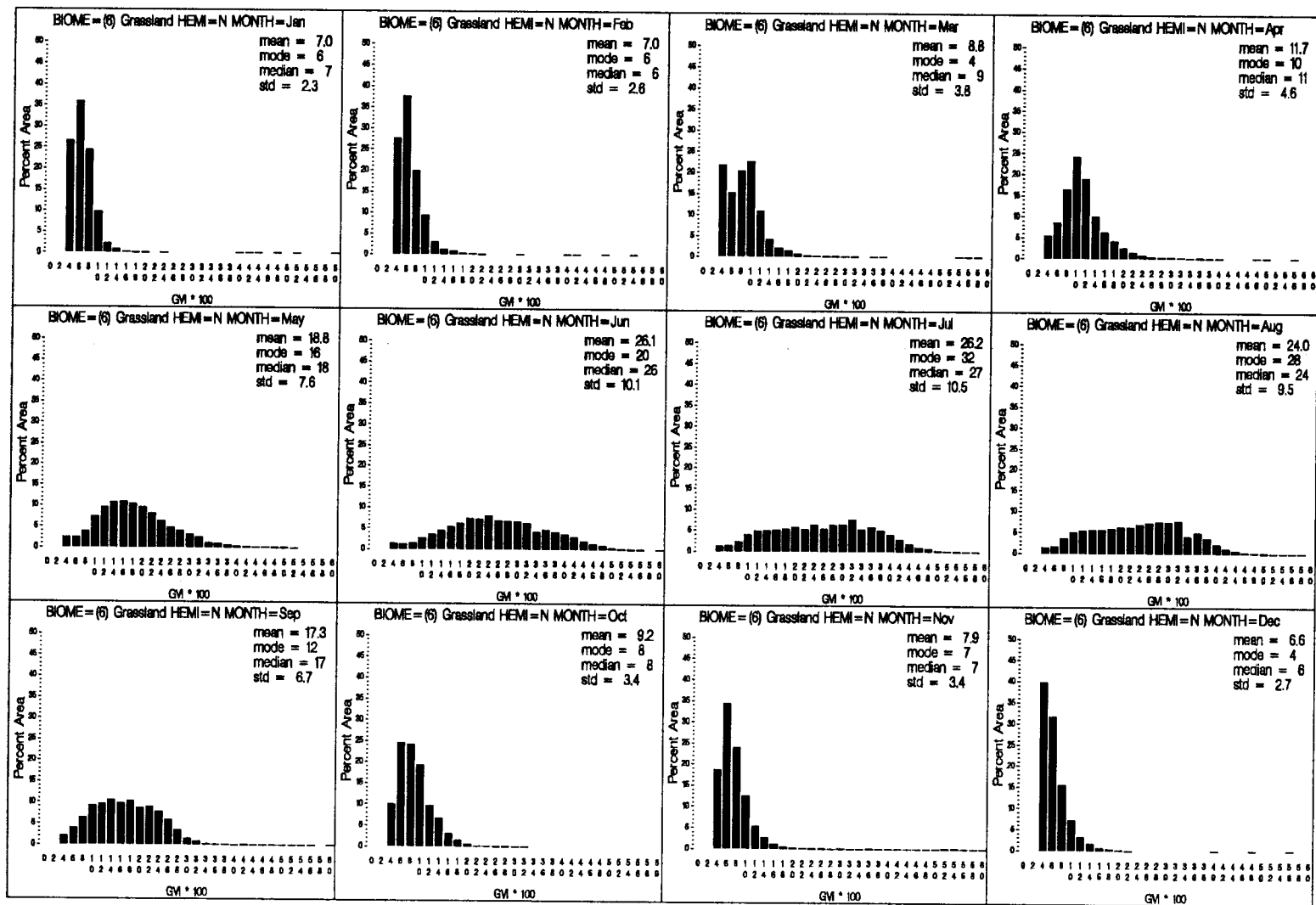




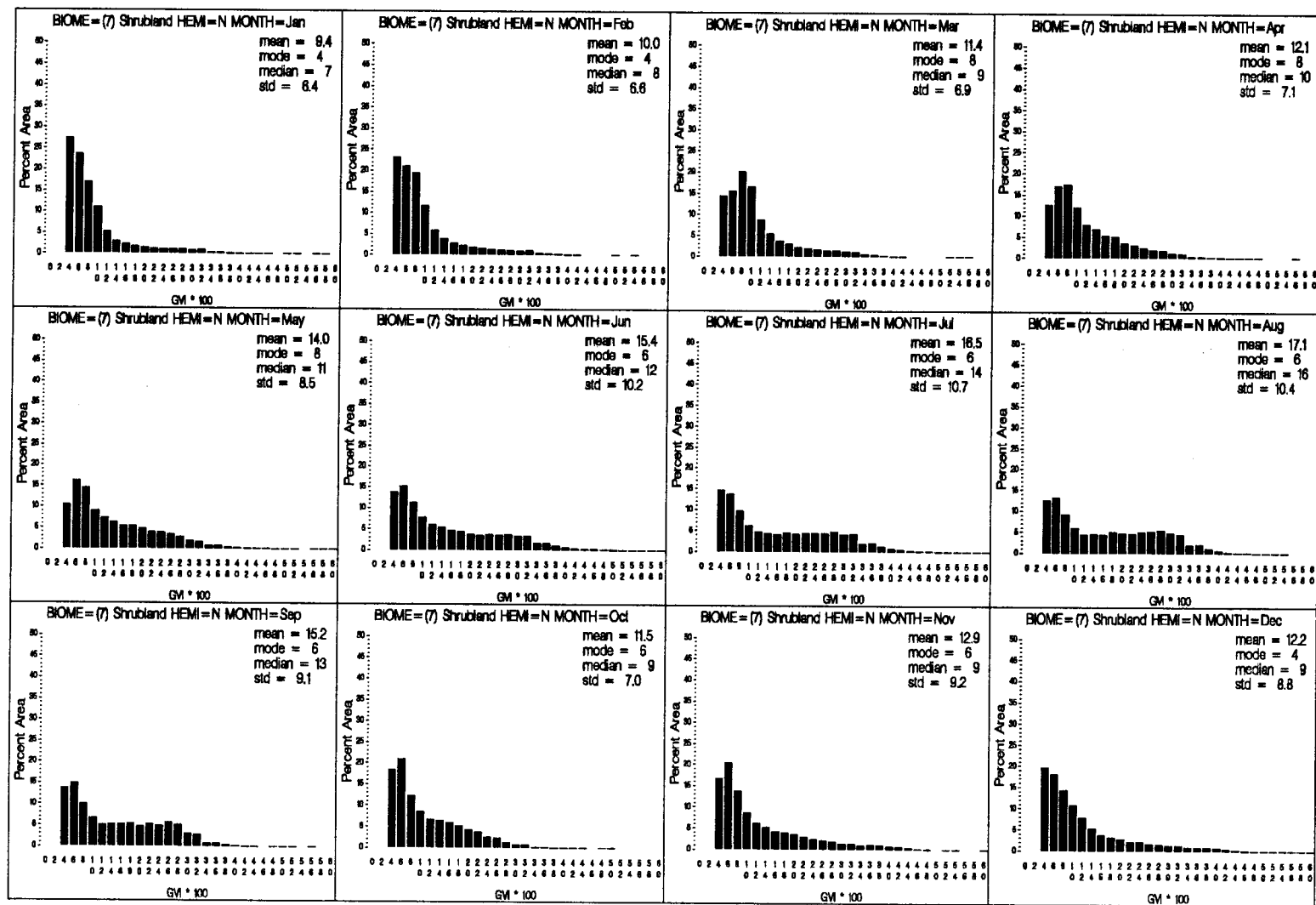


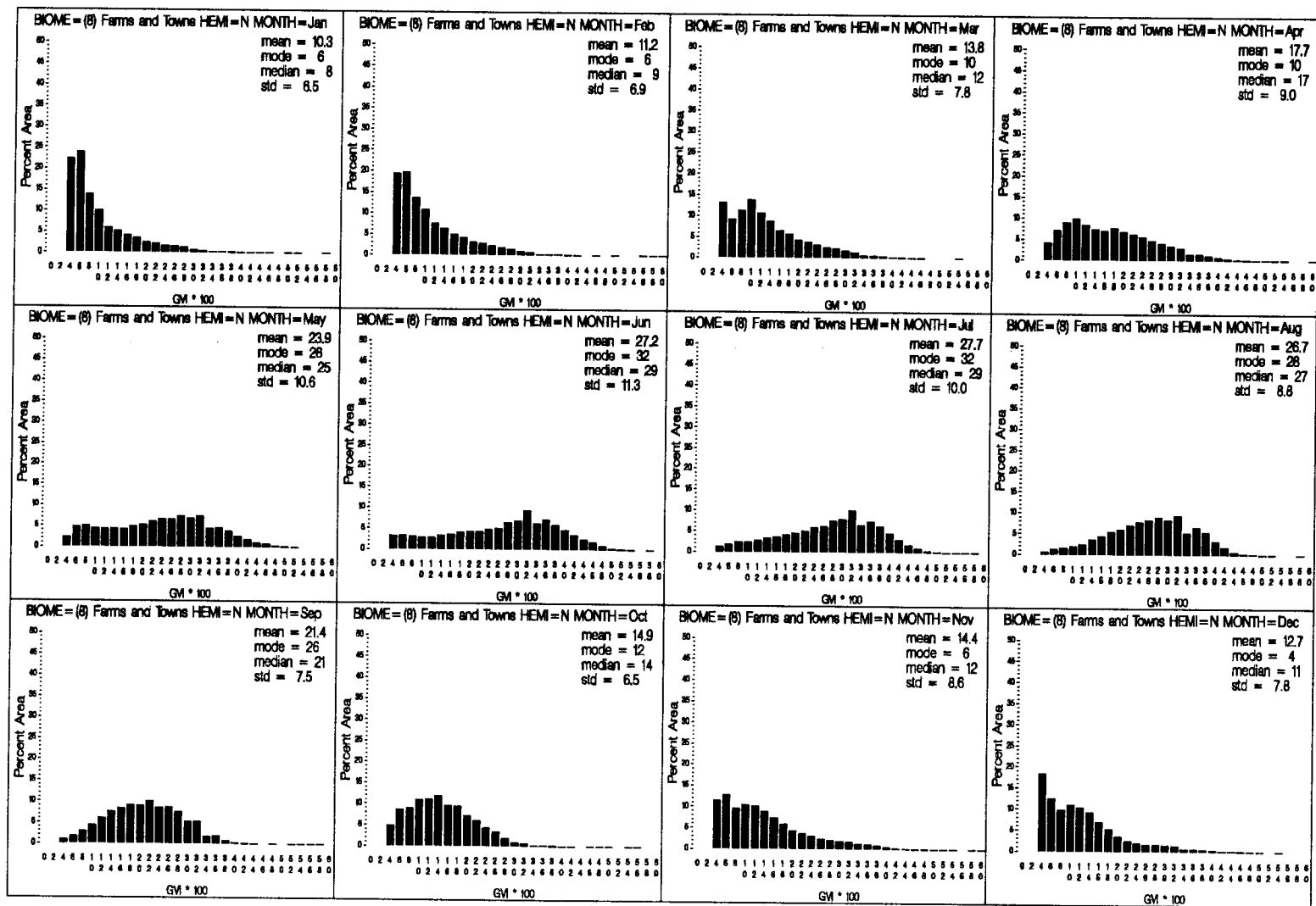


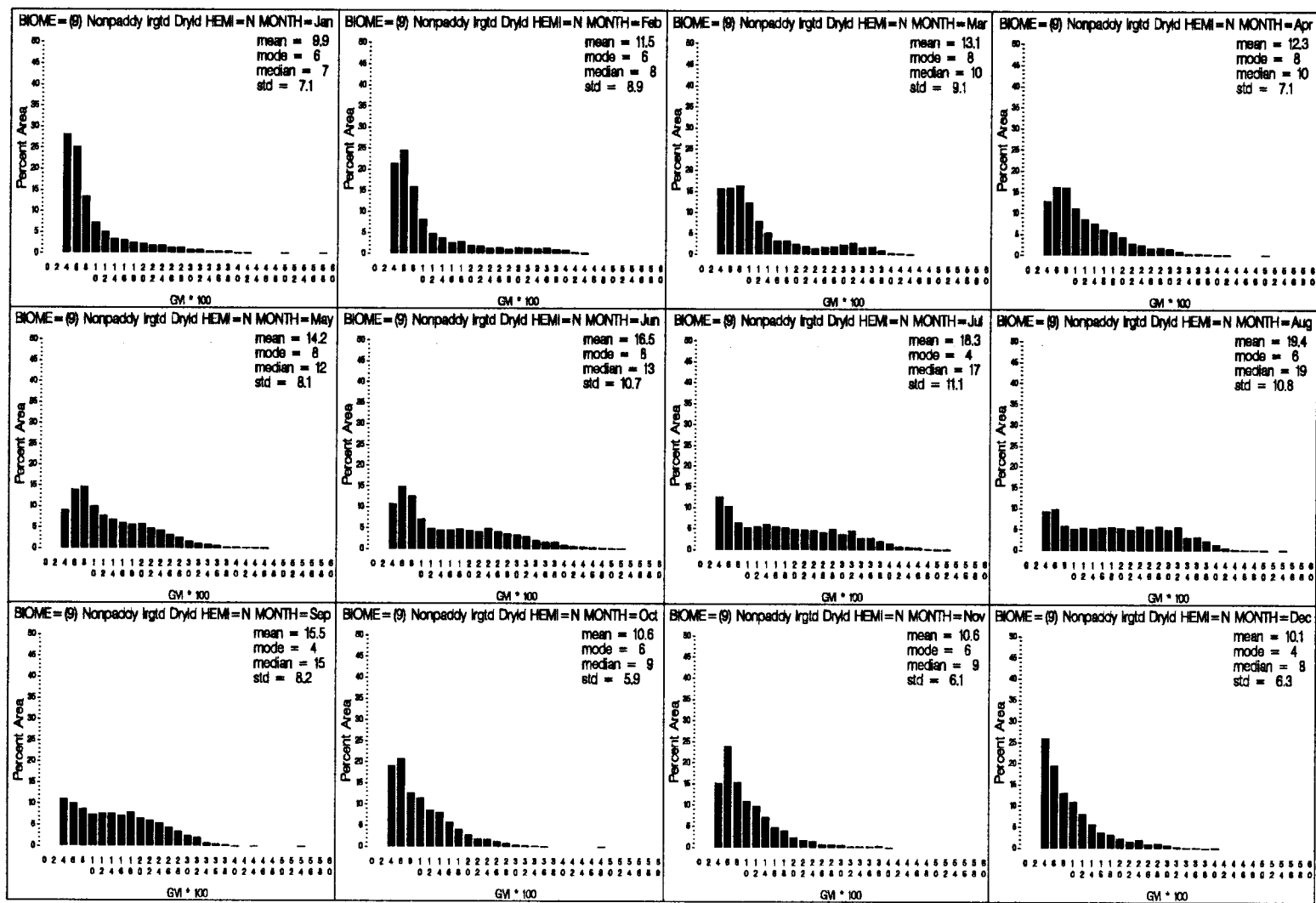


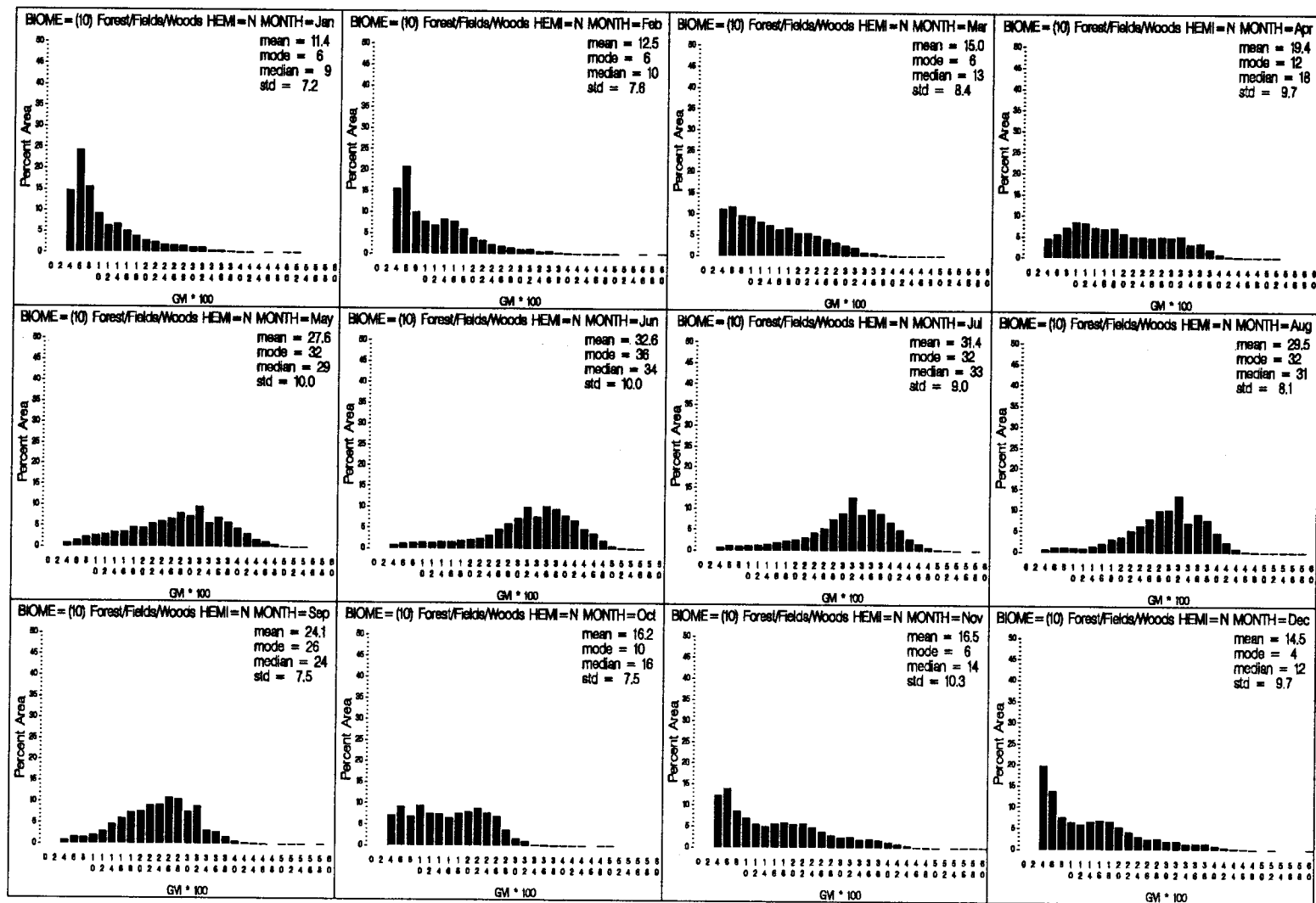


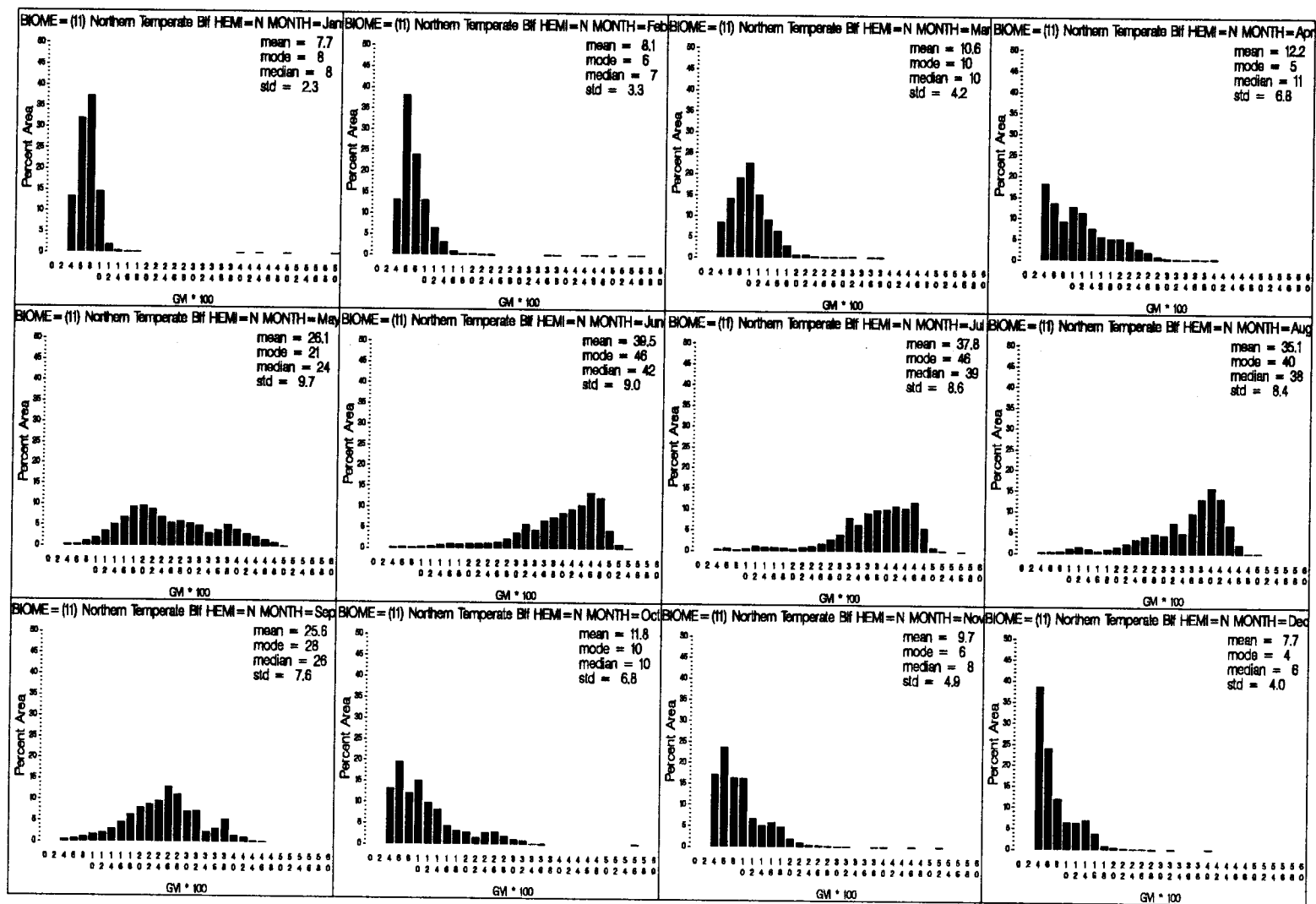


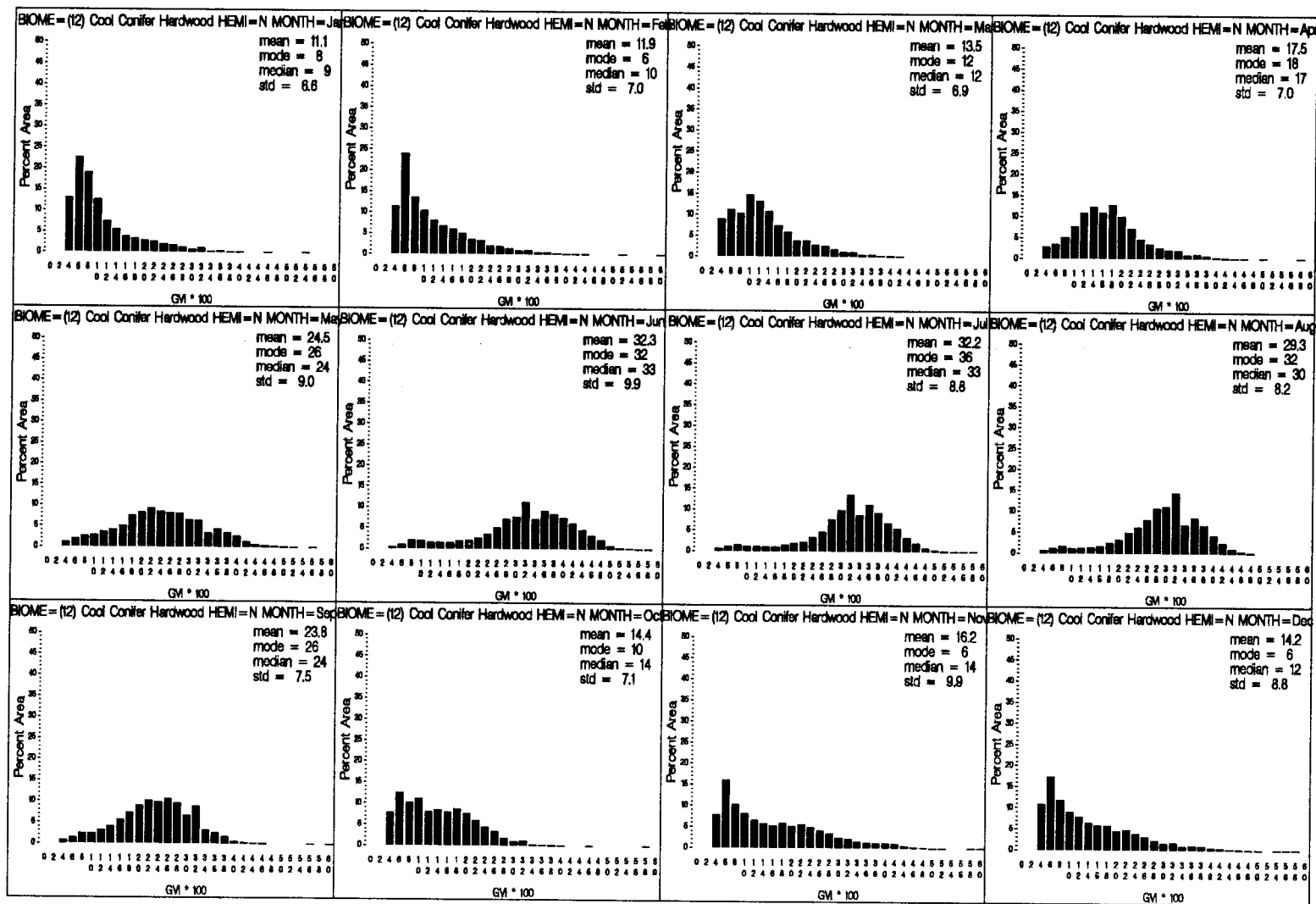


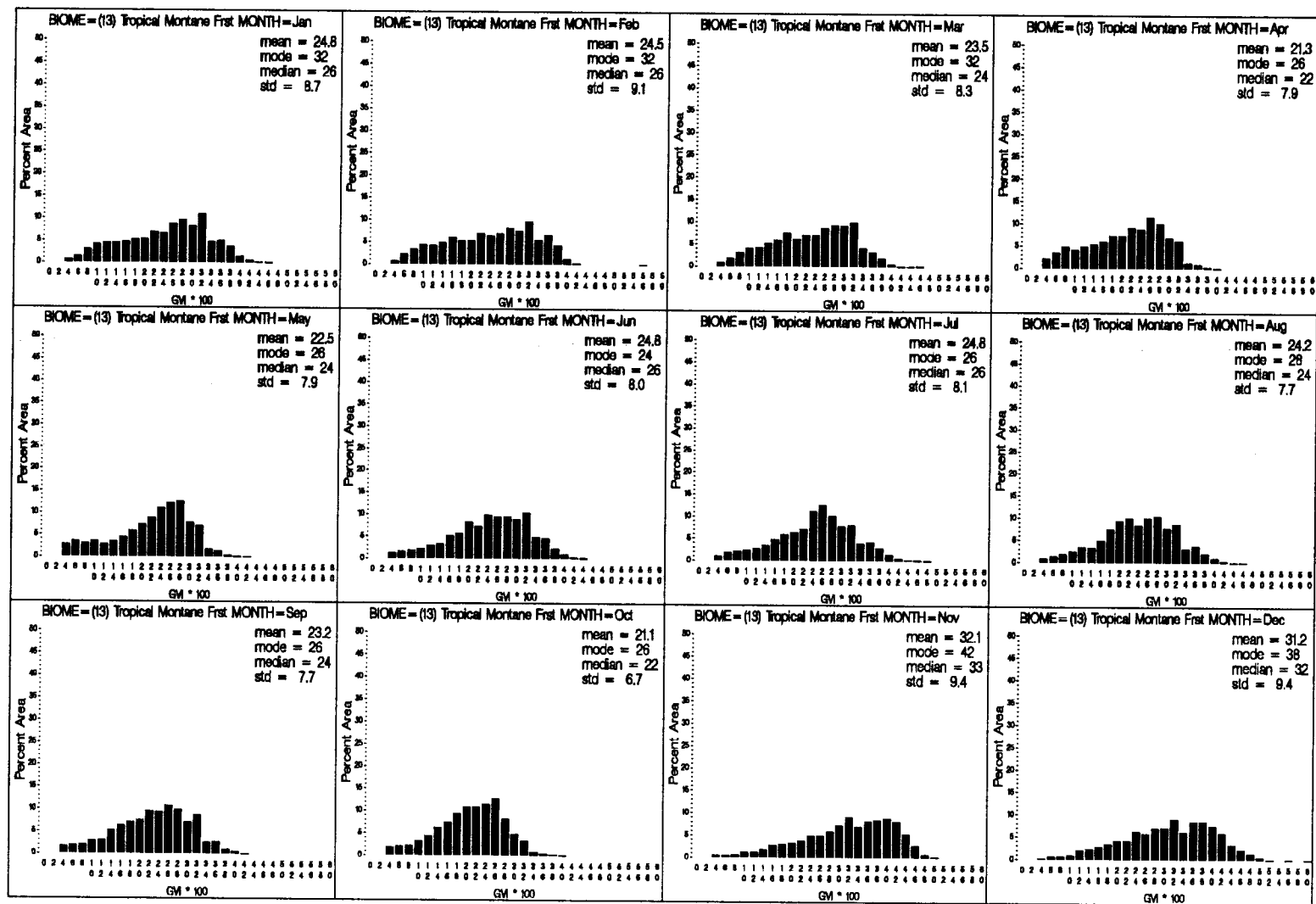


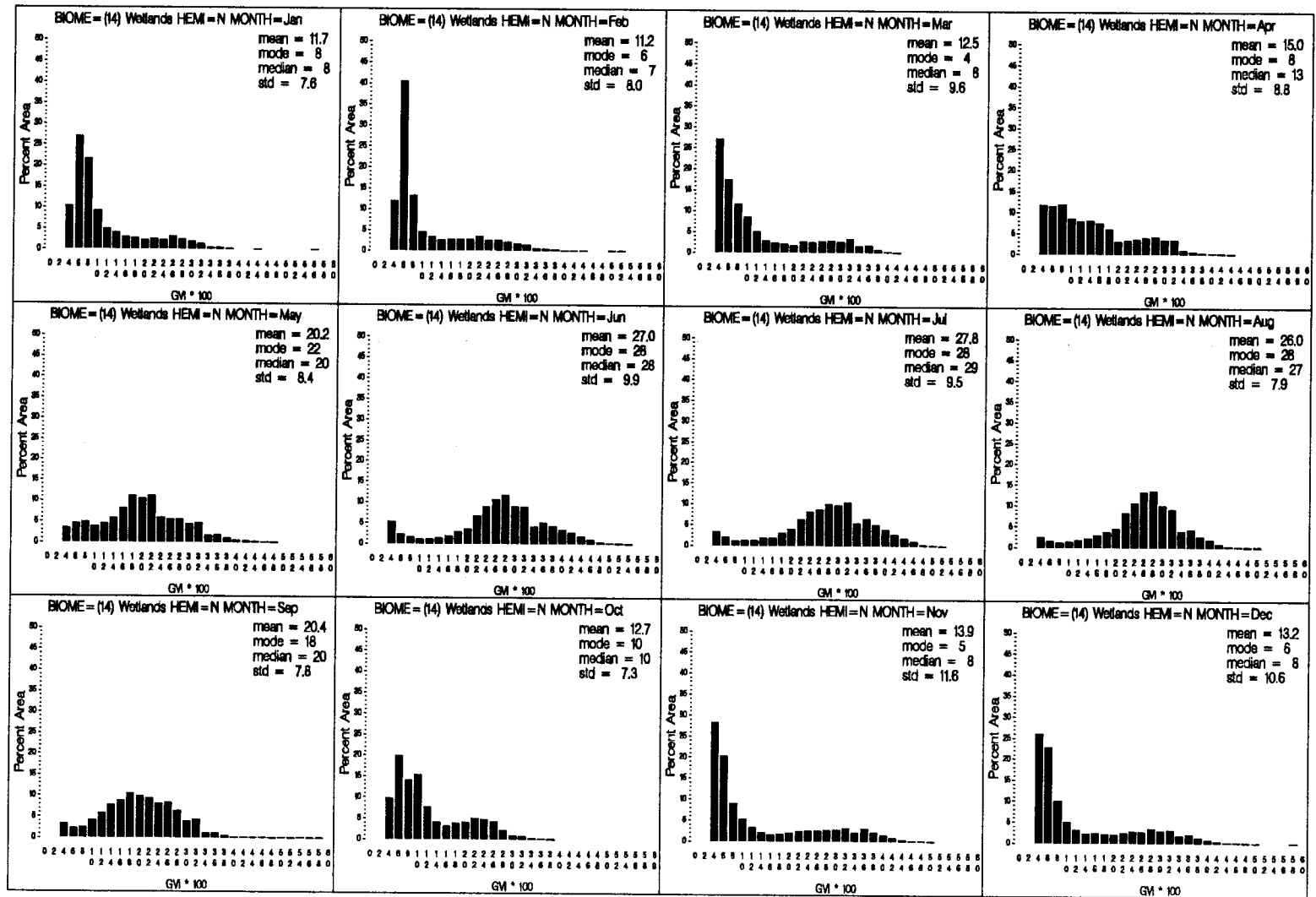




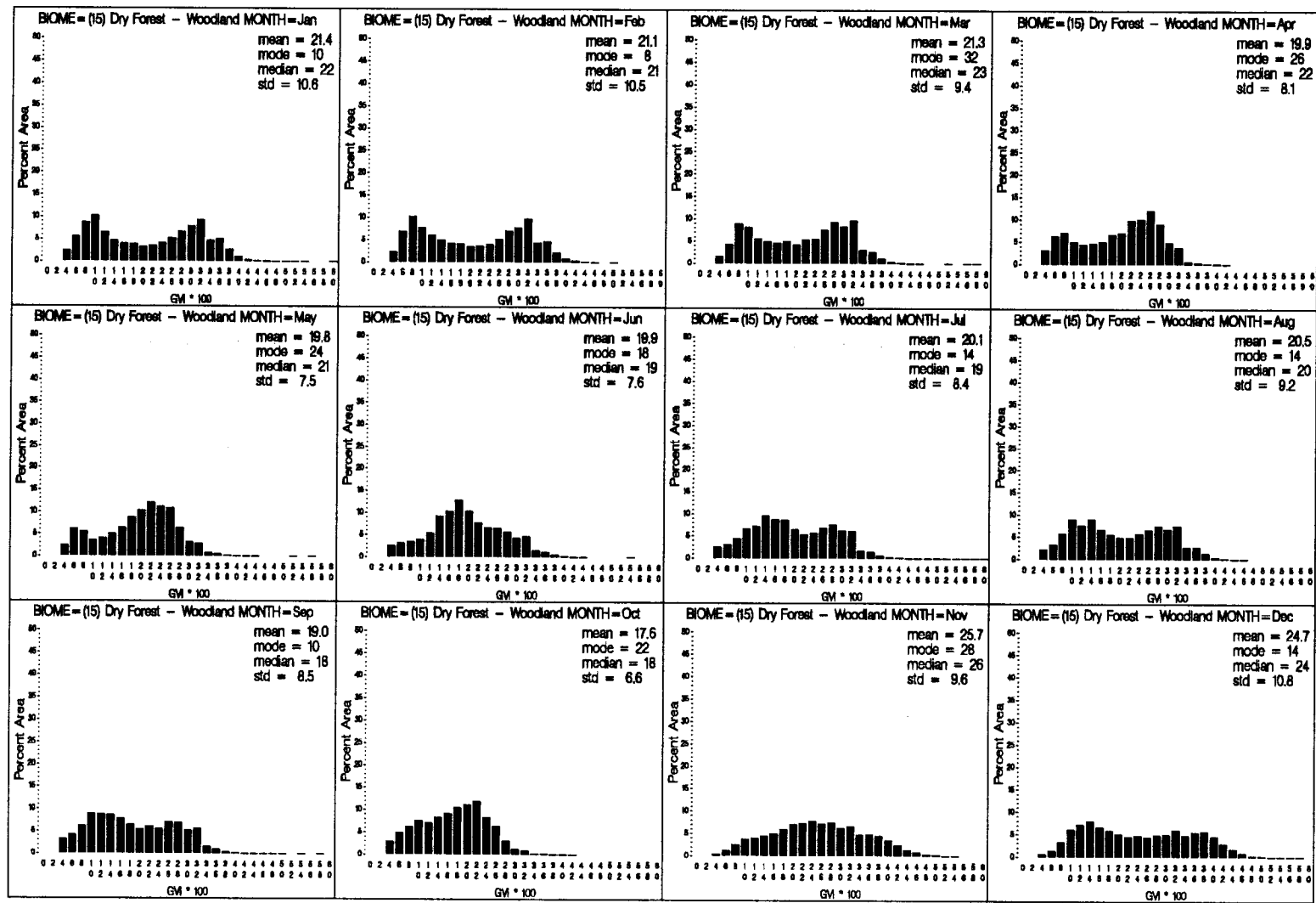


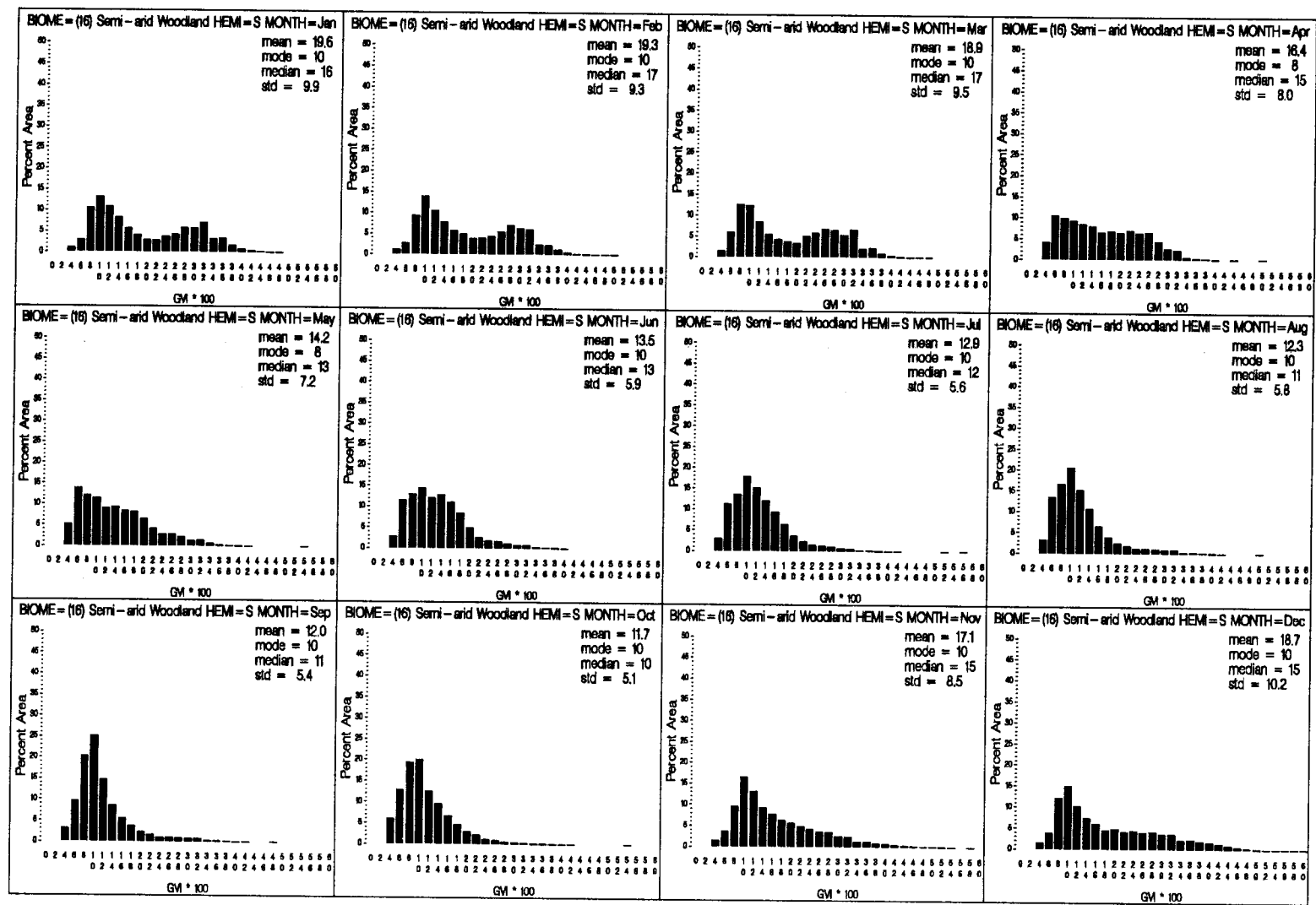


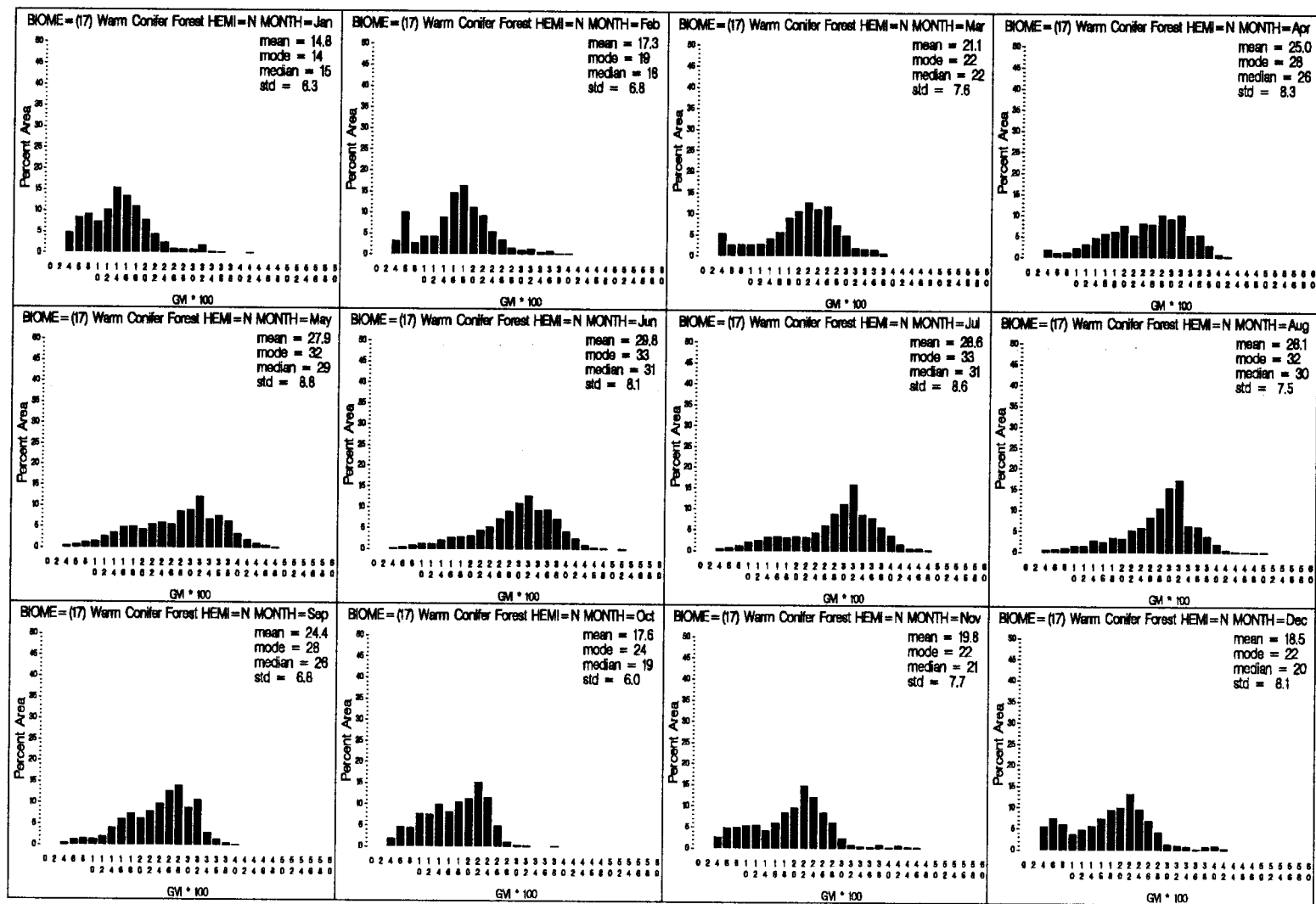


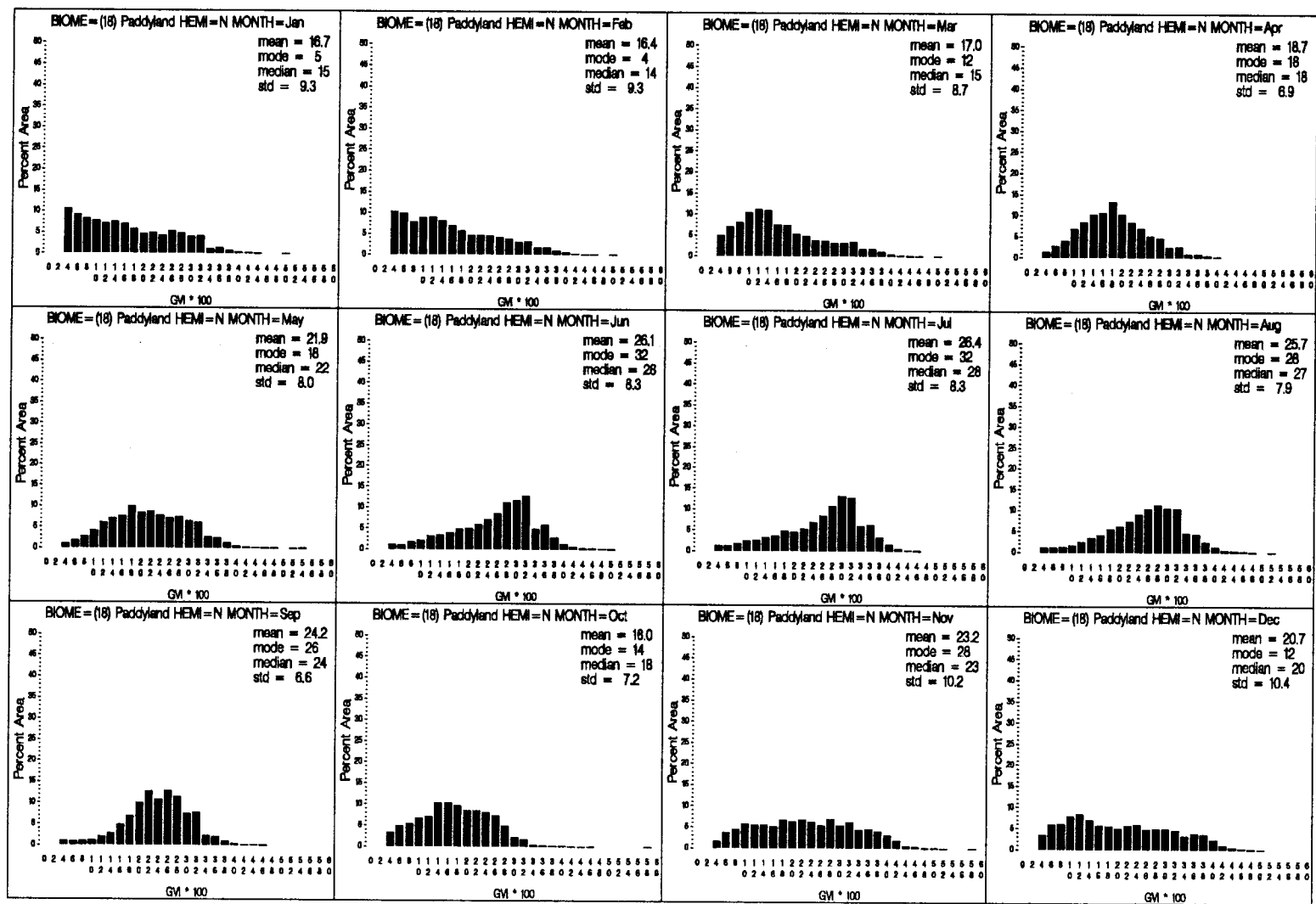


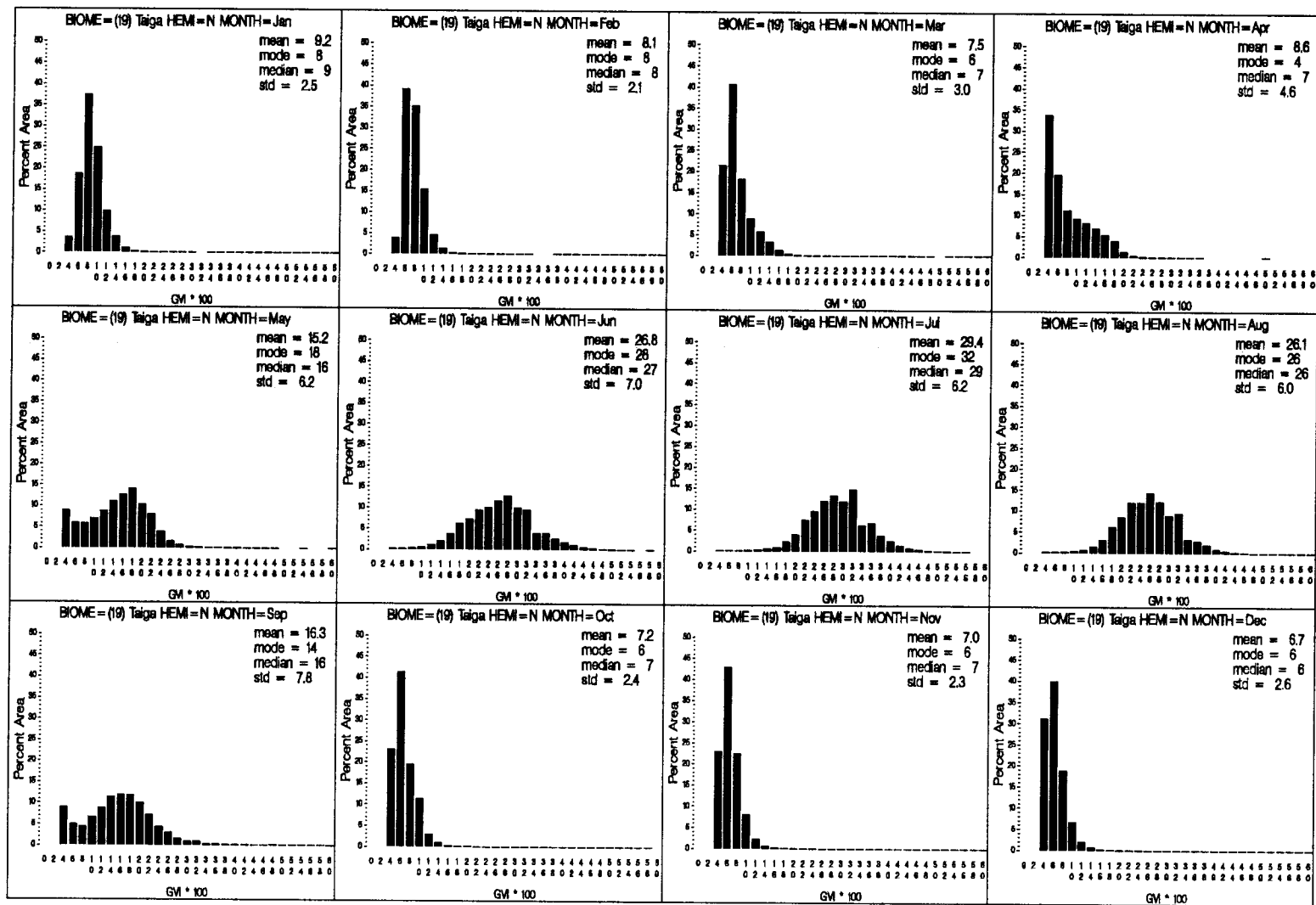


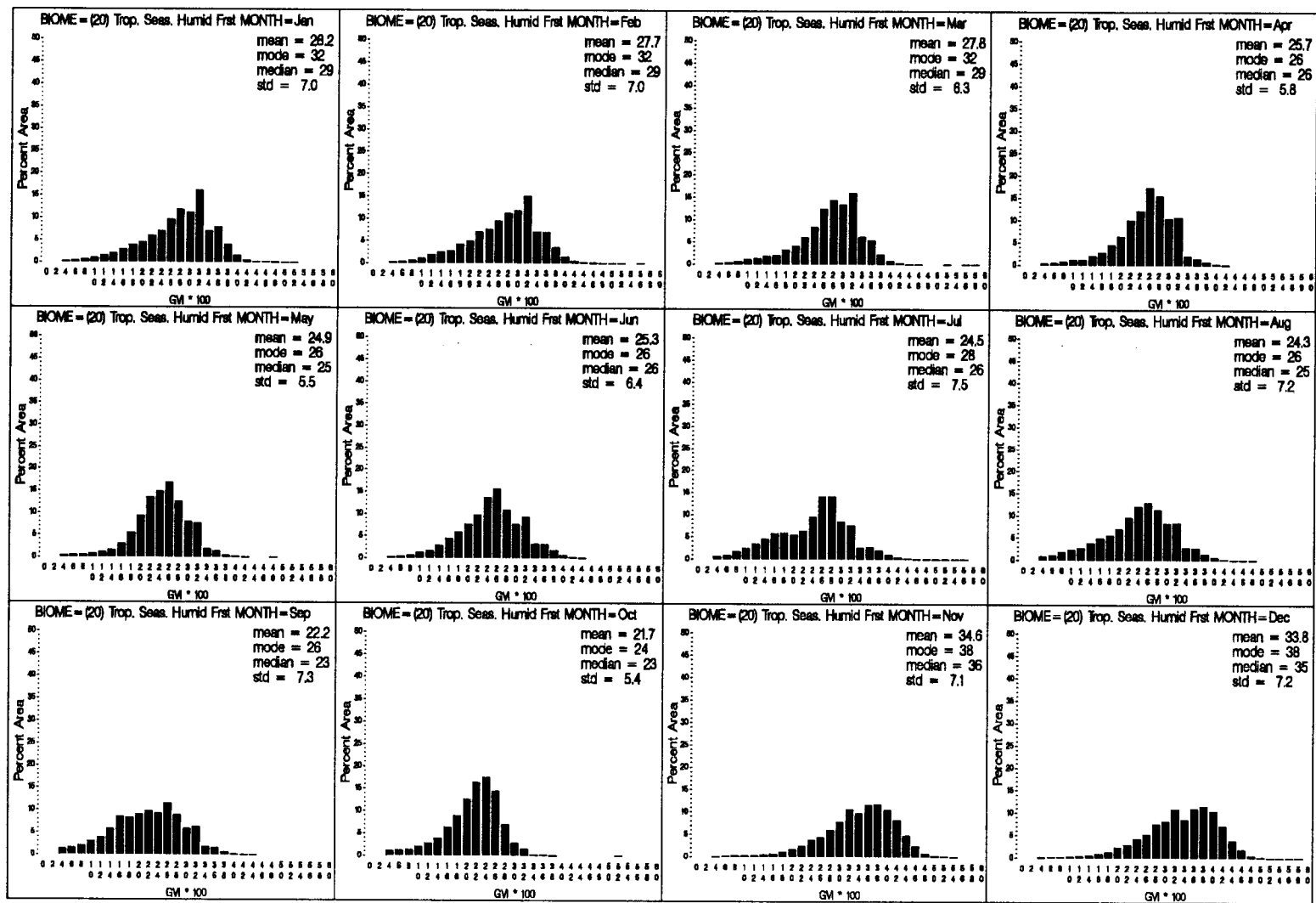


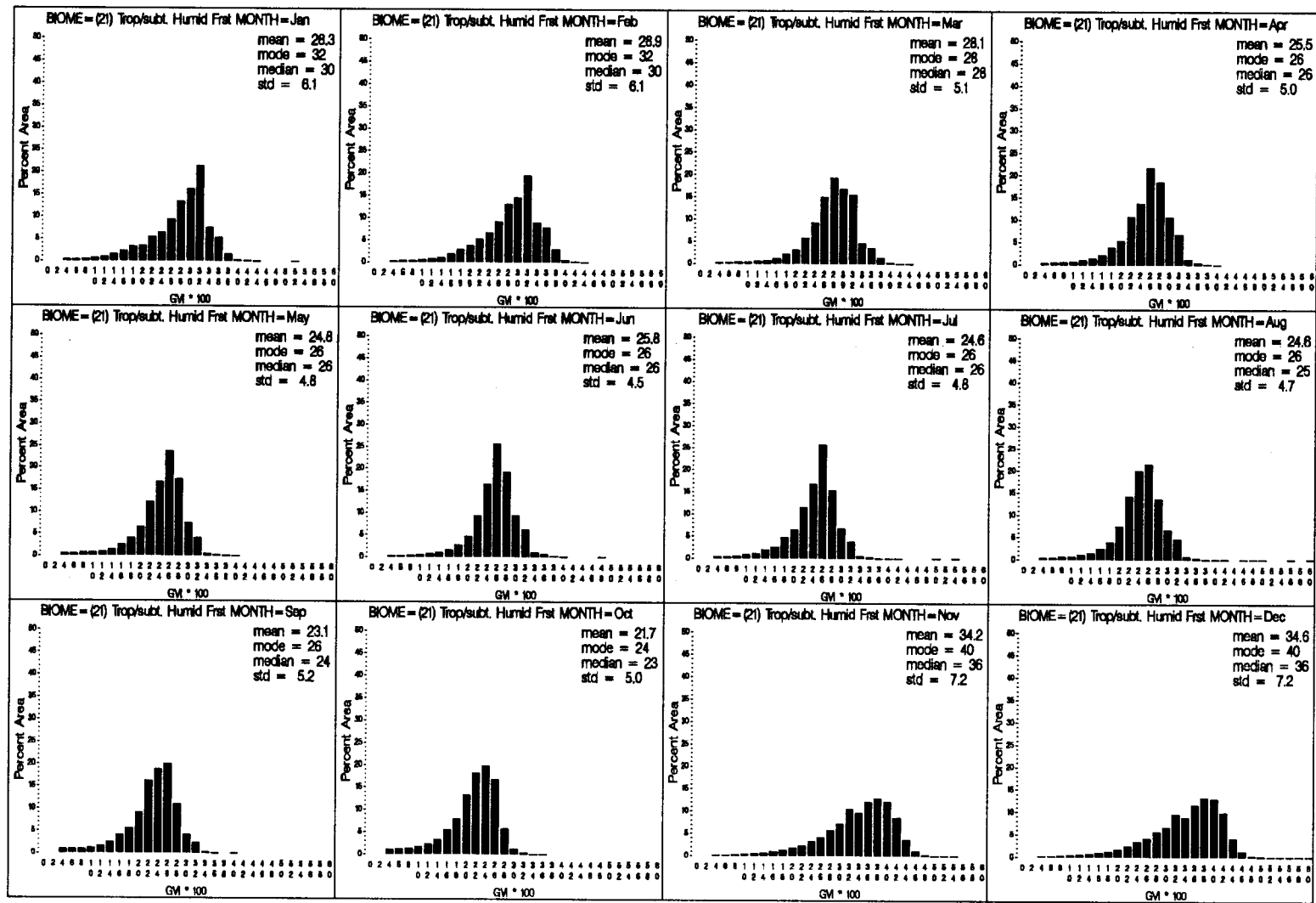


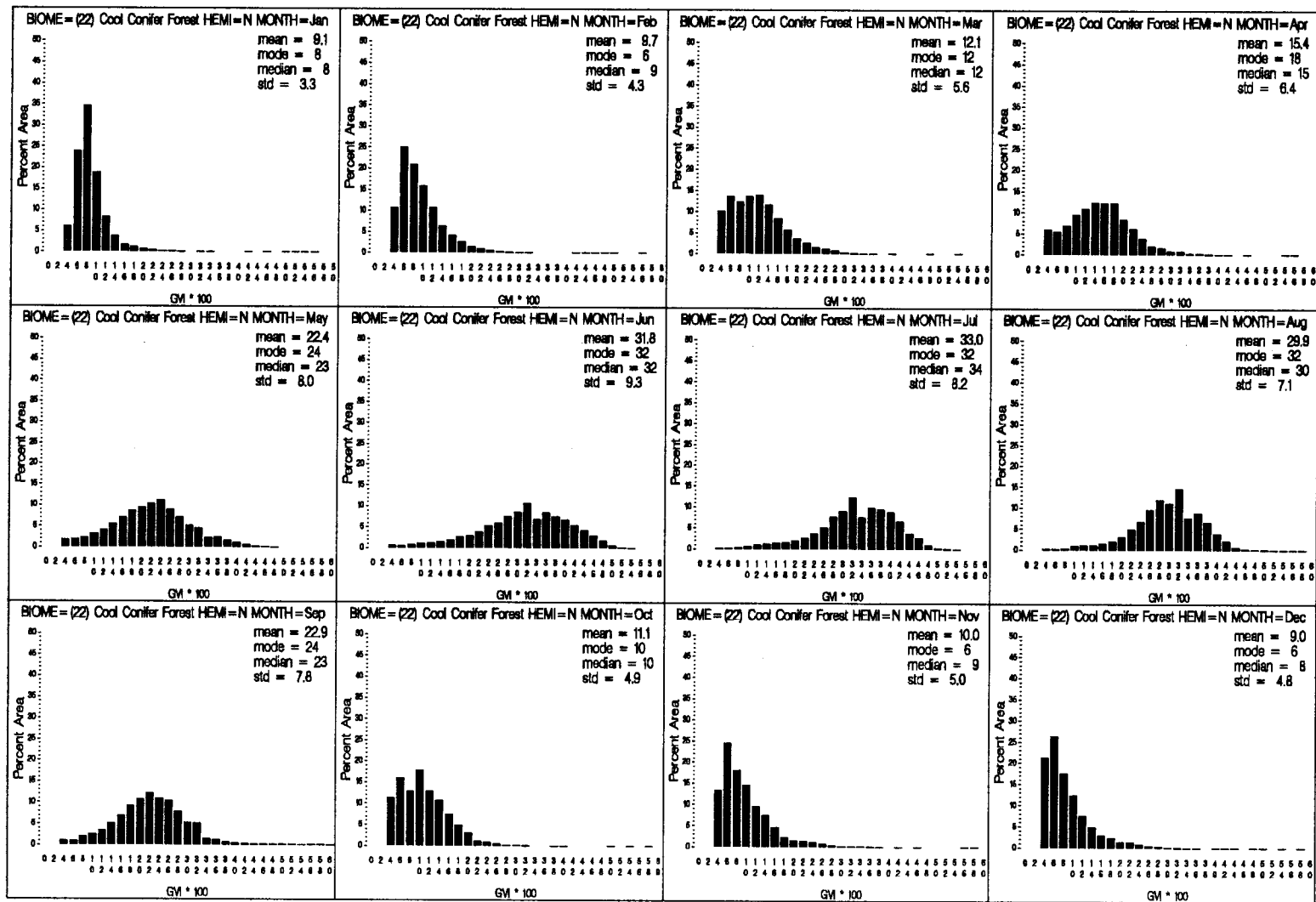














**APPENDIX I****Monthly Histograms of FBD per Biome**

